Department of Electrical and Computer Engineering

Reliable Indoor Power Line Communication Systems: via Application of Advanced Relaying Processing

Xiaolin Wu

This thesis is presented for the degree of

Doctor of Philosophy

of

Curtin University

May 2015

Declaration

To the best of my knowledge and belief this thesis contains no material previously published by any other person except where due acknowledgment has been made.

This thesis contains no material which has been accepted for the award of any other degree or diploma in any university.

Signature: . . . . . .

Date: . . . . . .

Xiaolin Wu
May 2015

In the memory of

my Physics teacher, Mr *Wu WenQing*,

who enlightened the once wild boy.

Acknowledgements

The PhD study is such a great experience. During these years, I devote myself to the academic research, try to contribute to the scientific community and have the opportunity to work with great people who helped me grow both professionally and culturally.

First of all, I would like to express my gratitude to my supervisor Dr. Yue Rong for his constant support and encouragement during the entire period of my PhD study. His invaluable guidance and timely correspondence directed me to reach the goal. Without his kind help, all this can never be achieved.

Also, I am grateful to the kindly emotional support that I got from my dear colleagues and friends, especially Ms Khandker Nadya Haq and Ms Helen Yang, for their soothing words that cheered me up during hard times.

Lastly, I would like to appreciate China Scholarship Council (CSC) and Curtin University for the financial and administrative support they have provided me during the course of my doctoral study.

Abstract

Recently, in order to provide indoor high speed information services, much effort of research has been made to improve the performance of the communication technologies used within buildings and houses. Among many wired and/or wireless solutions, indoor power line communication (PLC) is a very attractive technology for its unique advantage—power cables are preexisting around the house and can be used at any time without deploying any new wires. In addition to electricity delivery, the indoor power cables are used as medium, at the meantime, to support local area networks (LAN). However, as power cables are not manufactured for high frequency (HF) signal transmission purpose, indoor PLC channels demonstrate hostile characteristics for broadband communications. As a solution to this problem, a series of relay schemes are suggested in this thesis to improve the transmission performance.

As existing point-to-point (P2P) indoor PLC channel models cannot be directly used for the scenario where relay devices have been plugged into the indoor power grid, based on transmission line theory, we first propose a general method of modeling the relay-involved PLC channel. With this method, different signaling paths existing in the relay-involved channel can be transformed into a group of correlated P2P channels, while the latter one can be easily generated with some published P2P channel models. Then, the proposed relay schemes are examined under realistic channel environments generated from the relay-involved channel model.

In this thesis, we consider relay devices work in the amplify-and-forward (AF) mode for its lower complexity, shorter processing delay and lower implementation cost. Different relay schemes are addressed for various situations, where one or more relay devices are used for one-way transmission or two-way information exchange applications. Instead of considering the capacity performance of these schemes under given system power budget, we examine the power allocation problems from another angle of view, i.e. given certain quality-of-service (QoS) requirements, how to distribute power to the different nodes of the

network, on each subcarrier, to minimize the total power consumption. As PLC systems may produce serious electromagnetic interference (EMI) to other nearby communication systems, especially the amateur radio systems, we hope the proposed power saving algorithm for relay-assisted PLC systems can relieve this issue to some extent.

Simulation results show the efficiency of the proposed relay schemes. In particular, for the one-way relay-assisted transmission system, a novel transmission configuration for the source node can make the system benefit time diversity from the time-varying nature of the relay-involved PLC network. While the combined application of network coding and space-time coding can make the two-way information exchange system achieve a superior performance under certain power constraints.

Author's Note

Parts of this thesis and concepts from it have been previously published in the following journal and/or conference papers.

Journal Papers

[1] X. Wu and Y. Rong, "Joint Terminals and Relay Optimization for Two-way Power Line Information Exchange Systems with QoS Constraints", EURASIP Journal on Advances in Signal Processing, DOI: 10.1186/s13634-015-0265-3, accepted and to appear, Sep. 2015.

[2] X. Wu and Y. Rong, "Optimization for Relay-Assisted Broadband Power Line Communication Systems with QoS Requirements Under Time-varying Channel Conditions", AEÜ - International Journal of Electronics and Communications, submitted, Aug. 2015.

Conference Papers

[1] X. Wu and Y. Rong, "Optimal Power Allocation for Non-Regenerative Multicarrier Relay-Assisted PLC Systems with QoS Constraints", Proc. IEEE Int. Symposium Powerline Comm. Its Applications (ISPLC'2015), Austin, TX, USA, Mar. 29-Apr. 1, 2015.

[2] X. Wu and Y. Rong, "On the Location of Plug-In Relay Devices for Indoor Power Line Communication Environment", Proc. 8th Int. Conf. Signal Processing Communication Systems (ICSPCS'2014), Gold Coast, Australia, Dec. 15-17, 2014.

[3] X. Wu and Y. Rong, "Power Allocation for Relay-Assisted Indoor Power Line Communication Systems", The 7th Workshop on Power Line Communications,Bottrop, Germany, Sep. 11-12, 2014.

Contents

List of Figures

List of Tables

Chapter 1

Introduction

With the demand for communication and data sharing keeps increasing, various communication technologies have been developed. From the signal propagation medium of view, they can be cataloged in two broad groups, namely wired communication and wireless communication systems. Despite many obvious advantages of wireless communication, the most serious problem about wireless channel is its limited spectrum resource. For the wired systems, while equipping houses and neighborhoods with special signaling cables is expensive and time-consuming, power line communication (PLC) technology explores the "multi-use" of the preexisting and widespread power infrastructures to provide high speed networking capabilities. In other words, besides electricity delivery, power cables are used as the medium, at the meantime, to support high frequency (HF) signal transmissions.

However, as power cables are not manufactured for HF signal transmission purpose, PLC channels have demonstrated hostile characteristics for broadband communications. In summary [3], these hostile characteristics consist of (1) high attenuation in HF band; (2) frequency-selective fading in all available band; (3) time-varying property with different time scales; and (4) presence of considerable colored noise. Obviously, to overcome these disadvantages, advanced communication technologies need to be developed.

In this chapter, we first give an overview of PLC technology with its applications, general technical issues and some current standards. After this, some previous results of relay-assisted PLC systems have been reviewed. Finally, the organization of this thesis is presented.

Table 1.1: Classification of key PLC applications

	NARROW-BAND	BROADBAND
INDOOR	home automation	indoor high speed LAN
OUTDOOR	remote measurement and control	Internet access network

1.1 Overview of PLC

1.1.1 PLC applications

Power grids can be classified into three groups, namely the high voltage (HV) grid, medium voltage (MV) grid and low voltage (LV) grid. HV and MV power networks are usually properties of power suppliers and used for power transmission. At most of the time, power suppliers establish an accompany communication system, e.g. optical fiber system, when building the HV grid. Unless for special purposes, the application of PLC on HV grid is not necessary. On the other hand, the main motivations for PLC applications on MV grid are load management, e.g. ripple control, and to facilitate remote meter reading[4]. As the structure of MV grid is highly organized, the difficulties of deploying PLC are generally modest. Most current focuses have been put on the investigation of PLC on LV grids, which usually are used for power distribution and belong to communities or power users. As they have various structures, they are considered to be challenging communication channels.

Depending on the role it plays, PLC can be applied either as access networks (AN) or local area networks (LAN). Besides, with respect to the bandwidth occupied, PLC applications can also be classified as broadband PLC systems (BB-PLC) and narrow-band PLC systems (NB-PLC). For most of the case, PLC-based LAN is used for data-sharing and automation in houses or buildings, thus it is also called indoor PLC networks. While the others are classified as outdoor PLC systems. The most significant difference of the indoor environment, against the outdoor scenario, is its complex, heavily branched and irregular wiring topology. In this thesis, we focus on indoor PLC systems and its performance improvements. The above classification has been tabulated in Table 1.1, where red colored texts emphasize the focus of this thesis. Some currently available applications and one possible application in the future have been reviewed as follows.

Broadcasting over narrow-band PLC

Radio broadcasting over narrow-band PLC is widely used in European countries, such as Germany (supported by Drahtfunk), Switzerland (Telefonrundspruch), Norway (Linjesender) and some other countries[5]. In this case, radio program signals are injected into the public area LV power lines by special transformers.

In-vehicle networking

By using the battery supplied direct current (DC) power cable in aircraft and automotive, in-vehicle PLC provides the possibility to reduce the number of wires used for transmitting data, voice, music and video signals[6]. As all signals have been conducted on the preexisting power cables, the total weight of the cables becomes significant lighter. Note for some cases, e.g. the aircraft, the weight of networking cables is a critical concern[7].

Indoor networking

It is quite obvious that people can use the LV power network as a LAN for sharing data among computers and other peripheral equipment in the same residential house or commercial building. With multiple interconnected outlets preexisting in every room, indoor power lines have already formed a convenient network. By using this preexisting infrastructure, broadband network can be established without the need for expensive rewiring. Besides, since most of network devices need to obtain power from alternative current (AC) mains outlets, plugging a device into an outlet plays dual roles, i.e. enabling communication connection and power supply, at the same time.

Internet access network

The broadband PLC technology has also been used to deliver high speed Internet services from a local center. In this case, a computer equipped with a power line modem can obtain the Internet access through the local community LV power grid. This access-oriented application of PLC is also called broadband over power line (BPL).

Home automation

Essentially, home automation is a technology to monitor and/or remotely control "smart" electrical appliances in a house. For this reason, home automation is also called smart-home or intelligent-building. Besides the appliances need to be programming controllable, the key underlying technology is the communication system connecting these appliances. Considering usually the data rate of the information exchange between appliances is up to a few kbps, the narrow-band PLC provides a good solution.

Smart grid

With the emerging concept of smart grid, communication infrastructures used in the power grid have received much research interest recently. Compared with other communication systems, PLC technology has been considered as a competitive candidate for its unique advantage—the power cable itself is a part of the smart grid. In smart grid the power cables are used as medium, in addition to electricity delivery, to support information exchanges between appliances, power meters and/or transformers[8]. Just as the authors of [9] report, PLC is a "for the grid and through the grid" technology. At the mean time, some practical designs following this trend also appear. For example, the authors of [10] present a solution to remote detection of illegal electricity usage by using PLC, and in [11] the authors report that power quality can also be measured with PLC.

1.1.2 Technical challenges of PLC

As we mentioned, power distribution cables are not designed for data transmission. This fact poses several technical challenges for using these cables for high-speed data transmission.

Signal reflection, multipath fading and attenuation

Signal reflections happen whenever impedance mismatch occurs in an electric network. Besides, the equivalent impedance of a PLC signaling path can change significantly when electrical appliances are plugged in or unplugged from the grid. As a result, a power line channel is similar to a wireless channel from this aspect. The signal that arrives at the receiver is usually made up of several multipath components. Usually, multipath effects

become more severe for a long distance power line channel, as it is likely to consist of complex wiring topology[12].

On the other hand, PLC channels have highly frequency-selective attenuation. In other words, many deep notches present at certain frequencies and the attenuation can increase or decrease abruptly (up to 30 dB) within a small bandwidth.

Dependency on location of transceivers

The location of outlets, where PLC transceivers are deployed, can affect the communiaton quality significantly. For example, a receiver close to a noise source is likely to receive signals with low signal-to-noise ratio (SNR). Also, power grids are usually made up of cables with various lengths and types. These cables are connected together in a random fashion and terminated by loads with various impedance. Thus, channels between different outlet pairs in the same house often have quite different transfer functions. We will address this issue in detail in Chapter 4.

Time variation

PLC channels also present a time variation property. This is caused by the connected appliances and devices, which hold time-varying impedance. Due to this effect, the authors of [13] suggest that PLC channels can be represented as linear periodically time-varying (LPTV) systems, which are synchronized with the mains frequency.

Noise

The presence of noise in PLC channels is a significant problem for data transmission. These noises are generated from many different sources. Some typical noise sources are brush motors, fluorescent, halogen lamps, switching power supplies and dimmer switches. In addition to these, external interference, such as amateur radio transmission, can also decrease the system SNR at certain frequency ranges. We shall discuss this point in detail in the next chapter.

Table 1.2: Some current PLC standards in the market

IEEE P1675	standard for broadband over power line hardware installation and safety issues
IEEE P1775	electromagnetic compatibility (EMC) requirements and testing methods for PLC equipment
IEEE P1901	medium access control (MAC) and physical (PHY) layer specifications standard for broadband PLC
UPA Digital Home	inter-operable and coexisting PLC products
HomePlug 1.0	specification for connecting devices via indoor power lines
HomePlug AV	transmitting high-speed service, e.g. HDTV and VoIP , around the home
HomePlug AV2	follow IEEE 1901 standard and features gigabit-class PHY-rate, support for MIMO PHY and power saving modes
HomePlug BPL	assess network specification for "to-the-home" connection1
Homeplug CC	a low-speed, very low-cost specification for home automation

Compatibility regulation

Beside the above issues, government regulations usually forbid using PLC on certain frequency bands to avoid electromagnetic interference (EMI) to other radio systems. Therefore, practical frequency bands for PLC systems are not continuous.

1.1.3 PLC standards

For any modern communication technology, standardization plays a critical role. Currently, several competing organizations make their standards evolving. These organizations include HomePlug Powerline Alliance (HPPA), Universal Powerline Association (UPA), European Telecommunications Standards Institute (ETSI), Open PLC European Research Alliance (OPERA) and Institute of Electrical and Electronics Engineers (IEEE). A brief scanning of some current standards in the market is given in Table 1.2.

As this thesis focuses on physical (PHY) layer of the indoor broadband PLC system, we also give a brief summary of the PHY specification of HomgPlug AV[14] as a reference for later simulations.

(1) An up to 200 Mbps PHY layer rate is provided via using orthogonal frequency-division multiplexing (OFDM), where 1024 subcarriers are equally spaced in the frequency band between 2MHz and 28MHz.

(2) Turbo coding with varying code rates is employed to gain immunization to noisy environments.

(3) Coherent modulation is supported.

(4) Channel adaption is achieved by using AC mains period synchronization and variable bit-loading.

(5) Several robust modes of operation are provided for the communication of network synchronization information.

1.2 Relay-assisted PLC systems

There are certain similarities between PLC and wireless transmission characteristics, e.g. the frequency-selective nature of the propagation channel, as we mentioned earlier. Thus, many signal processing techniques, which originally have been developed for wireless communication systems, can be adopted into PLC, such as compressed sensing[15] and cognitive radio[16].

Recently, diversity techniques have attracted much research interest in PLC. Considering indoor power grid cables usually consist of three conductors, namely Line, Neutral, and Ground lines, every two of them can be seen as an independent port, i.e. sub-channel, so that a low diversity order multiple-input multiple-output (MIMO) system can be realized if all three conductors are used at the same time[17, 18]. Obviously, this strategy is constrained by the number of the available conductors.

From another aspect, restricted to one single pair of signal transmission cables, the idea of cooperative communication can be adapted into the indoor PLC environment, usually by plugging relay devices into the outlets located between the transceivers. Due to the similar broadcasting nature between the wireless signal propagation and the power-cable guided signal transmission, relay-assisted communication schemes can be readily introduced into PLC systems.

However, as is pointed out in [19] that we should pay careful attention to the difference of the relay-involved PLC channel from its wireless peer. In wireless relaying channels, the source-to-destination, source-to-relay and relay-to-destination signaling paths can be treated

as independent to each other. On the other hand, in PLC environment these paths are highly correlated, as they share the same power cable grid all the time.

Furthermore, under wireless environment the introduction of relay node does not influence the characteristics of the direct path, given the distance between the transceivers is much larger than the size of relay devices. However, this conclusion does not hold for the PLC case as the appearance of impedance of the relay devices affects the matching state of the whole network. We refer to this situation as the relay-involved PLC channel and will discuss this issue in detail in Chapter 3.

Some publications concerning relaying techniques in PLC are summarized as follows. In [20], the author described a relay-assisted PLC system based on single-frequency networking condition. The authors of [2] have investigated the optimal time-slot duration allocation between the direct transmission phase and the relay phase, when there is only one relay node. With an opportunistic decode-and-forward (ODF) proposal, the authors of [21] discussed power saving issue of indoor PLC. This proposal has been generalized to both DF and amplify-and-forward (AF) relay modes in [22], and the authors demonstrated its benefits on rate improvement as well. Under the assumption that each outlet on the power grid is a potential relay node, the authors of [23] proposed a multihop transmission scheme combined with the application of distributed space-time block code (DSTBC) in PLC networks. From another angle of analysis, authors of [24] and [15] considered cooperative multihop relaying and cooperative coding, respectively.

1.3 Thesis organization

This thesis is organized as follows.

After this introduction chapter, Chapter 2 prepares the fundamental knowledge about the indoor PLC environment, in which the indoor power grid topology, indoor point-to-point (P2P) PLC channel models, noise analysis and modeling and the basic relay processing methods have been addressed.

Chapter 3 plays an important role. A basic method for the relay-involved PLC channel modeling is proposed. Besides, we present a simple approach, which is based on a verified P2P PLC channel model, to simulate the relay-involved PLC channel.

Chapter 4 focuses on the location selection for the relay devices under a practical indoor grid topology. Criteria and suggestion are given.

The problem of joint optimization of relay and source power allocations has been proposed in Chapter 5. To solve this highly non-convex problem, an alternative optimization (AO) approach has been adapted. Analysis and simulation show benefits of the proposed relay scheme. Chapter 6 introduces a simple form of network coding into indoor PLC systems. Its power saving property has been explored by using the AO algorithm. Based on this, Chapter 7 takes a further step and considers the performance improvement from both network coding and space-time coding (STC) at the same time. Simulation results are given to demonstrate the efficiency of this combined technology.

Finally, we conclude this thesis in Chapter 8 and give out some interesting topics for future research.

The structure of the thesis is summarized in Fig. 1.1.

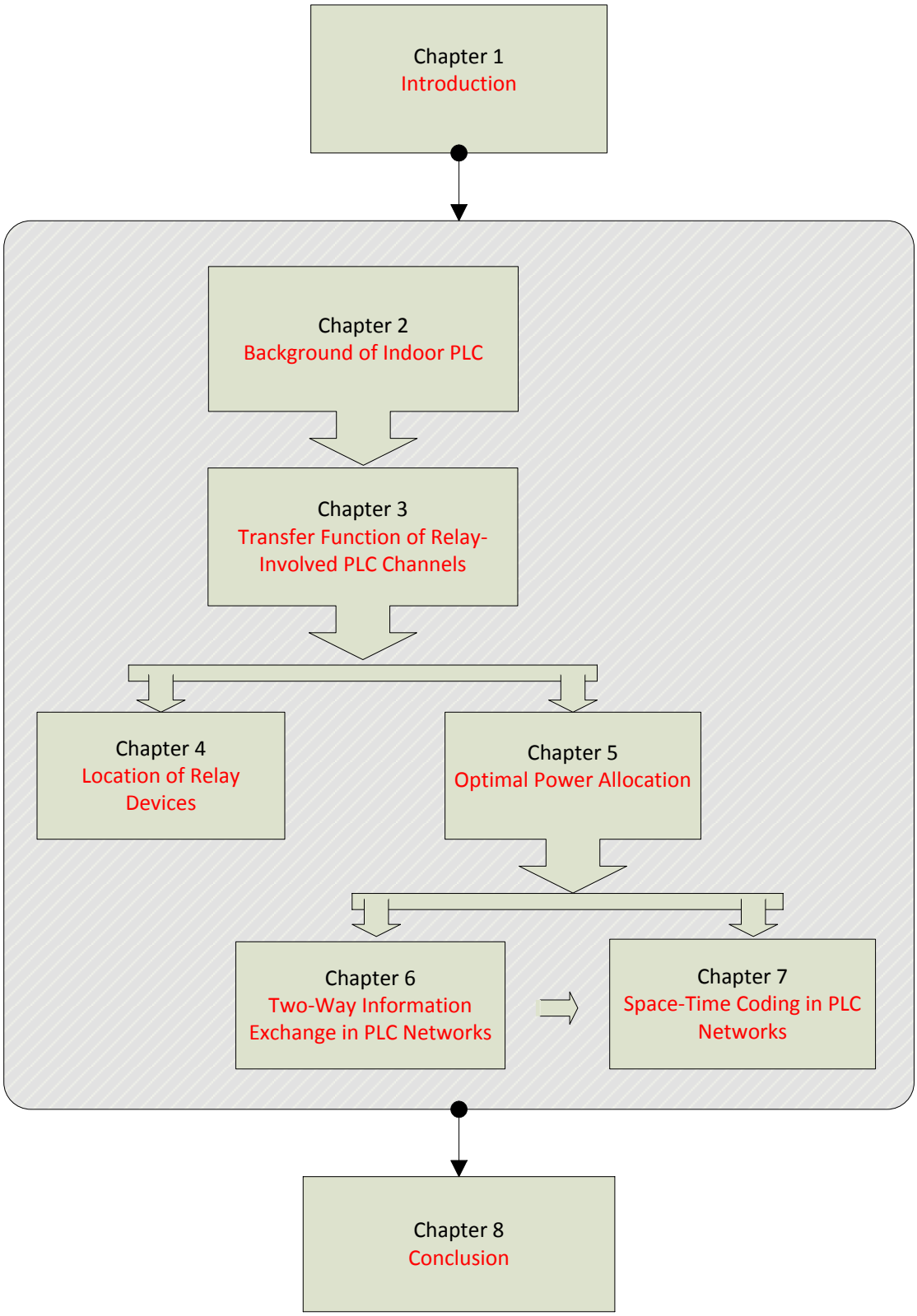

Figure 1.1: Thesis structure.

Chapter 2

Background of Indoor PLC

This chapter serves the purpose of establishing the fundamental knowledge about the indoor PLC environment. This knowledge is a start point for all topics discussed in this thesis. In Section 2.1, the indoor power grid topology is analyzed and this allows us to understand how the relay nodes can be practically implemented in the indoor power grid. Considering the cabling implementation practice varies from house to house, a statistical indoor topology model is mentioned. Following this, the point-to-point (P2P) PLC channel models published in the literature are reviewed in Section 2.2. Although these channel models cannot be directly applied for the relay-involved PLC network (as we shall see this in Chapter 3), they provide the basics to allow us to take a further step. Noise analysis and modeling are discussed in Section 2.3. Beside giving the different types of noise detected on the PLC channel, we also describe a well-recognized noise model. In Section 2.4, we discuss two basic relay processing methods, namely amplify-and-forward (AF) and decode-and-forward (DF), used in most of the relay devices.

2.1 Indoor power grid topology

Although the indoor power grid topology changes with the structure of different houses and user's preference, it is reported in [1] that observation of common wiring practices and norms reveals a regular wiring deployment existing. A typical example has been given in Fig. 2.1, where a two-layer structure can be observed. The lower layer consists of a collection of outlets in different rooms, which are associated with one derivation box, while

the higher layer is constructed by connecting these derivation boxes to the main panel of the house. Note usually the cables used for different layer, even sometimes within the same layer, have different types according to certain power delivery capacity requirements.

By ignoring some non-electrical properties, we can simplify this cabling structure as given in Fig. 2.2, which allows us to understand how a relay-assisted PLC system can be practically implemented. Under this arrangement, every pair of outlets can be employed as a P2P communication system and the corresponding channel are characterized by the wiring topology and load impedance between this outlet pair. For example, in Fig. 2.2, we can choose outlet T_1 and T_2 to implement the transceiver pair and refer to the shortest wring between them as the backbone path and its length as the channel length. Other wirings are treated as tap-brunches[1] attached to the backbone, which contribute to the multipath nature of the channel. The outlets located on this backbone (e.g. R_2) or on a branch of this backbone (e.g. R_1) can be deployed with plug-in relay devices, which we refer to as the relay nodes.

The authors of [1] suggest that this whole topology can be divided into a group of clusters. Each cluster contains a derivation box and the outlets connected it. Furthermore, these clusters usually have rectangular shapes with certain statistical characteristics. Based on these observations, they proposed a statistical topology model which classifies various clusters into three common structure types, namely scattering structure, star structure and bus structure. These common structures are given in Fig. 2.3. For each common structure type, statistical distribution has been examined to its parameters, such as the number of cables, cable length, cable type and so on, thus random indoor grid topologies can be generated from this model.

2.2 Channel modeling

In practice not only the power grid deployment practice varies in different parts of the world, even in a particular network the selection of outlets to connect transceivers has a strong influence on the final channel response characteristics. These factors make a generally accepted channel model not available. On the other hand, design of advanced PLC systems requires the knowledge of the channel characteristics and using of verified models. Currently, several PLC channel simulation models exist. Depending on their modeling approaches, these models can be classified into three groups as given in Table 2.1.

[1] We will also refer to it shortly as branches.

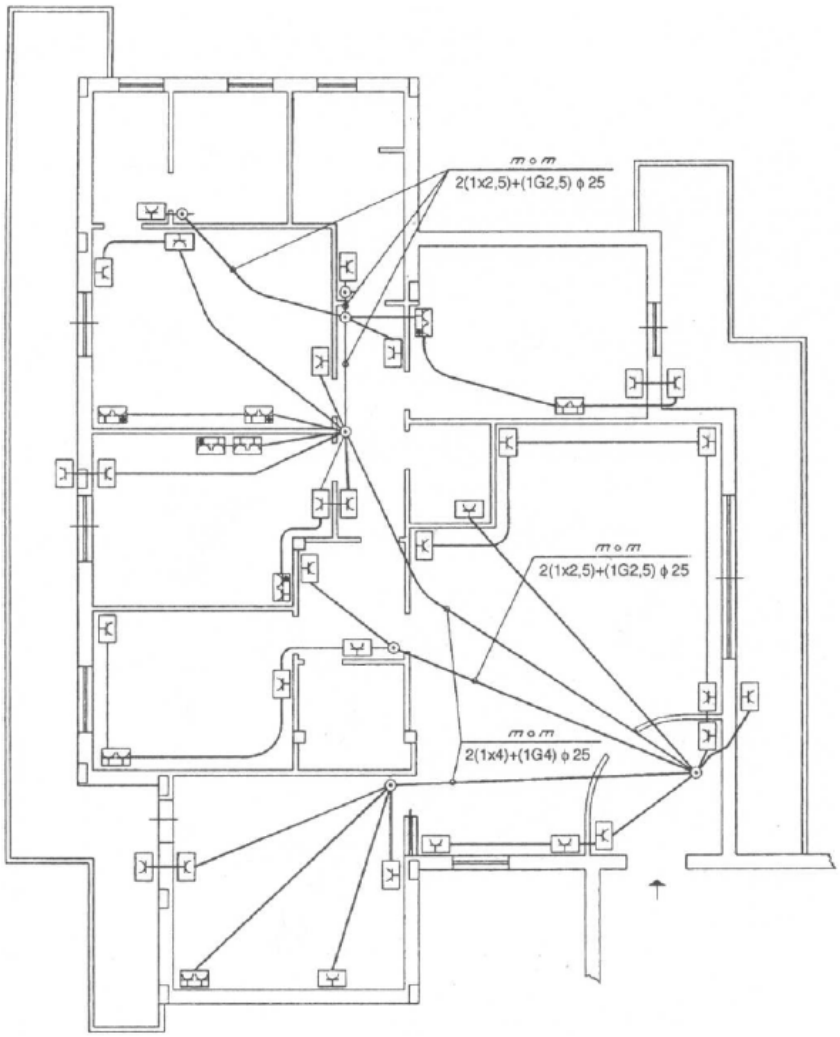

Figure 2.1: A real wiring topology of power grid in a house[1].

Table 2.1: Overview of PLC channel models with key references

	BOTTOM-UP	TOP-DOWN
DETERMINISTIC	[17, 25, 26]	N/A
STATISTICAL	[1, 27]	[12, 28–30]

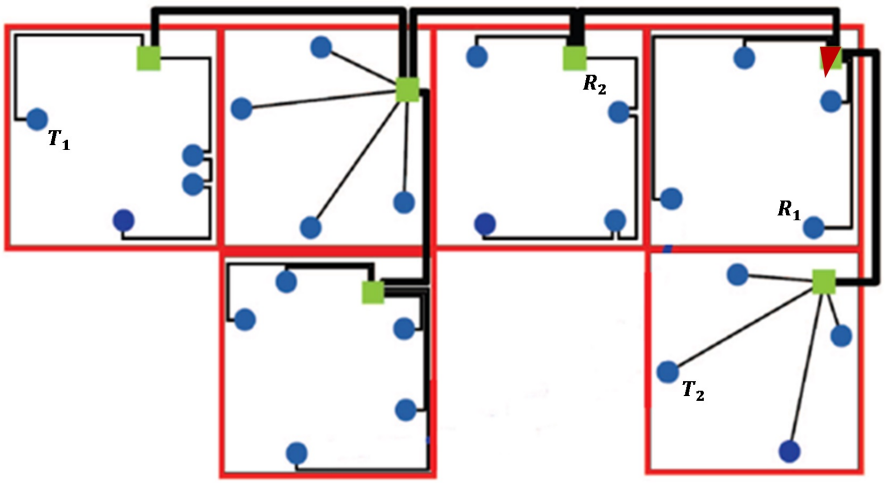

Figure 2.2: A simplified wiring topology of power grid in a house, showing main panel (triangle), derivation boxes (squares) and outlets (dots)[2].

From Table 2.1 we can see that the statistical approach can be implemented following either the top-down or bottom-up sequence. The top-down approach characterizes the external behavior characteristics of PLC networks and use a set of high-level parameters to describe the channel. Note this approach has been used extensively for the modeling of radio propagation channels. In this model group, the parameter values are usually derived from the statistical analysis based on extensive measurement campaigns. Specifically, this approach can be done either in the time domain[30] or in the frequency domain[12]. Despite the difficulty of setting a large number of test loops with selection of physical characteristics and configurations, its results lack connections with the physical topology.

From another angle of view, the bottom-up approach starts from a physical model and derives a group of low-level parameters to represent a particular indoor PLC channel. Note this approach was successfully applied in the digital subscriber line (DSL) channel model. It ensures a strong connection with physical structures. Usually, by using the ABCD matrix method, the signal propagation characteristics can be tackled in the frequency domain. However, for indoor PLC channels, it is a hard task to define a fixed structural model which can represent the various physical network behaviors. Recently, with a statistical indoor grid topology generator, the authors of [31] presented a random channel simulator following the bottom-up approach, although the calculations involved in this method are extensive.

As a trade-off between the above mentioned two approaches, the authors of [32] proposed

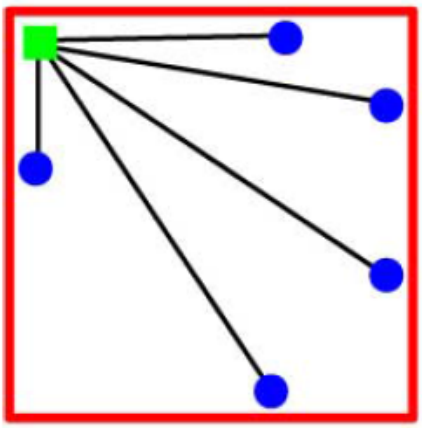

(a) scattering structure

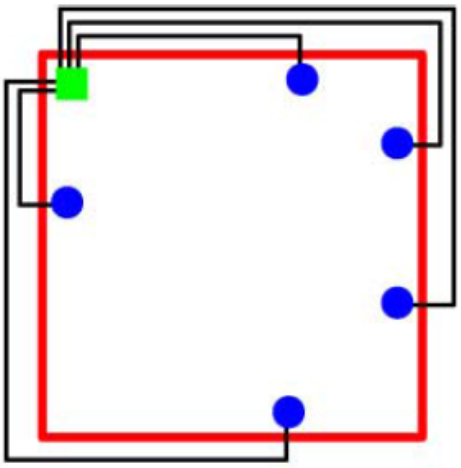

(b) star structure

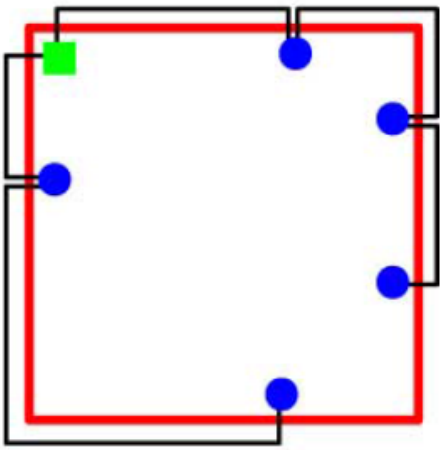

(c) bus structure

Figure 2.3: Three common cluster structures[1].

a hybrid model. This model provides physics-oriented channel simulations by setting values to a simplified network structure. In addition, statistical distributions for the low-level parameters of this structure are suggested so that generation of random channels is also allowed. The authors also reported that the validity of the generated channels from this model is assessed by comparing their behavior with measurements.

In addition, as reported in [13] that the indoor PLC channel has a time-varying nature, and a more accurate representation for it should be a linear periodical time-varying (LPTV) system, rather than a linear time-invariant (LTI) system. An example response of this LPTV channel is shown in Fig. 2.4, where its frequency response gain varies over a main period[2]. From Fig. 2.4 we can see that in addition to the gradual variation of the channel gain along with the mains period, some rapid transitions also happen.

Let us define the period of one signal being transmitted from one node to another node as a signaling phase. Then, considering the relative long coherent time of these LPTV channels, i.e. around $600\mu s$[32], we can reasonably treat the P2P PLC channel as quasi-stationary, namely the channel parameters do not change whithin one signaling phase. However, if a relay scheme has been applied, then more than one signaling phase need to be considered. In other words, the relay-involved PLC channel state changes over different signaling phases. We shall discuss this point in detail in Chapter 3.

It is worth to mention that above mentioned channel models are built for P2P communications. The relay-involved PLC channel modeling problem is not addressed very often in the literature. In this thesis, this problem will be addressed. As we use Canate's hybrid P2P channel model as a basic tool for our research[32–34], some details about this model are given as follows.

Network structure

The simplified network layout of this model is given in Fig. 2.5. It consists of seven segments, i.e. four sections on the backbone between transceivers, three branches terminated with loading impedance (Z_1, Z_2 and Z_3).

[2]In Australia, the mains frequency for household application is 50Hz.

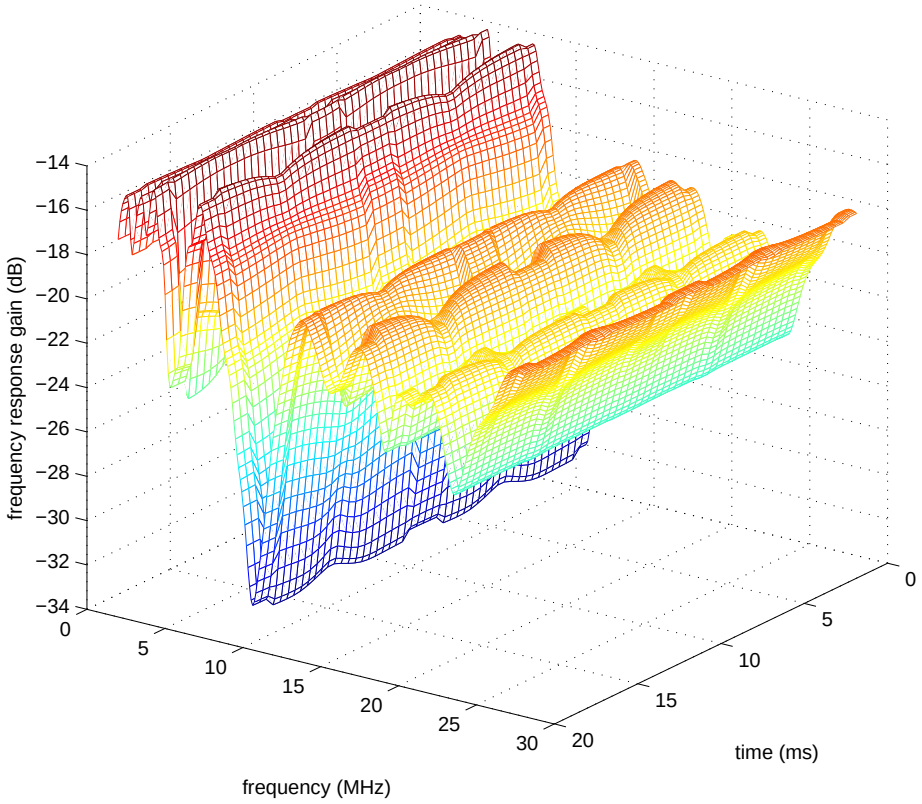

Figure 2.4: Frequency response of an LPTV channel.

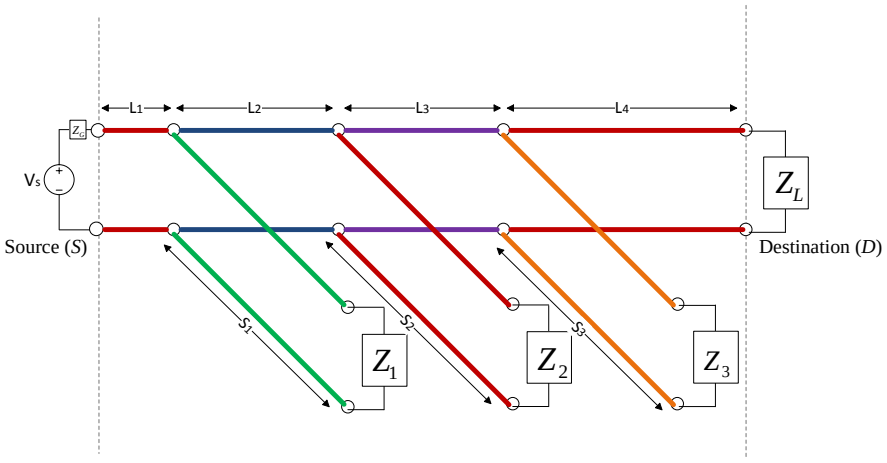

Figure 2.5: Network topology of Canate's channel model.

Table 2.2: Characteristic data of indoor power cables

Cable type index	1	2	3	4	5
section (mm^2)	1.5	2.5	4	6	10
ε_{eq}	1.45	1.52	1.56	1.73	2
$Z_0(\Omega)$	270	234	209	178	143
$C(pF/m)$	15	17.5	20	25	33
$L(\mu H/m)$	1.08	0.96	0.87	0.78	0.68
R_0	12	9.34	7.55	6.25	4.98
G_0	30.9	34.7	38.4	42.5	49.3
$R = R_0 10^{-5}\sqrt{f}(\Omega/\mathrm{m})$			$G = 5G_0 10^{-14} 2\pi f$		

Cables

Each segment includes a power cable pair. In addition to its length, this cable pair is chartered by its type, which in turn depends on its manufacture parameters. Five most commonly used cables with their characteristic data are given in Table 2.2, where ε_{eq}, Z_0 are the relative permittivity of the phase-screen insulator material and characteristic impedance, while C, L, R, G are the capacitance, inductance, resistance and conductance per-unit-length. Besides, with these characteristic data it is easy to calculate the cable's propagation constant γ.

Loads

The three loads in this P2P model can behavior in three states, namely: (1) constant impedance; (2) time-invariant but frequency-selective impedance; and (3) time-varying and frequency-selective impedance. For simplicity, in this thesis we only consider the first two cases[3].

This topology along with its loading information can be summarized in Table 2.3. Using transmission line theory with the information in Table 2.3, the frequency response of a P2P indoor PLC channel between the transceivers can be calculated. An example generated from this model, under the time-invariant configuration, are given in Fig. 2.6.

[3]In other words, we consider each P2P channel in each signaling phase is time-invariant. Note this does not indicate that the relay-involved channel, which consists of more than one P2P path and involves more than one signaling phase, is also time-invariant. Actually as we shall see in Chapter 3, the changing of the impedance of relay devices over different signaling phases result in a time-varying relaying channel.

Table 2.3: Parameters for the Canate's PLC channel model

line section name	length	cable type	terminated load
backbone 1	L_1	n_{L1}	*N/A*
branch-tap 1	S_1	n_{S1}	Z_1
backbone 2	L_2	n_{L2}	*N/A*
branch-tap 2	S_2	n_{S2}	Z_2
backbone 3	L_3	n_{L3}	*N/A*
branch-tap 3	S_3	n_{S3}	Z_3
backbone 4	L_4	n_{L4}	*N/A*
Transmitting inner impedance:			Z_G
Receiving load impedance:			Z_L

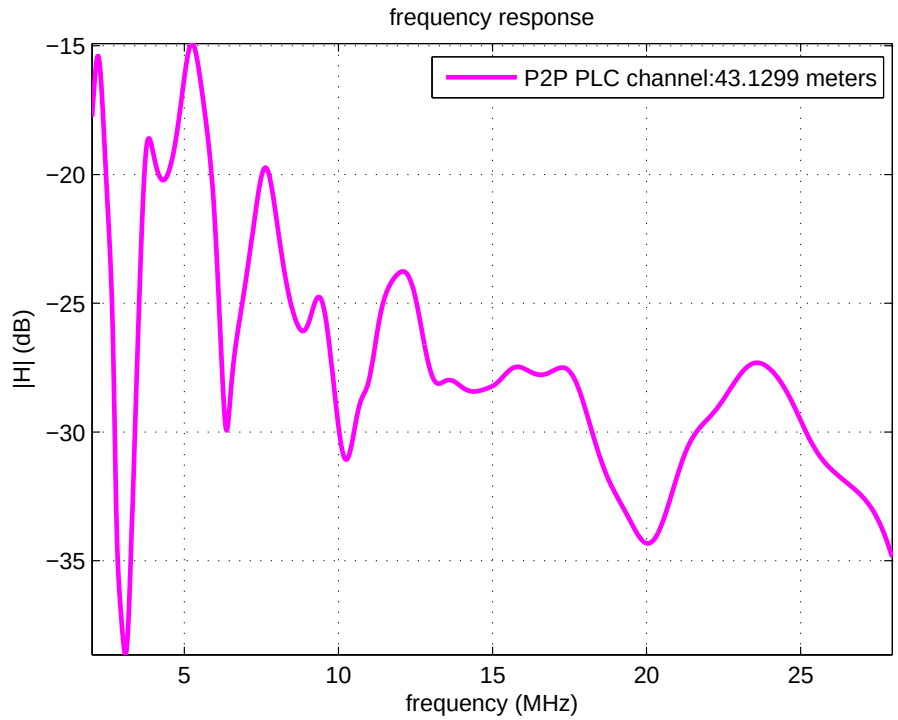

Figure 2.6: An example of time-invariant channel response.

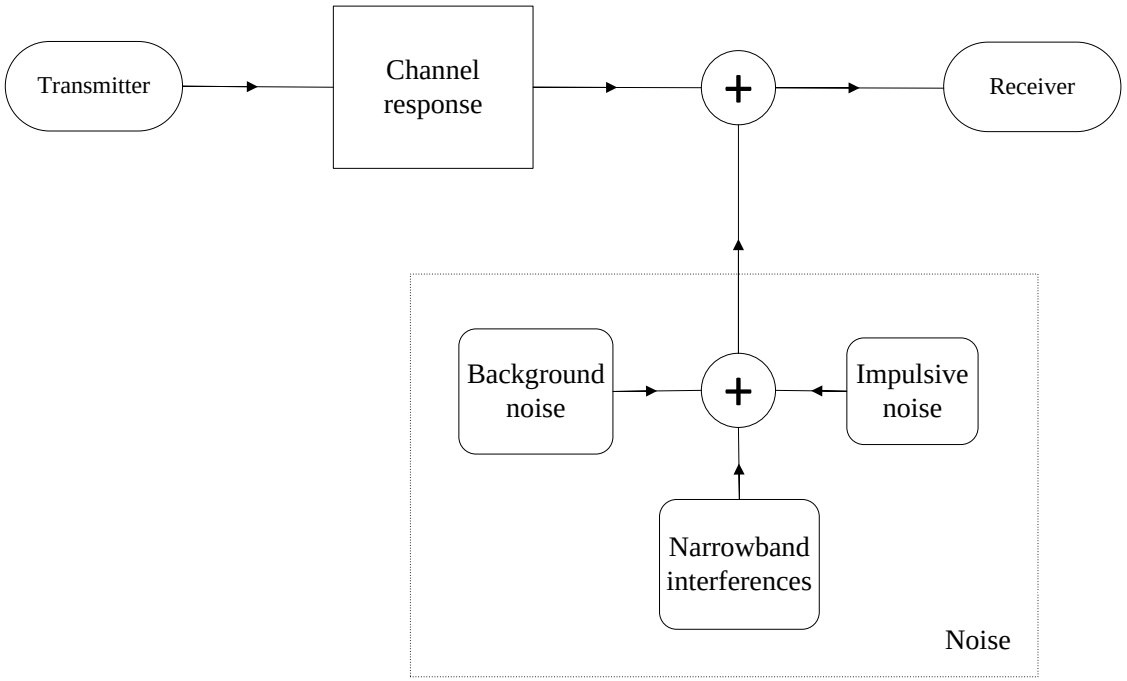

Figure 2.7: Categories of PLC noise.

2.3 Noise analysis and modeling

Noise in PLC is complicated due to the presence of different source of disturbance. According to [35], generally they can be classified into two board categories, namely the general background noise (GBN) and the impulsive noise. The former in turn consists of two classes, i.e. colored background noise and narrow-band interference. This is illustrated in Fig 2.7. The background noise is the sum effect caused from several low power noise sources, e.g. residential electronic equipment, and its power spectral density (PSD) decreases when the frequency becomes higher. The narrow-band interference is introduced by medium and short wave broadcasts. In common, the GBN often has a stable PSD over seconds, minutes and even hours. In [36] the authors reported that the noise's PSD is not white, but in any narrow band its probability density function (PDF) can be approximated as Gaussian.

On the other hand, the impulse noise may change rapidly within microseconds and milliseconds. According to their different characteristics, they also can be divided into three groups, i.e. the periodic impulsive noise synchronized with the mains frequency, the asynchronously periodic impulsive noise and the aperiodic impulsive noise. The periodic impulsive noise

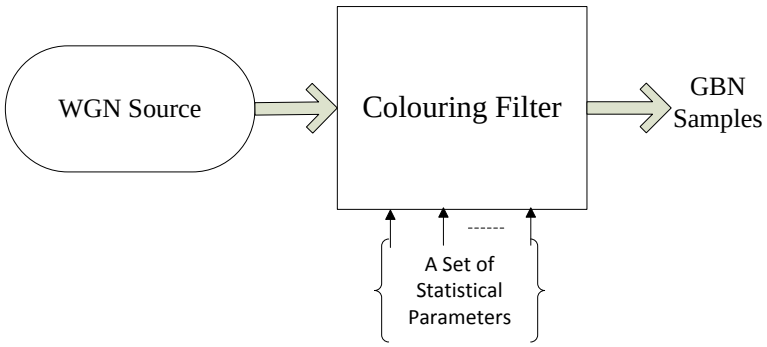

Figure 2.8: Synthesis diagram of Benyousef's noise model.

is commonly generated by silicon controlled rectifiers (SCR) when power supplies and this leads to its synchronization with the mains frequency. Conversely, as is caused by switching power supplies, e.g. low-energy lamps, the asynchronously periodic impulsive noise shows repetition rates which are independent from the mains power cycles. The aperiodic impulsive noise is with a sporadic nature and mainly caused when connection or disconnection of electrical devices happens in the power grid.

The impulsive noise can be modeled with random process, in which statistical distributions of amplitude, inter-arrival time and duration need to be examined. On the amplitude aspect, Middleton's classified noise models have often been used [37]. While for the temporal characteristics, Markov chains are suitable mathematical models[35]. As there is still no generally accepted impulsive noise model available, in this thesis we only consider the impact of the GBN, so that we can reasonably assume that the noise PSD is stationary over a relatively long period.

Based on extensive measurements, Benyousef in [38] proposes a synthesis process where a White Gaussian noise (WGN) is passed through a colored filter. Thus as long as a statistical transfer function of the colored filter is identified, it is easy to approximate the GBN as a stationary process. The diagram of this noise synthesis approach is shown in Fig. 2.8. As we use Benyousef's noise model to generate noise samples for testing our relay schemes in this thesis, some details of this model are given as follows.

The principle of modeling the GBN is the superposition of background noise and the narrowband interference. Each of these two components requires the coloring filter to synthesize a suitably statistical PSD function independently. If we use f to denote the frequency, then

Table 2.4: PDF of the parameters for background noise approximation

PARAMETER	N_0	N_1	f_1
UNIT	dBm/Hz	dBm/Hz	MHz
DISTRIBUTION	Normal	Uniform	Shifted Exponential
	$\sigma_{N_0} = 1.29$	$a_{N_1} = 23.06$	$\lambda_{f_1} = 1.3$
	$\mu_{N_0} = -135$	$b_{N_0} = 74.97$	$f_{shift} = 0.096$

mathematically we can express this as

$$S_G(f) = S_B(f) + \sum_{k=1}^{N} S_I^{(k)}(f) \tag{2.1}$$

where $S_G(f)$ is the required PSD for the GBN, while $S_B(f)$ and $S_I^{(k)}(f)$ are the background noise PSD and the PSD of the kth narrow-band interference.

Background noise

The extensive measurements show that the PSD of background noise can be approximated by a first-order exponential function, i.e.

$$S_B(f) = N_0 + N_1 e^{-\frac{f}{f_1}} \tag{2.2}$$

where N_0, N_1 and f_1 are the statistical parameters of the exponential function. Table 2.4 gives the PDF of these three parameters under office building scenario.

Narrow-band interference

For the kth (out of N) independent narrow-band interference, a Gaussian function can be used to model its PSD as

$$S_I^{(k)}(f) = A^{(k)} \exp\left[-\frac{\left(f - f_0^{(k)}\right)^2}{2\left(B^{(k)}\right)^2} \right] \tag{2.3}$$

Table 2.5: PDF of the parameters for interference generation

PARAMETER	N	$B^{(k)}$	$A^{(k)}$
UNIT		MHZ	dBm/Hz
DISTRIBUTION	Normal	Shifted Exponential	Normal
$f \in$(0,30MHz)	$\sigma_N = 12$ $\mu_N = 1.4$	$\lambda_{B^{(k)}} = 0.33$ $B_{shift} = 0.19$	$\sigma_{A^{(k)}} = 16.6$ $\mu_{A^{(k)}} = 4.8$

where three parameters, $A^{(k)}$, $B^{(k)}$ and $f_0^{(k)}$ and the total number of interference N follow the distributions given in Table 2.5 for the office building scenario.

Substituting (2.2) and (2.3) into (2.1), the sum PSD used for the coloring filter to generate the GBN samples can be written as

$$S_G(f) = N_0 + N_1 e^{-\frac{f}{f_1}} + \sum_{k=1}^{N} A^{(k)} \exp\left[-\frac{\left(f - f_0^{(k)}\right)^2}{2\left(B^{(k)}\right)^2} \right]. \tag{2.4}$$

An example of the GBN generated by this model is given in Fig. 2.9. We mention that generally the noise PSD depends on the location of the outlet, e.g. an outlet near a noise-generating appliance usually has a stronger PSD than the one which is located further away from that appliance.

2.4 Signal processing at relay nodes

Depending on the signal processing method used at relay nodes, relay-assisted transmission systems work in two modes, namely regenerative and non-regenerative modes. In the regenerative mode, the relay node first decodes the received signal and then re-encodes and forwards it to the destination node. This process is also called decode-and-forward (DF) relaying. Depending on whether an error correction coding (ECC) is used in the DF process, the relay node can work in two different ways. Firstly, the relay node can simply keep working in each transmission round, without caring the quality of its received signal.

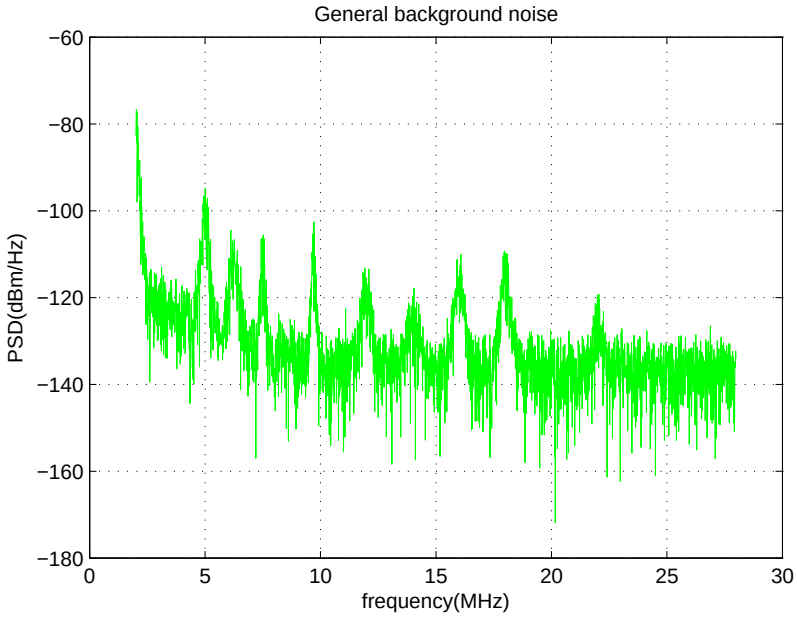

(a) PSD

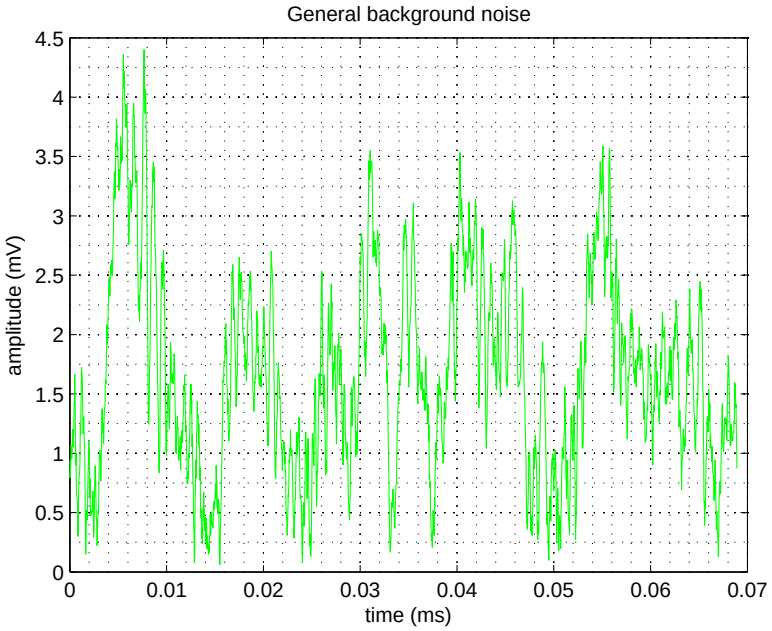

(b) waveform

Figure 2.9: Example of generated GBN.

However, when the received signal has a very low signal-to-noise ratio (SNR), the relatively complex DF processing cannot make positive contributions to the system performance. As an improved way, the DF relay node can also work in an opportunistic manner. For example, with a cyclic redundancy check (CRC) coding, the relay node only forwards signal when it is sure that the revived signal is successfully decoded. This idea has been discussed in [21, 22].

On the other hand, despite a relatively inferior performance, the non-regenerative scheme only requires the relay node to amplify-and-forward (AF) its received signal, thus it has lower complexity, shorter processing delay and lower implementation cost. In this thesis, we focus on a serial of relay schemes, where the relay nodes work in the AF mode.

2.5 Chapter summary

In this chapter we reviewed the background information of the indoor PLC system, namely the wiring topology, channel modeling and noise approximation. In particular, we examined Canate's hybrid channel model and Benyousef's GBN model. These two models act as a toolkit for our research starting from the next chapter. As our interest in this thesis is concerned about the PHY layer of indoor PLC systems, we skipped reviews about the medium access control (MAC) protocols and standards which are applied for indoor PLC.

Chapter 3

Transfer Function of Relay-Involved PLC Channel

The emerging cooperative communication technology has attracted a lot of research attention in the wireless communication society. However, this idea can also be adapted into the indoor PLC environment, usually by plugging relay devices into the outlets which located between the transceivers. The first attempt of evaluating this idea has been done in [2], where the authors considered the possible locations in a house where the relay device can be introduced practically. Due to the similar broadcasting nature between the wireless signal propagation and the power-cable guided signal transmission, the three-node relay system (which consists a source node S, a destination node D and a relay node R) can be readily introduced into PLC systems. However, there are some notable difference between PLC relay channels and the wireless relay case.

In wireless channel, the source-to-destination path H_{SD}, source-to-relay path H_{SR} and relay-to-destination path H_{RD} can be treated as independent to each other, and they usually share the same channel model. Furthermore, under wireless environment, the introduction of relay node will not influence the characteristics of the direct path considering the distance between the transceivers are much larger than the size of the relay device.

On the other hand, in PLC environment three signaling paths H_{SD}, H_{SR} and H_{RD} are highly correlated, as they share the same power cable grid all the time. Furthermore, in the PLC scenario the appearance of the relay device (and its impedance) will influence all the three channel paths. In other words, if we indicate the channel transfer function (CTF) of the three paths as $H_{SD}(f)$, $H_{SR}(f)$ and $H_{RD}(f)$ *before* the relay node is introduced, while use $\tilde{H}_{SD}(f)$,

$\tilde{H}_{SR}(f)$ and $\tilde{H}_{RD}(f)$ to denote the CTF of the corresponding paths *after* the introduction of the relay node, we can express, in general, that

$$\tilde{H}_{SD}(f) \neq H_{SD}(f) \tag{3.1}$$

$$\tilde{H}_{SR}(f) \neq H_{SR}(f) \tag{3.2}$$

$$\tilde{H}_{RD}(f) \neq H_{RD}(f) \tag{3.3}$$

where f means the frequency.

We refer to this situation as the relay-involved PLC channel condition, which was firstly mentioned in [19], however has not been discussed in detail in the literature. In this chapter, we will fill this gap. By addressing this issue, we will develop a basic method for the relay-involved PLC channel generation, which will be used for simulations in this thesis. The reminder of this chapter is organized as follows. In Section 3.1, we introduce the CTF computation of a point-to-point (P2P) PLC channel, using the chain matrix theory (ABCD mothod), which is a classical analysis method for the distributive parameter circuits modeling. Based on this, in Section 3.2 we introduce the relay node into the P2P channel model, and derive its CTF expression. Rather than rebuilding a new CTF simulation model from scratch, Section 3.3 shows that how we can strategically reuse a well verified P2P PLC channel model to simulate the relay-involved PLC channel conditions. Lastly, Section 3.4 concludes this chapter.

3.1 CTF for P2P PLC channel

Let us start with the basic CTF computation by using the chain matrix theory [39], which is also called the ABCD method. Based on this method, we will firstly consider the different situations occurred in PLC systems, and then show how to compute the CTF in general.

3.1.1 ABCD matrix

The ABCD representation for any two-port circuit is very useful for the calculation of the CTF of PLC. A general representation of a P2P PLC network in ABCD method is shown in Fig. 3.1, where the ideal voltage source V_s cascades its corresponding inner impedance Z_s to build the information source S, while the load impedance Z_L represents the receiver D.

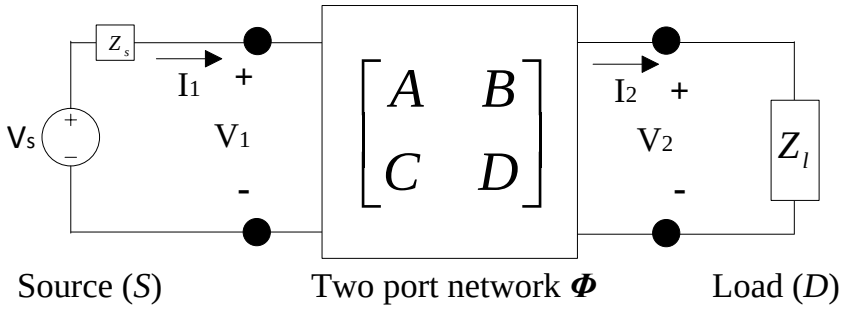

Figure 3.1: A P2P PLC system represented by a two-port network.

The PLC network Φ, in the middle, is represented by the two-port network ABCD model. In the two-port network, the V_1 (input voltage), I_1 (input current), V_2 (output voltage), and I_2 (out current) in general hold the relations as

$$\begin{bmatrix} V_1 \\ I_1 \end{bmatrix} = \begin{bmatrix} A & B \\ C & D \end{bmatrix} \begin{bmatrix} V_2 \\ I_2 \end{bmatrix} \tag{3.4}$$

where A, B, C, and D are appropriately chosen constants, which only depend on the inner topology and components of the two-port network and are not influenced by the outside associated circuits.

It is easy to show that if we have a cascade of two-port circuits, as shown in Fig. 3.2, the ABCD representation of this cascaded circuit is the matrix multiplication of the ABCD matrices for the two individual two-port circuits, i.e.

$$\begin{bmatrix} A_0 & B_0 \\ C_0 & D_0 \end{bmatrix} = \begin{bmatrix} A_1 & B_1 \\ C_1 & D_1 \end{bmatrix} \begin{bmatrix} A_2 & B_2 \\ C_2 & D_2 \end{bmatrix}. \tag{3.5}$$

To ease our following discussion, we give out some frequently used circuit components and its corresponding ABCD representations.

(1) A transmitter/ information source: a transmitter consisting of an ideal voltage source V_s and a source inner impedance Z_s shown in Fig. 3.3a can be represented by matrix

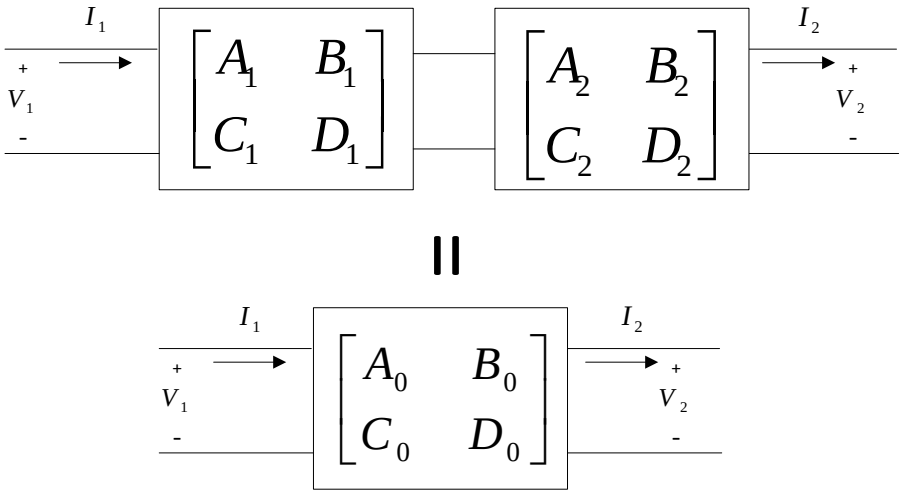

Figure 3.2: A cascade consists of two two-port networks and its multiplication equivalence.

$$\begin{aligned} \Phi_S &= \begin{bmatrix} A & B \\ C & D \end{bmatrix} \\ &= \begin{bmatrix} 1 & Z_s \\ 0 & 1 \end{bmatrix}. \end{aligned} \tag{3.6}$$

(2) A general impedance: impedance Z shown in Fig. 3.3b can be represented by matrix

$$\begin{aligned} \Phi_Z &= \begin{bmatrix} A & B \\ C & D \end{bmatrix} \\ &= \begin{bmatrix} 1 & 0 \\ Z & 1 \end{bmatrix}. \end{aligned} \tag{3.7}$$

(3) Paired power cable: two parallel cables, for example the Line phase and Neutral cables, as shown in Fig. 3.3c can be modeled as a transmission line, which can then be characterized by its characteristic impedance Z_c, and its propagation constant γ [40]. By measuring the per-unit-length parameters of a cable, it is easy to calculate the characteristic impedance and

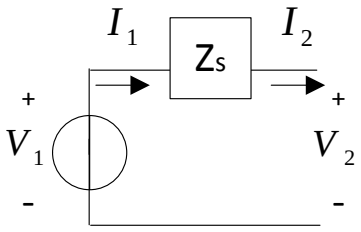

(a) Transmitter

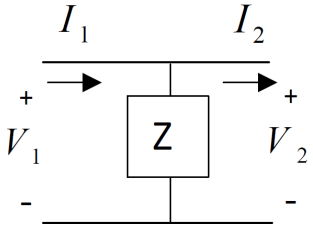

(b) Impedance

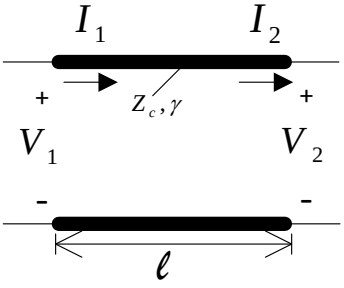

(c) Paired power cable

Figure 3.3: ABCD representation of common components of circuit.

propagation constant of the cable with the following equations

$$Z_c(f) = \sqrt{\frac{R + j2\pi fL}{G + j2\pi fC}} \tag{3.8}$$

$$\gamma(f) = \sqrt{(R + j2\pi fL)(G + j2\pi fC)} \tag{3.9}$$

where R, L, G, and C are the per-unit-length resistance (Ω/m), inductance (H/m), conductance (S/m) and capacitance (F/m), respectively. And f denotes frequency (in Hz)[1]. Thus the ABCD matrix for a paired power cable with characteristic impedance Z_c and propagation constant γ with its length l can be calculated as

$$\begin{aligned} \Phi_C &= \begin{bmatrix} A & B \\ C & D \end{bmatrix} \\ &= \begin{bmatrix} \cosh(\gamma l) & Z_c \sinh(\gamma l) \\ \frac{1}{Z_c}\sinh(\gamma l) & \cosh(\gamma l) \end{bmatrix}. \end{aligned} \tag{3.10}$$

3.1.2 Equivalent input impedance

For any two part network, from its ABCD representation, we can easily derive its equivalent input impedance Z_{eq}. To illustrate this point, we use a typical example as shown in Fig. 3.4, which is a general network with a load impedance Z_l. Using (3.4) and noticing the fact

$$I_2 = \frac{V_2}{Z_l}, \tag{3.11}$$

we can directly calculate the equivalent input impedance of this network as

$$\begin{aligned} Z_{eq} &= \frac{V_1}{I_1} \\ &= \frac{AZ_l + B}{CZ_l + D}. \end{aligned} \tag{3.12}$$

As a preparation for the relay-involved PLC channel condition analysis, specially we use this result to find the equivalent input impedance of a tap-branched cable-pair closed with an impedance Z_b, which is as shown in Fig. 3.5. By using (3.12) and (3.10), we can readily get this equivalent input impedance value Z_{eqb} as

[1] Unless it is necessary, we drop the notation f in the expression of characteristic impedance $Z_c(f)$ and propagation constant $\gamma(f)$ for simplicity.

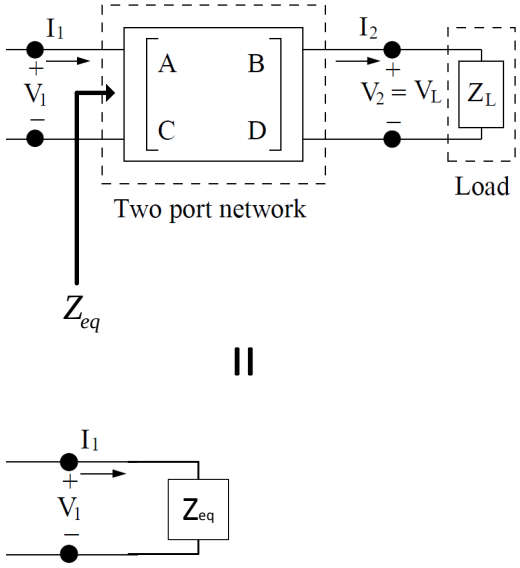

Figure 3.4: Equivalent input impedance for a general network.

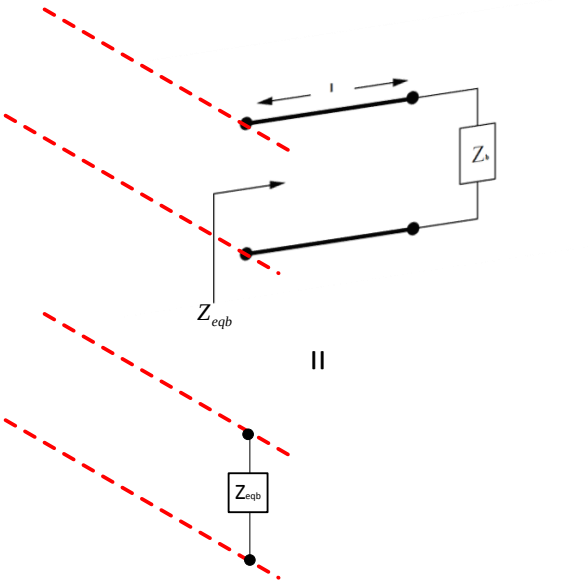

Figure 3.5: Equivalent input impedance of a tap-branched cable pair closed with impedance Z_b, where the backbone cable pair has been indicated by the dash lines.

$$Z_{eqb} = Z_c \frac{Z_b + Z_c \tanh(\gamma l)}{Z_c + Z_b \tanh(\gamma l)} \tag{3.13}$$

where Z_c ,γ and l are the characteristic impedance, propagation constant and the length of this branched cable-pair, respectively.

3.1.3 Transfer function from ABCD matrix

Simple transmission line case

Let us consider the circuit in Fig. 3.1, where all voltages and currents are expressed in the frequency domain. Fig. 3.1 shows a network located in one plane, i.e. no any branch involved. Using the ABCD model for the two-port box in this figure it is straightforward to calculate the transfer function between the voltage source and the receiving load as

$$\begin{aligned} H_{sl}(f) &= \frac{V_l}{V_s} \\ &= \frac{Z_l}{AZ_l + B + CZ_lZ_s + DZ_s}. \end{aligned} \tag{3.14}$$

From (3.14) we notice that the CTF of a network not only depends on its inner ABCD parameters, but also depends on the inner impedance of its stimulating source (Z_s) and its connected load (Z_l).

Branched transmission line case

Now let us consider a more realistic situation, namely a transmission line with branch circuits. As an example shown in Fig. 3.6, a transmission line with a branch, consisting of a pair of cable terminated with impedance Z_b, has been constructed. We can notice that there are two planes in this structure, namely the backbone circuit plane (shown as the horizontal one) and the branch circuit plane (the vertical one). The intersection of these two planes are the line which connects points A and B. We can find the CTF between the voltage source V_s and the main load (i.e. the load on the backbone) Z_l by the following steps:

(1) Depending on the different type of circuit component, divide the whole structure (between the source and load) into three cascaded sub-circuits, namely the first backbone trans-

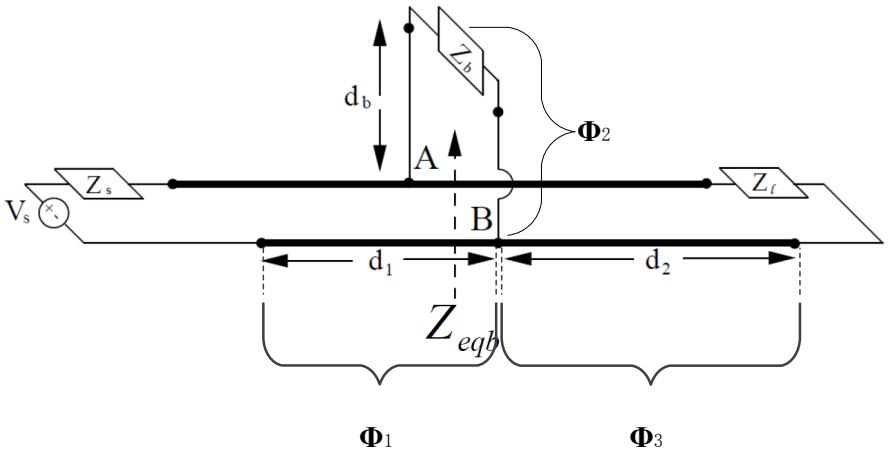

Figure 3.6: A transmission line with a branch circuit.

mission line segment Φ_1, the branched-circuit segment Φ_2 and the second backbone transmission line segment Φ_3. Each of these segments is a two-port network.

(2) For the segments located on the backbone plane, directly calculate its ABCD matrix; for the segment located on the branch plane, firstly substitute it with its equivalent input impedance (which must be located on the intersection of these two planes), and then calculate its ABCD matrix with this equivalent input impedance. Thus, by using the knowledge discussed in Section 3.1.1, we can show that each segment's ABCD matrix Φ_i $(i = 1, 2, 3)$ can be calculated as

$$\Phi_1 = \begin{bmatrix} \cosh(\gamma_1 d_1) & Z_1 \sinh(\gamma_1 d_1) \\ \frac{1}{Z_1} \sinh(\gamma_1 d_1) & \cosh(\gamma_1 d_1) \end{bmatrix} \tag{3.15}$$

where Z_1, γ_1 and d_1 in (3.15) are the characteristic impedance, propagation constants and cable length, respectively, for the first backbone transmission line segment.

And

$$\Phi_2 = \begin{bmatrix} 1 & 0 \\ \frac{1}{Z_{eqb}} & 1 \end{bmatrix} \tag{3.16}$$

$$\Phi_3 = \begin{bmatrix} \cosh(\gamma_2 d_2) & Z_2 \sinh(\gamma_2 d_2) \\ \frac{1}{Z_2}\sinh(\gamma_2 d_2) & \cosh(\gamma_2 d_2) \end{bmatrix} \tag{3.17}$$

where Z_{eqb} in (3.16) is the equivalent input impedance of branched-circuit segment; while Z_2, γ_2 and d_2 in (3.17) are the characteristic impedance, propagation constants and cable length, respectively, for the second backbone segment.

(3) Thus the ABCD matrix Φ_T for the whole structure, i.e. from the voltage source (V_s) to the receiving impedance (Z_l), is the multiplication of the ABCD matrix Φ_i ($i = 1,2,3$) of each segment, i.e.

$$\Phi_T = \prod_{i=1}^{3} \Phi_i \tag{3.18}$$

$$= \begin{bmatrix} A_T & B_T \\ C_T & D_T \end{bmatrix} \tag{3.19}$$

where

$$A_T = \cosh(\gamma_2 d_2)\alpha + \frac{\sinh(\gamma_2 d_2)}{Z_2}\beta \tag{3.20}$$

$$B_T = Z_2 \cosh(\gamma_2 d_2)\alpha + \cosh(\gamma_2 d_2)\beta \tag{3.21}$$

$$C_T = \cosh(\gamma_2 d_2)\xi + \frac{\sinh(\gamma_2 d_2)}{Z_2}\vartheta \tag{3.22}$$

$$D_T = Z_1 \sinh(\gamma_1 d_1)\xi + \cosh(\gamma_2 d_2)\vartheta \tag{3.23}$$

and

$$\alpha = \cosh(\gamma_1 d_1) + \frac{\sinh(\gamma_1 d_1) Z_s}{Z_1} \tag{3.24}$$

$$\beta = Z_1 \sinh(\gamma_1 d_1) + Z_s \cosh(\gamma_1 d_1) \tag{3.25}$$

$$\xi = \frac{Z_1 \cosh(\gamma_1 d_1) + Z_s \sinh(\gamma_1 d_1) + Z_{eqb} \sinh(\gamma_1 d_1)}{Z_1 Z_{eqb}} \tag{3.26}$$

$$\vartheta = \frac{Z_1 \sinh(\gamma_1 d_1) + Z_s \cosh(\gamma_1 d_1)}{Z_{eqb}} + \cosh(\gamma_1 d_1). \tag{3.27}$$

(4) By using (3.14) with the whole structure's ABCD matrix Φ_T, we get the CTF of the proposed problem, i.e.

$$H_T(f) = \frac{Z_l}{A_T Z_l + B_T + C_T Z_l Z_s + D_T Z_s}. \tag{3.28}$$

This procedure has been been illustrated in Fig. 3.7. For channels with more branches or more complex branched circuit, the calculation of the channel transfer function based on this method is straightforward, but the formula is more complex. Furthermore, we mention that some published P2P PLC channel model, such as [1, 25] and [32] are results of following this approach.

3.2 CTF for relay-involved PLC channel

As the half-duplex constraint holds in many practical relay devices, we consider that the time-division duplexing (TDD) mode is used in this thesis for its easy implementation, although the frequency-division duplexing (FDD) mode is also possible. Thus, the procedure to complete a message transmission form a source node (S) to a destination node (D) with an amplify-and-forward (AF) processing in the relay node (R) consists of two phases as shown in Fig. 3.8. In the first phase, the source node broadcasts its message to the relay node and the destination node; in the second phase, the destination node receives multiaccess signals from both the source and the relay nodes. Note that we allow the source node broadcasts the same massage twice in two phrases/stages, and this configuration leads to the most general form of the AF relay scheme, namely the broadcast-and-multiaccess (BMA) scheme, which includes two special cases, i.e. two-hop scheme and broadcast-and-forward (BF) scheme. The reason about this point will become clear in Chapter 5.

3.2.1 Circuit modeling for the relay node

As discussed in Section 3.1.1, for the source node, we can model it as a transmitter consisting a voltage source (V_s) and a inner impedance (Z_s); and for the destination node, as a receiving load (Z_l). However, as the relay node changes its working role in two different phases, we need to consider it as follows.

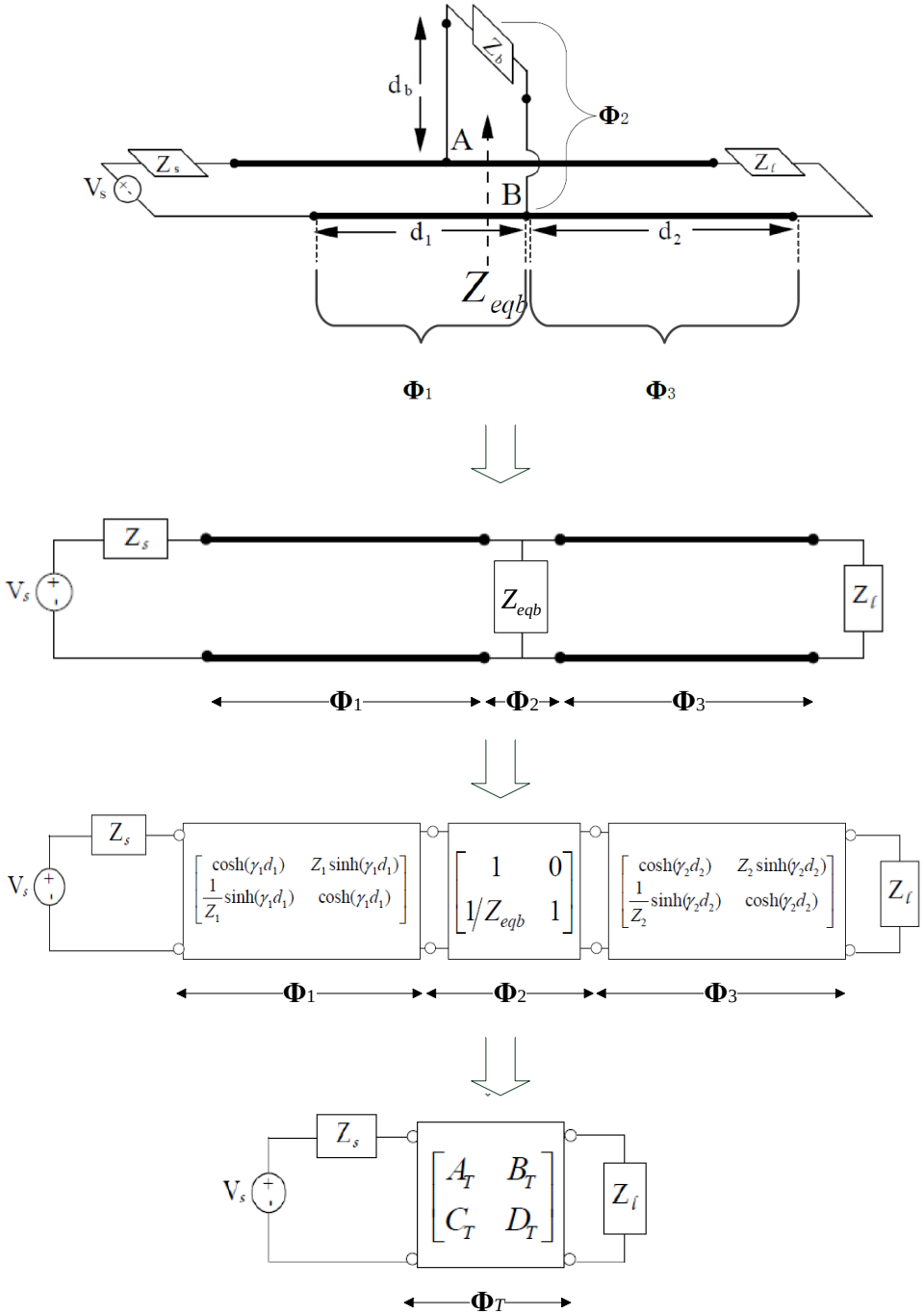

Figure 3.7: Procedure to find the CTF of a one-branched channel.

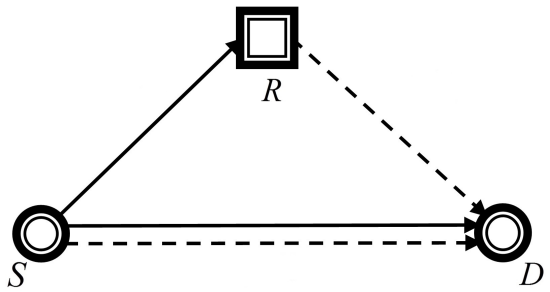

Figure 3.8: Broadcast-and-multiaccess (BMA) relay scheme, where the dash lines denote the second phase.

In the first stage, the relay node works in the receiving mode, thus a load impedance (Z_{lR}) is appropriate to model it, as shown in Fig 3.9a. In the second stage, the relay node acts as a transmitter, which can be modeled by a controlled voltage source with a source voltage V_R and a inner source Z_{sR} as shown in Fig. 3.9b. As we assume the relay node works in the AF model, then we can express its output voltage

$$V_R = \beta V_{lR} \tag{3.29}$$

where β is the amplitude gain of the AF processing, while V_{lR} is the voltage received by the relay node in the first phase.

3.2.2 Circuit modeling for relay-involved channels

For any given indoor PLC cabling topology and a pair of outlets implemented with the source and destination nodes, we can firstly identify the backbone, i.e. the shortest signaling path between the transmitter and the receiver nodes[1]. Then, the topology can be remapped along with the backbone, as shown by a typical example given in Fig. 3.10. For the complex network between the transceivers, we can treat them as a cascade of different segments. As we can see in Fig. 3.10, each segment contains at most one branch circuit, which is connected to the backbone at an intersection point (i.e. points P_i, $i = 1,2,..,5$). Particularly, the end segments (segment 1 and 6) are associated with the source and destination nodes.

As there are different type of branches, we can classify them into four groups:

(1) pure cable single branch, e.g. branch 4;

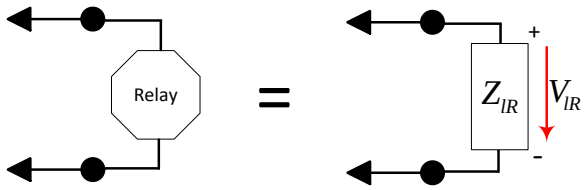

(a) model of relay node in the first phase

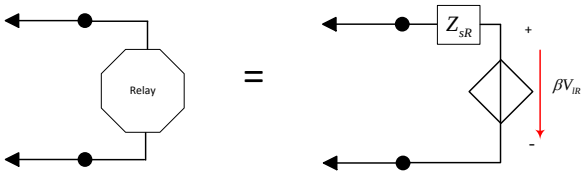

(b) model of relay node in the second phase

Figure 3.9: Relay node's model in different phases.

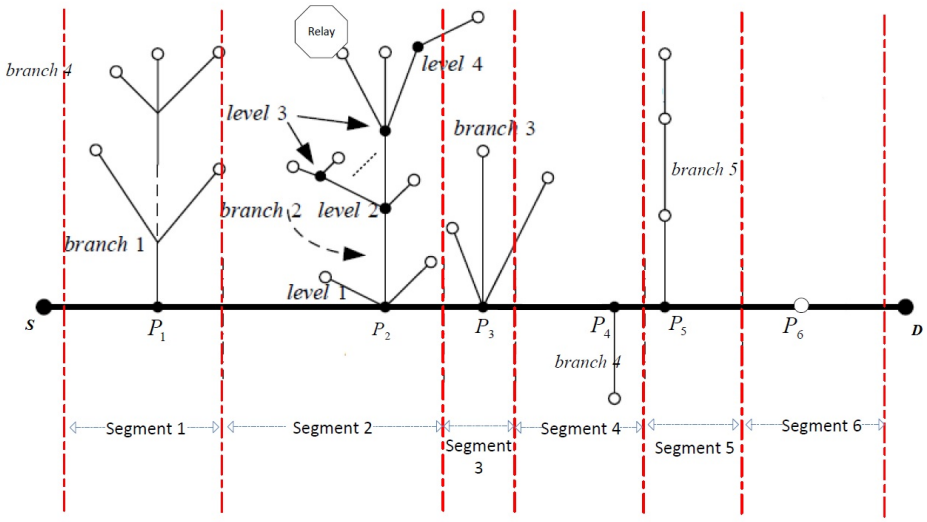

Figure 3.10: Remap of a typical topology of indoor PLC network, where the bold line indicates the backbone.

(2) multi-level single branch, which constructed by the cascade of different type of cables, e.g. branch 5;

(3) star branch, with several cables connected at the same level, such as branch 3;

(4) general multi-level branch, which is the combination of type (2) and (3), e.g branch 1 and 2.

For the segment with a branch (e.g. segment 1-5), the relay device can be introduced at any outlet on the branch (e.g. the location as shown in Fig. 3.10), while for the segment without a branch (e.g. segment 6), the relay can be directly mounted at the outlet on the backbone. Obviously, the latter situation can be seen as a special case and be included in the former case, if we treat the branch as ideal conductor pair. Thus, without losing generality, we assume the relay node is implemented at one outlet (e.g. branch 2 here), which intersects with the backbone at the point P.

Thus the network between the transmitter S and point P can be modeled as a two-port network represented in ABCD matrix as

$$\Phi_1 = \begin{bmatrix} A_1 & B_1 \\ C_1 & D_1 \end{bmatrix}. \tag{3.30}$$

Also, we can treat the network between the point P and the receiver D as another two-port network denoted by its ABCD matrix

$$\Phi_2 = \begin{bmatrix} A_2 & B_2 \\ C_2 & D_2 \end{bmatrix} \tag{3.31}$$

and the branched network, between the point P and the relay node R, as still another two-port network denoted by its ABCD matrix

$$\Phi_b = \begin{bmatrix} A_b & B_b \\ C_b & D_b \end{bmatrix}. \tag{3.32}$$

Considering the outlet, where the relay device chooses to plug in, may have a preexisting load Z_b, then the relay node R should be paralleled to it. For the situation where the outlet keeps open circuit (unloaded), we can treat this as a spacial loaded case as $Z_b \to \infty$. Thus, the circuit modeling for relay-involved channels can be given in Fig. 3.11.

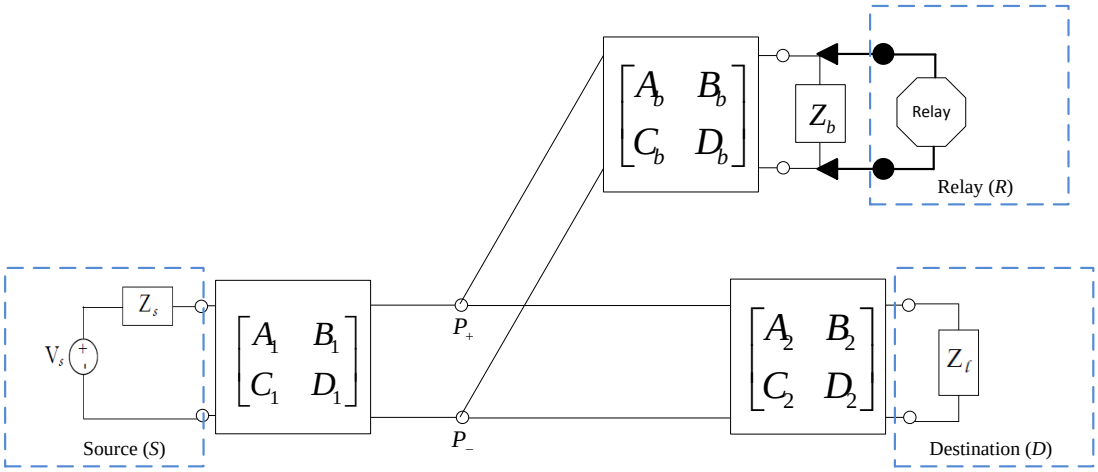

Figure 3.11: Circuit model for relay-invovled PLC channels.

3.2.3 CTF derivation of relay-involved channels

Transfer function from *S* to *D* in the *first* phase

As in the first phase the relay node can be treated as a load, then the CTF of the direct path (i.e. the signaling path from the source to the destination node along the backbone) can be found by using the chain matrix method as illustrated in Fig. 3.12, where the input equivalent impedance of the relay branch is computed as

$$Z_{eqb} = \frac{A_b Z'_{lR} + B_b}{C_b Z'_{lR} + D_b} \tag{3.33}$$

where Z'_{lR} is the paralleling equivalent impedance of Z_b and Z_{lR}, namely

$$\begin{aligned} Z'_{lR} &= Z_b \,/\!/\, Z_{lR} \\ &= \frac{Z_b Z_{lR}}{Z_b + Z_{lR}}. \end{aligned} \tag{3.34}$$

As also shown in Fig. 3.12, the multiplication matrix between S and D in the first phase,

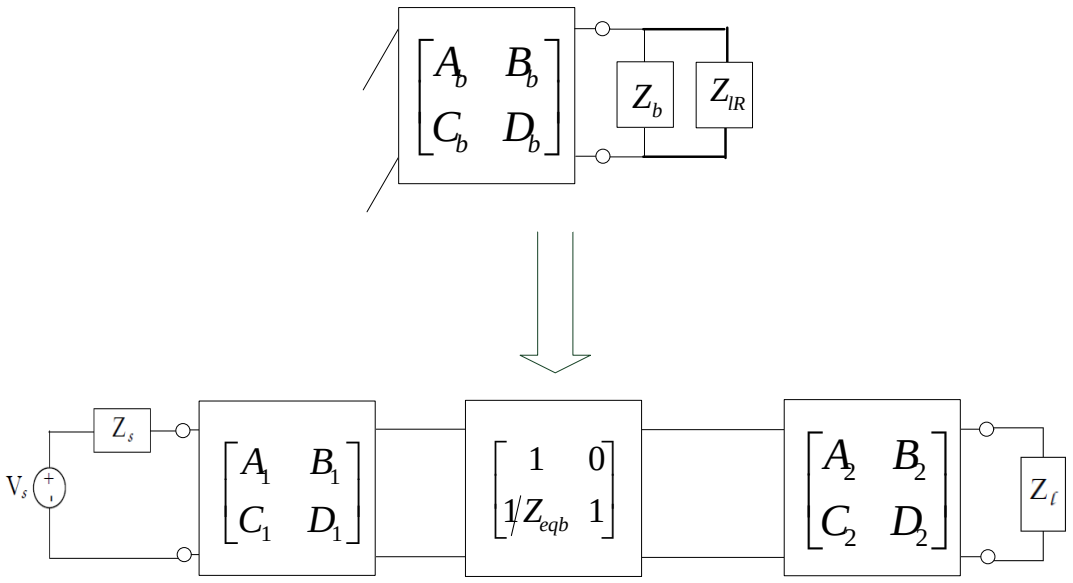

Figure 3.12: CTF derivation: from the source node to the destination node in the first phase.

denoted as $\Phi_{SD}^{(1)}$, can be expressed as

$$\begin{aligned}\Phi_{SD}^{(1)} &= \begin{bmatrix} A_{SD}^{(1)} & B_{SD}^{(1)} \\ C_{SD}^{(1)} & D_{SD}^{(1)} \end{bmatrix} \\ &= \begin{bmatrix} A_1 & B_1 \\ C_1 & D_1 \end{bmatrix} \begin{bmatrix} 1 & 0 \\ \frac{1}{Z_{eqb}} & 1 \end{bmatrix} \begin{bmatrix} A_2 & B_2 \\ C_2 & D_2 \end{bmatrix}\end{aligned} \tag{3.35}$$

which in turn leads to the CTF between S and D in the first phase, denoted as[2] $\tilde{H}_{SD}^{(1)}$, can be expressed as

$$\begin{aligned}\tilde{H}_{SD}^{(1)} &= \frac{V_l}{V_s} \\ &= \frac{Z_l}{A_{SD}^{(1)} Z_l + B_{SD}^{(1)} + C_{SD}^{(1)} Z_l Z_s + D_{SD}^{(1)} Z_s}.\end{aligned} \tag{3.36}$$

Note for the two-hop relay scheme case, we should treat $Z_l \to 0$ in (3.36), as there is no direct path available in the first phase.

[2]Note for simplicity, we drop the notation of the frequency f in the following.

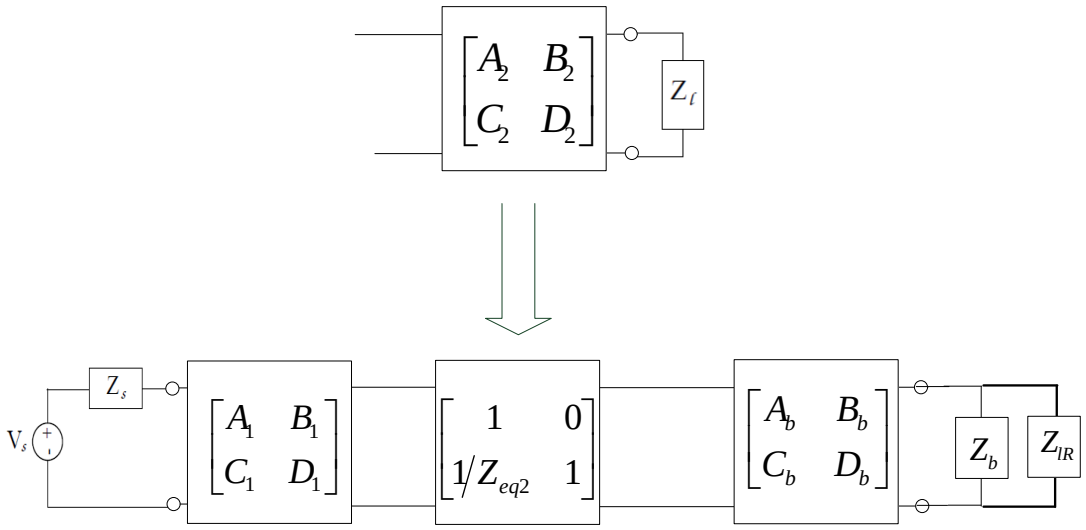

Figure 3.13: CTF derivation: from the source node to the relay node in the first phase.

Transfer function from S to R in the *first* phase

In the first phase, the relay node receives the information signal through the path from Φ_1 to Φ_b as shown in Fig. 3.11, then from the relay node's point of view, the second segment Φ_2 on the the backbone should be treated as a "branch". This has been shown in 3.13, where the input equivalent impedance of the Φ_2 branch is computed as

$$Z_{eq2} = \frac{A_2 Z_l + B_2}{C_2 Z_l + D_2}. \tag{3.37}$$

Note we should treat $Z_l \to 0$ in (3.37) when we consider the two-hop relay scheme case without the direct link.

In Fig. 3.13, the multiplication matrix between S and R in the first phase, denoted as $\Phi_{SR}^{(1)}$, can be expressed as

$$\begin{aligned} \Phi_{SR}^{(1)} &= \begin{bmatrix} A_{SR}^{(1)} & B_{SR}^{(1)} \\ C_{SR}^{(1)} & D_{SR}^{(1)} \end{bmatrix} \\ &= \begin{bmatrix} A_1 & B_1 \\ C_1 & D_1 \end{bmatrix} \begin{bmatrix} 1 & 0 \\ \frac{1}{Z_{eq2}} & 1 \end{bmatrix} \begin{bmatrix} A_b & B_b \\ C_b & D_b \end{bmatrix} \end{aligned} \tag{3.38}$$

which in turn leads to the CTF between S and R in the first phase, denoted as $\tilde{H}_{SR}^{(1)}$, can be expressed as

$$\begin{aligned}\tilde{H}_{SR}^{(1)} &= \frac{V_{lR}}{V_s} \\ &= \frac{Z_{lR}^{'}}{A_{SR}^{(1)}Z_{lR}^{'} + B_{SR}^{(1)} + C_{SR}^{(1)}Z_{lR}^{'}Z_s + D_{SR}^{(1)}Z_s}\end{aligned} \tag{3.39}$$

where $Z_{lR}^{'}$ is the paralleling equivalent impedance of Z_b and Z_{lR}, i.e.

$$\begin{aligned}Z_{lR}^{'} &= Z_b /\!\!/ Z_{lR} \\ &= \frac{Z_b Z_{lR}}{Z_b + Z_{lR}}.\end{aligned} \tag{3.40}$$

Transfer function from R to D in the *second* phase

As in the second phase the relay node should be treated as transmitter (where$V_R = \beta V_{lR}$), which forwards signal to the destination node through the path from Φ_b to Φ_2 as shown in Fig. 3.11. Form the relay node's point of view, now the first segment Φ_1 on the the backbone should be treated as a branch. This has been shown in 3.14, where input equivalent impedance of the Φ_1 branch is computed as

$$Z_{eq1} = \frac{A_1 Z_s + B_1}{C_1 Z_s + D_1}. \tag{3.41}$$

Note for the two-hop and BF relay schemes, the source should be treated as open circuit (high impedance state) as it does not work in the second phase. This can be configured by setting $Z_s \to \infty$ in (3.41); on the other hand, for the BMA relay scheme, the source node repeat a transmission. Following the superposition theorem, its transmission voltage V_s should be set as zero, as here we only intend to find the response on Z_l stimulated by the relay node's effect.

After using the ABCD matrix of Z_b, the multiplication matrix between R and D in the second

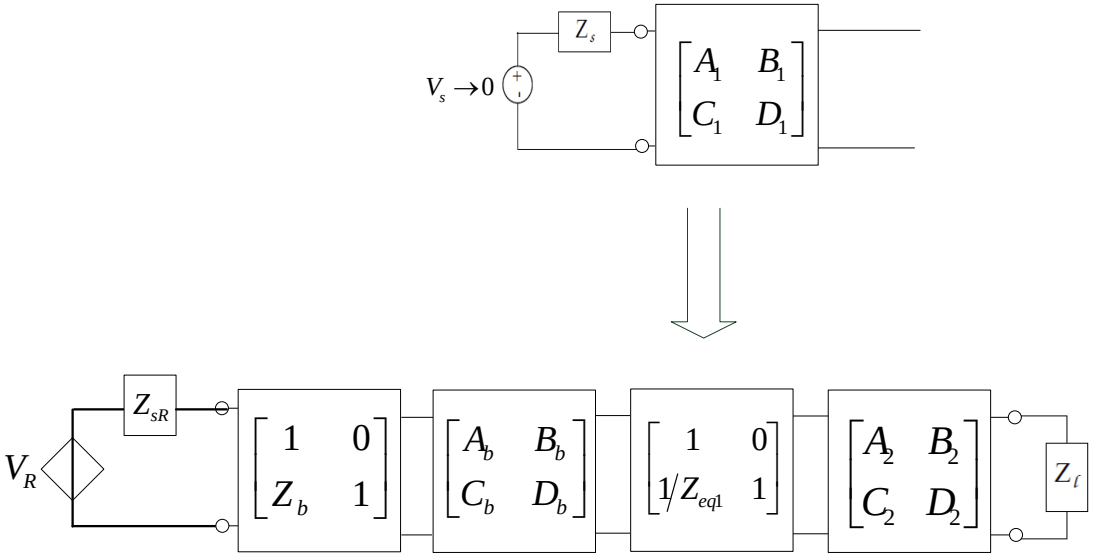

Figure 3.14: CTF derivation: from the relay node to the destination node in the second phase.

phase, denoted as $\Phi_{RD}^{(2)}$, can be expressed as

$$\begin{aligned}\Phi_{RD}^{(2)} &= \begin{bmatrix} A_{RD}^{(2)} & B_{RD}^{(2)} \\ C_{RD}^{(2)} & D_{RD}^{(2)} \end{bmatrix} \\ &= \begin{bmatrix} 1 & 0 \\ Z_b & 1 \end{bmatrix} \begin{bmatrix} A_b & B_b \\ C_b & D_b \end{bmatrix} \begin{bmatrix} 1 & 0 \\ \frac{1}{Z_{eq1}} & 1 \end{bmatrix} \begin{bmatrix} A_2 & B_2 \\ C_2 & D_2 \end{bmatrix}\end{aligned} \tag{3.42}$$

which in turn leads to the CTF between R and D in the second phase, denoted as $\tilde{H}_{RD}^{(2)}$, can be expressed as

$$\begin{aligned}\tilde{H}_{RD}^{(2)} &= \frac{V_l}{V_R} \\ &= \frac{Z_l}{A_{RD}^{(2)} Z_l + B_{SD}^{(2)} + C_{SD}^{(2)} Z_l Z_{sR} + D_{SD}^{(2)} Z_{sR}}\end{aligned} \tag{3.43}$$

where Z_{sR} is the inner impedance of the relay node when it works in the transmission mode.

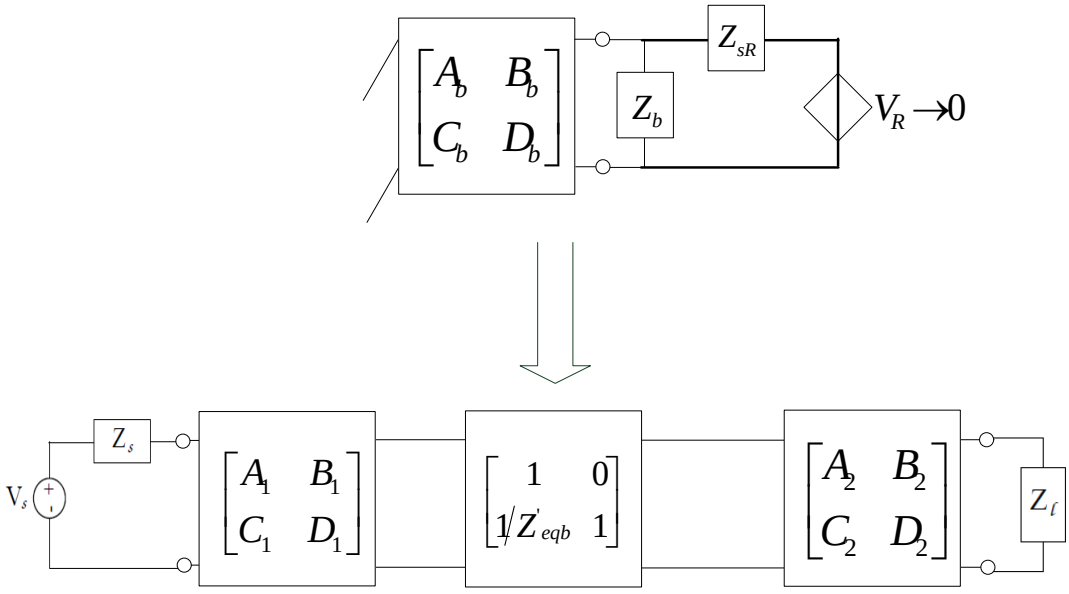

Figure 3.15: CTF derivation: from the source node to the destination node in the second phase.

Transfer function from S to D in the *second* phase

For the two-hop and BF relay schemes, there is no need to discuss this problem; on the other hand, with the BMA scheme, the source node will repeat a transmission. Again, as here we only have interesting about the response on Z_l stimulated by the source node's effect, the relay node's transmission voltage V_R should be set as $V_R \to 0$. Similar to the first phase situation, we illustrate the circuit model as shown in Fig. 3.15, where the input equivalent impedance of the relay branch Φ_b in the second phase, is computed as

$$Z'_{eqb} = \frac{A_b Z''_{lR} + B_b}{C_b Z''_{lR} + D_b} \tag{3.44}$$

where $Z_{lR}^{''}$ is the parallel equivalent impedance of Z_b and relay node's inner impedanceZ_{sR}, namely

$$\begin{aligned} Z_{lR}^{''} &= Z_b /\!/ Z_{sR} \\ &= \frac{Z_b Z_{sR}}{Z_b + Z_{sR}}. \end{aligned} \tag{3.45}$$

Thus the multiplication matrix between S and D in the second phase, denoted as $\Phi_{SD}^{(2)}$, should be written as

$$\begin{aligned} \Phi_{SD}^{(2)} &= \begin{bmatrix} A_{SD}^{(2)} & B_{SD}^{(2)} \\ C_{SD}^{(2)} & D_{SD}^{(2)} \end{bmatrix} \\ &= \begin{bmatrix} A_1 & B_1 \\ C_1 & D_1 \end{bmatrix} \begin{bmatrix} 1 & 0 \\ \frac{1}{Z_{eqb}^{'}} & 1 \end{bmatrix} \begin{bmatrix} A_2 & B_2 \\ C_2 & D_2 \end{bmatrix} \end{aligned} \tag{3.46}$$

which in turn leads to the CTF between S and D in the second phase, denoted as $\tilde{H}_{SD}^{(2)}$, can be expressed as

$$\begin{aligned} \tilde{H}_{SD}^{(2)} &= \frac{V_l}{V_s} \\ &= \frac{Z_l}{A_{SD}^{(2)} Z_l + B_{SD}^{(2)} + C_{SD}^{(2)} Z_l Z_s + D_{SD}^{(2)} Z_s}. \end{aligned} \tag{3.47}$$

As the relay node changes its working mode from phase 1 to phase 2 and in general $Z_{eqb} \neq Z_{eqb}^{'}$, by comparing (3.36) and (3.47), we can see that in general,

$$\tilde{H}_{SD}^{(1)} \neq \tilde{H}_{SD}^{(2)}. \tag{3.48}$$

In addition, by using (3.36), (3.39), (3.43) and (3.47) we can also easily examine that, in general,

$$\tilde{H}_{SD}^{(1)} \neq \tilde{H}_{SR}^{(1)} \tilde{H}_{RD}^{(2)} \tag{3.49}$$

$$\tilde{H}_{SD}^{(2)} \neq \tilde{H}_{SR}^{(1)} \tilde{H}_{RD}^{(2)}. \tag{3.50}$$

From the discussion in Section 3.1 and 3.2, we can see that for any power line topology between a pair of transceivers and the load impedance information of the network nodes, we

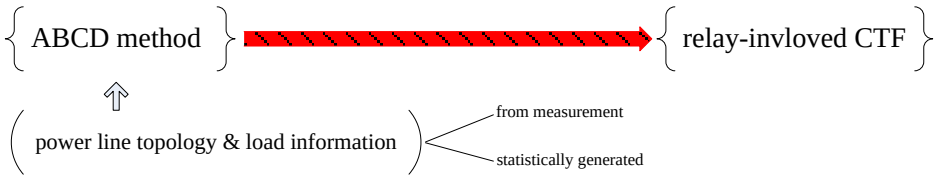

(a) ground-up approach

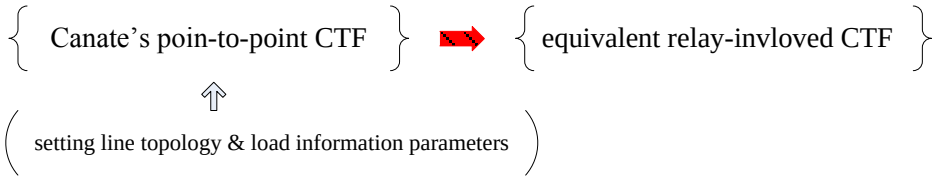

(b) the simple approach

Figure 3.16: Two approaches for relay-involved CTF generation.

can use the ABCD method to calculate its corresponding CTF, no matter the PLC network is used as a P2P channel or relay-involved channel. Furthermore, by adopting the indoor PLC random topology generation method in [1], a statistical CTF model of relay-involved channels can also be built. We refer to this way as the ground-up approach as illustrated in Fig. 3.16a.

3.3 A simple CTF generation approach for relay-involved channels

Rather than following the computationally intensive ground-up approach, we can reuse the published P2P channel models for our relay-involved channel model. For its simple parameterization system and verified performance, in this thesis we adopt the hybrid model proposed by Canate et al [32], which we discussed in Chapter 2. Specifically, we can directly (but also strategically) use this P2P PLC channel model to generate a series of realistic relay-involved PLC channels, and these results will be used as a test platform for our simulation of various relay schemes proposed in the later chapters. we refer to this approach as the simple CTF generation approach as illustrated in Fig. 3.16b.

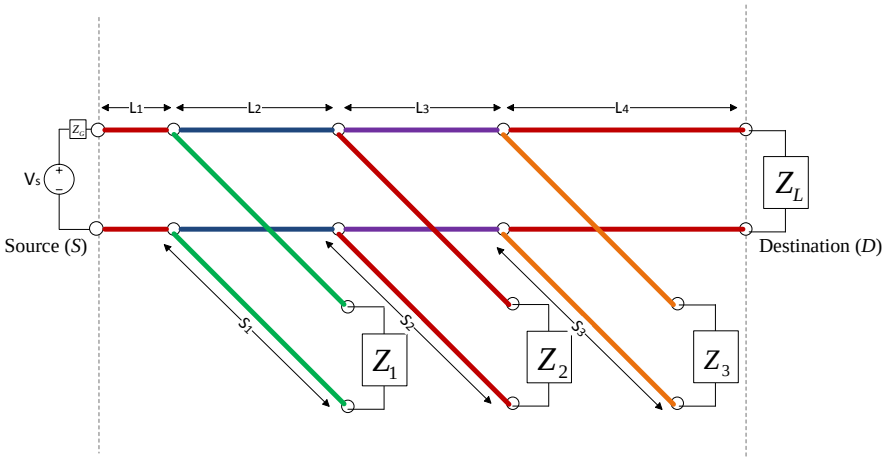

Figure 3.17: Network topology of the hybrid PLC channel model.

For discussion convenience, we redraw the topology of Canate's hybrid channel model in Fig. 3.17, where altogether seven line sections (i.e. backbone segments 1 to 4 and branch-taps 1 to 3) were used. By setting the parameters of this model as in Table 3.1, we can further simplify this network layout to a three-segment channel model, so that the relay device can be introduced on the only available branch (i.e. branch-tap 1) as shown in Fig. 3.18. As we will see, this configuration will significantly reduce the difficulty of the CTF generation problem for the relay-involved channels. On the other hand, as Canate's channel model has been verified by measurement [32], our relay-involved results generated from this model are reasonably realistic. For simplicity, in the following we only consider the time-invariant case, i.e $Z_1(f,t) = Z_1(f)$, as the time-varying case can be done in the same way. An example of the frequency response of $Z_1(f)$ has been given in Fig. 3.19.

For latter comparison purpose, we firstly give the P2P CTF H_{SD} by using the parameters in Table 3.1. This is shown in Fig. 3.20. On the other hand, for the relay-involved CTF generation problem, the parameters configuration for the different signaling paths in the different transmission phases need to be addressed sequentially as follows.

Generate transfer function $\tilde{H}_{SD}^{(1)}$

As analysis shown in Section 3.2, in the first phase the relay node can be treated as a load, then the CTF of the direct path $\tilde{H}_{SD}^{(1)}$ can be generated from the equivalent network layout as illustrated in Fig. 3.21, and this model can be directly obtained by setting the parameters

Table 3.1: Parameters for the three-segment channel realization

line section name	length	cable type	terminated load
backbone 1	L_1=*50.2m*	n_{L1}=*3*	*N/A*
branch-tap 1	S_1=29.1m	n_{S1}=1	$Z_1(f,t)$
backbone 2	L_2=*77.8m*	n_{L2}=*4*	*N/A*
branch-tap 2	S_2=0	N/A	Z_2=∞
backbone 3	L_3=*0*	*N/A*	*N/A*
branch-tap 3	S_3=0	N/A	Z_3=∞
backbone 4	L_4=*0*	*N/A*	*N/A*
	Transmitting inner impedance:		Z_G=5Ω
	Receiving load impedance:		Z_L=150Ω

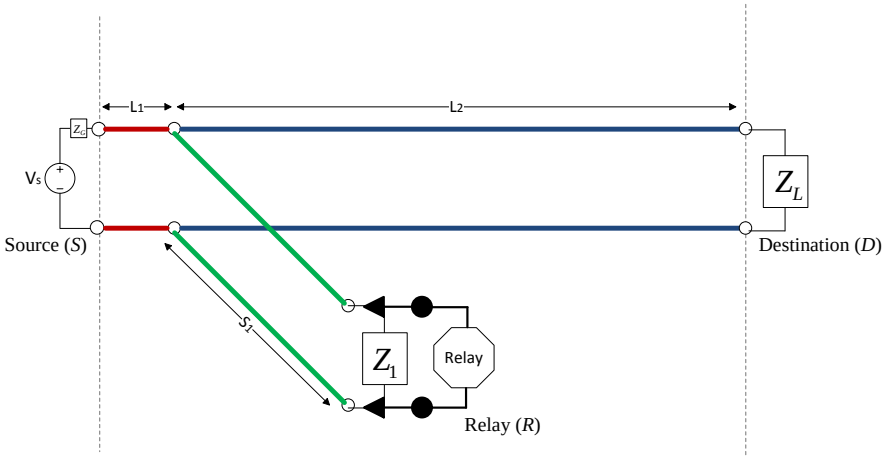

Figure 3.18: Network layout for the three-segment case.

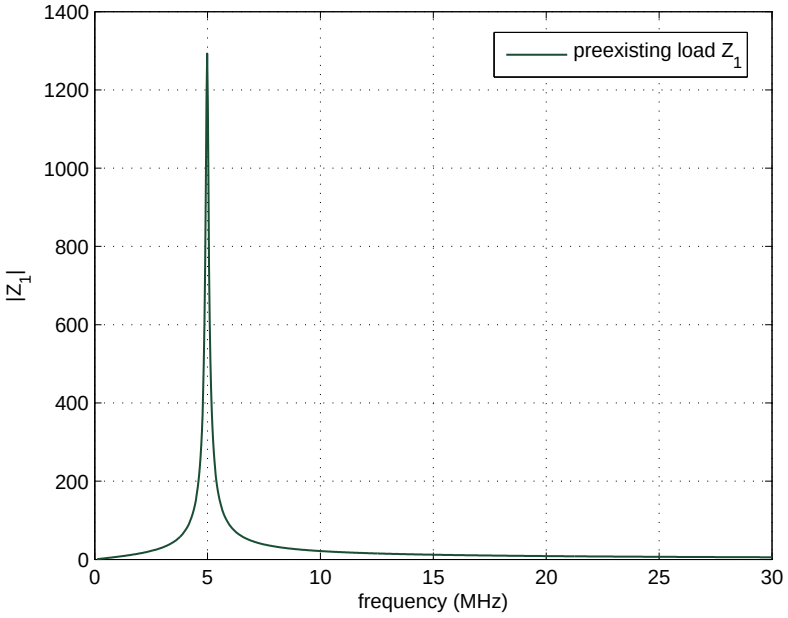

Figure 3.19: An example of the frequency response of $Z_1(f)$

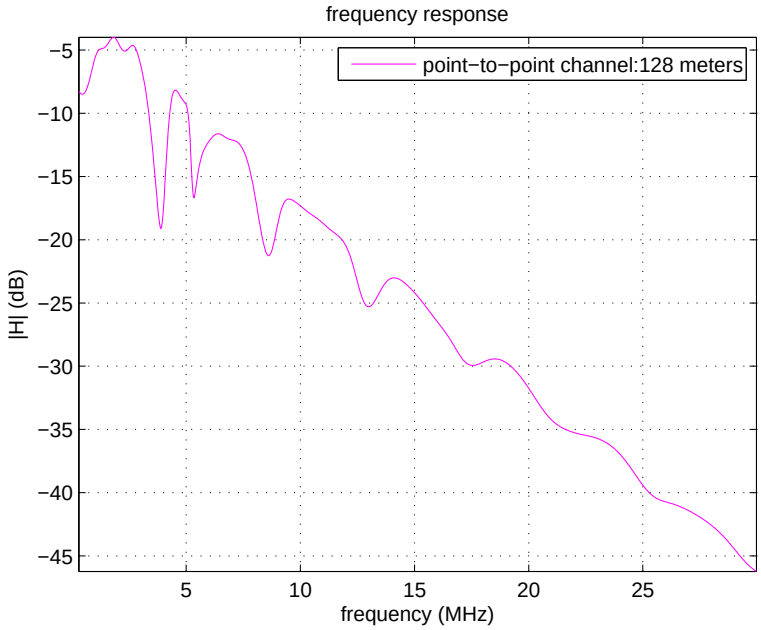

Figure 3.20: P2P CTF for the source-to-destination path before the introduction of the relay node.

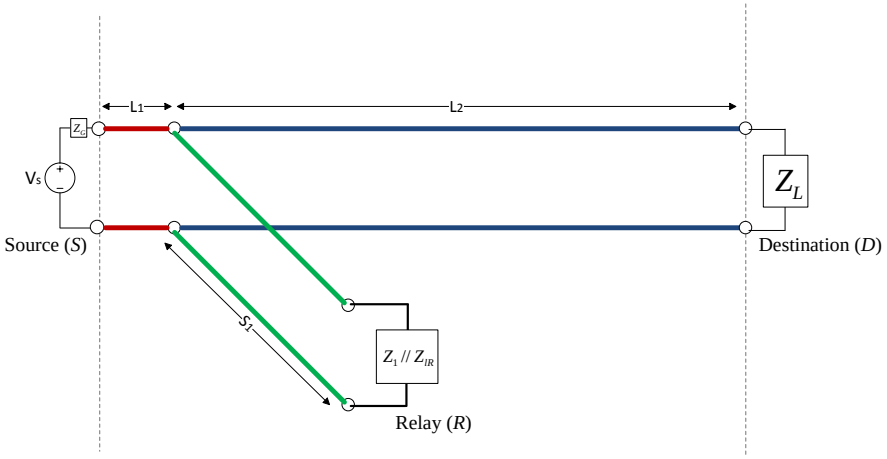

Figure 3.21: Equivalent network layout for CTF generation of source-to-destination path in the first phase.

of the hybrid model (Fig. 3.17) as in Table 3.2. Note we set the receiving impedance of the relay node has the same value as the destination node, i.e. $Z_{lR} = Z_L$=150Ω, so that the paralleling equivalent impedance of Z_1 and Z_{lR} can be calculated by using (3.34). Its CTF result has been plotted in Fig. 3.22.

Generate transfer function $\tilde{H}_{SR}^{(1)}$

Similarly, the CTF of the source-to-relay path in the first phase $\tilde{H}_{SR}^{(1)}$ can be generated from the network layout shown in Fig. 3.23, and this model can be obtained by setting the parameters as in Table 3.3. Note to treat the paralleling equivalent impedance of Z_1 and Z_{lR} as the receiving load and the backbone segment 2 as a "branch". Its CTF result has been plotted in Fig 3.24.

Generate transfer function $\tilde{H}_{RD}^{(2)}$

In the second phase the relay node works in the transmitting mode. We set the inner impedance of the relay node has the same value as the source node, i.e. $Z_{sR} = Z_G$=5Ω. Note to treat the backbone segment 1 as a "branch" and the source voltage V_s as zero following the superposition theorem. Thus, the CTF of the relay-to-destination path in the second phase $\tilde{H}_{RD}^{(2)}$ can be generated from the equivalent network layout as illustrated in Fig.

Table 3.2: Parameters for generating CTF $\tilde{H}_{SD}^{(1)}$

line section name	length	cable type	terminated load
backbone 1	L_1=*50.2m*	n_{L1}=*3*	*N/A*
branch-tap 1	S_1=29.1m	n_{S1}=1	$Z_1(f) /\!/ Z_{lR}$
backbone 2	L_2=*77.8m*	n_{L2}=*4*	*N/A*
branch-tap 2	S_2=0	N/A	Z_2=∞
backbone 3	L_3=*0*	*N/A*	*N/A*
branch-tap 3	S_3=0	N/A	Z_3=∞
backbone 4	L_4=*0*	*N/A*	*N/A*
Transmitting inner impedance:			Z_G=5Ω
Receiving load impedance:			Z_L=150Ω

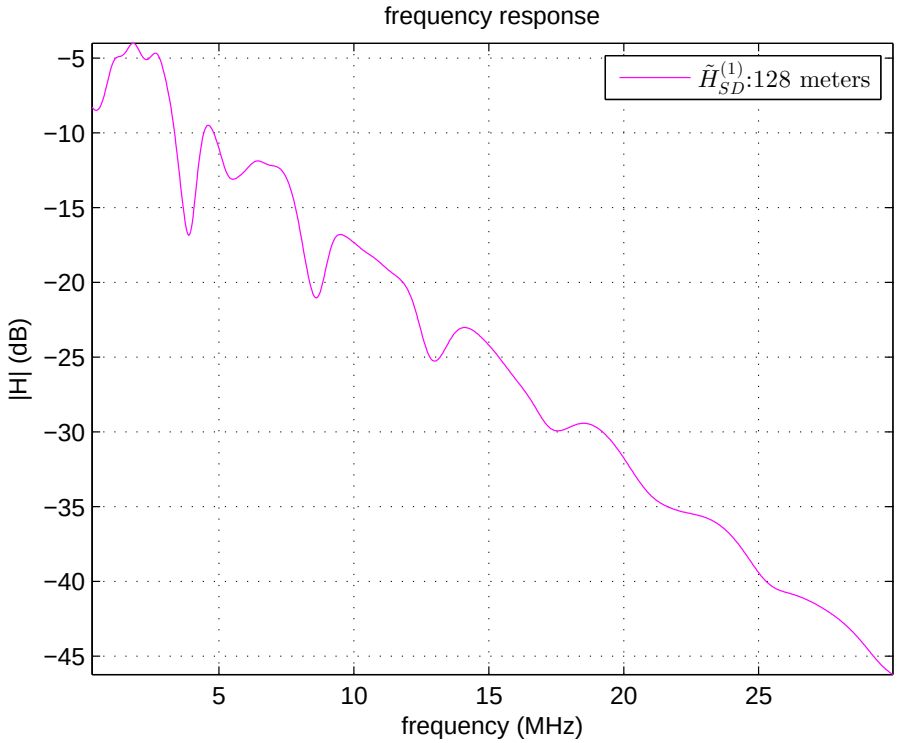

Figure 3.22: CTF result for the source-to-destination path in the first phase.

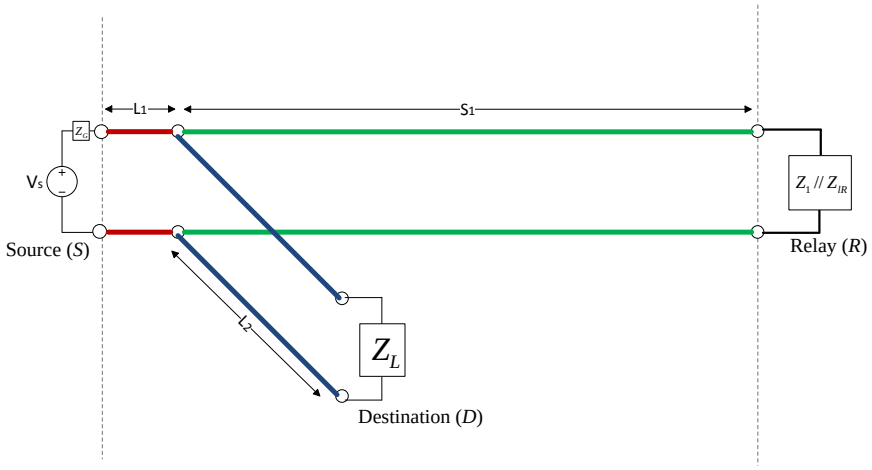

Figure 3.23: Equivalent network layout for CTF generation of source-to-relay path in the first phase.

Table 3.3: Parameters for generating CTF $\tilde{H}_{SR}^{(1)}$

line section name	length	cable type	terminated load
backbone 1	L_1=*50.2m*	n_{L1}=*3*	*N/A*
branch-tap 1	L_2=77.8m	n_{L2}=4	Z_L
backbone 2	S_1=*29.1m*	n_{S1}=*1*	*N/A*
branch-tap 2	S_2=0	N/A	Z_2=∞
backbone 3	L_3=*0*	*N/A*	*N/A*
branch-tap 3	S_3=0	N/A	Z_3=∞
backbone 4	L_4=*0*	*N/A*	*N/A*
Transmitting inner impedance:			Z_G=5Ω
Receiving load impedance:			$Z_1 /\!/ Z_{lR}$

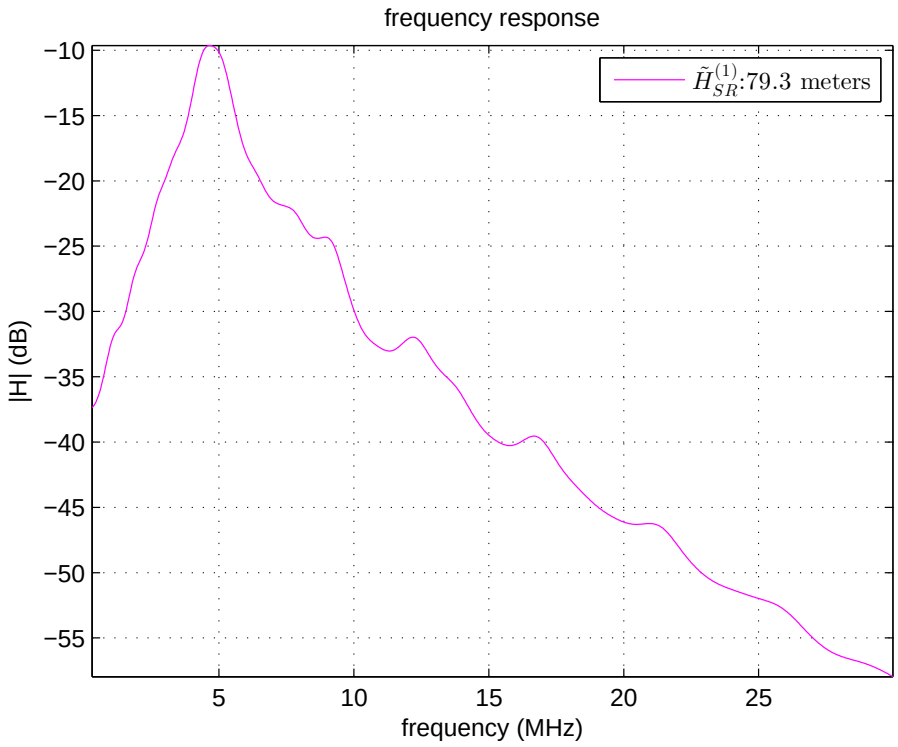

Figure 3.24: CTF result for the source-to-relay path in the first phase.

3.25, and this model can be obtained by setting the parameters in Table 3.4. Also, its CTF result has been plotted in Fig. 3.26.

Generate transfer function $\tilde{H}_{SD}^{(2)}$

As the relay node changes its working mode from phase 1 to phase 2, to find the the CTF of the direct path in the second phase $\tilde{H}_{SD}^{(2)}$, it is necessary to reconstruct its corresponding equivalent network layout as illustrated in Fig. 3.27, which can be obtained by setting the parameters of the hybrid model as values in Table 3.5. Noting to treat he paralleling equivalent impedance of Z_1 and Z_{sR} as the terminated load on the branch and the relay voltage V_R as zero following the superposition theorem. Its CTF result has been plotted in Fig. 3.28.

By summarizing the results from Fig. 3.20, 3.22, 3.24, 3.28 and 3.28 into Fig. 3.29, and comparing them with each other, we can see clearly that in general,

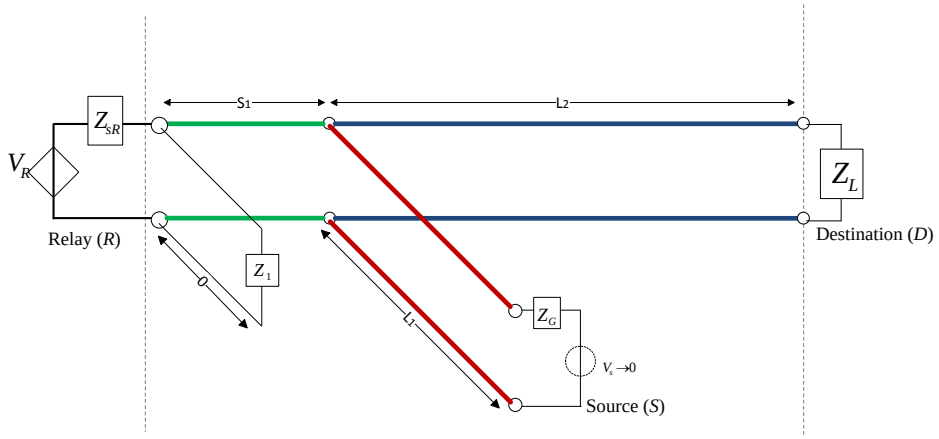

Figure 3.25: Equivalent network layout for CTF generation of relay-to-destination path in the second phase.

Table 3.4: Parameters for generating CTF $\tilde{H}_{RD}^{(2)}$

line section name	length	cable type	terminated load
backbone 1	L_0=0	N/A	*N/A*
branch-tap 1	S_0=0	N/A	$Z_1(f)$
backbone 2	S_1=29.1m	n_{S1}=1	*N/A*
branch-tap 2	L_1=50.2m	n_{L1}=3	Z_G=5Ω
backbone 3	L_2=77.8m	n_{L2}=4	*N/A*
branch-tap 3	S_3=0	N/A	Z_3=∞
backbone 4	L_4=0	N/A	*N/A*
Transmitting inner impedance:			Z_{sR}=5Ω
Receiving load impedance:			Z_L=150Ω

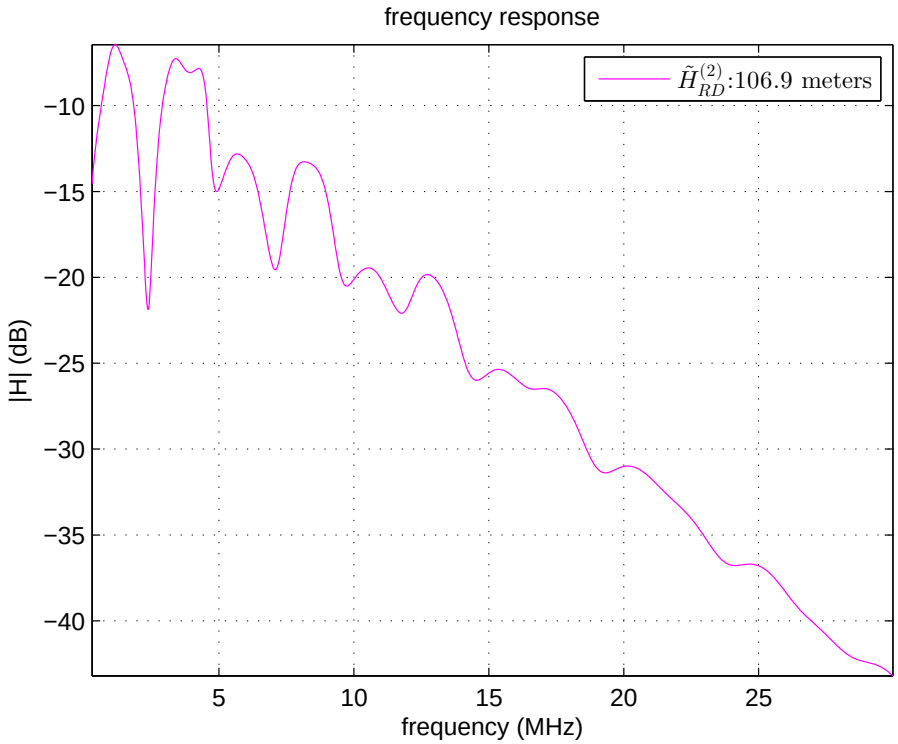

Figure 3.26: CTF result for the relay-to-destination path in the second phase.

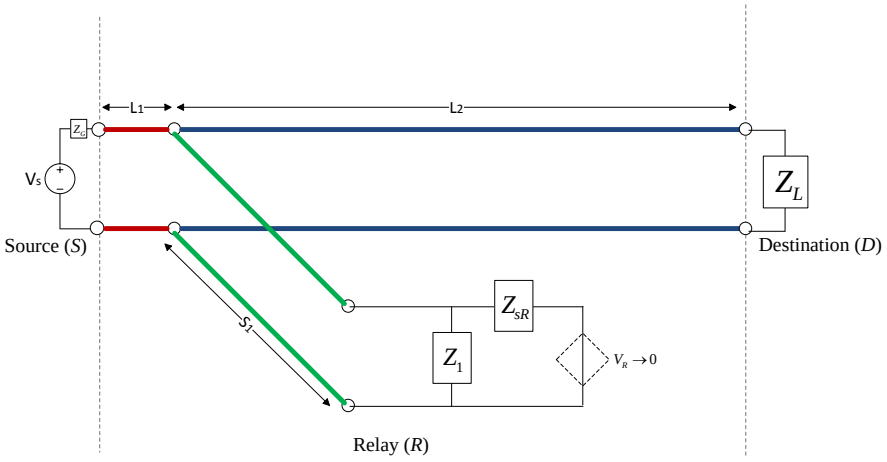

Figure 3.27: Equivalent network layout for CTF generation of source-to-destination path in the second phase.

Table 3.5: Parameters for generating CTF $\tilde{H}_{SD}^{(2)}$

line section name	length	cable type	terminated load
backbone 1	L_1=50.2m	3	*N/A*
branch-tap 1	S_1=29.1m	1	$Z_1 /\!/ Z_{sR}$
backbone 2	L_2=77.8m	4	*N/A*
branch-tap 2	S_2=0	N/A	Z_2=∞
backbone 3	L_3=0	N/A	*N/A*
branch-tap 3	S_3=0	N/A	Z_3=∞
backbone 4	L_4=0	N/A	*N/A*
	Transmitting inner impedance:		Z_G=5Ω
	Receiving load impedance:		Z_L=150Ω

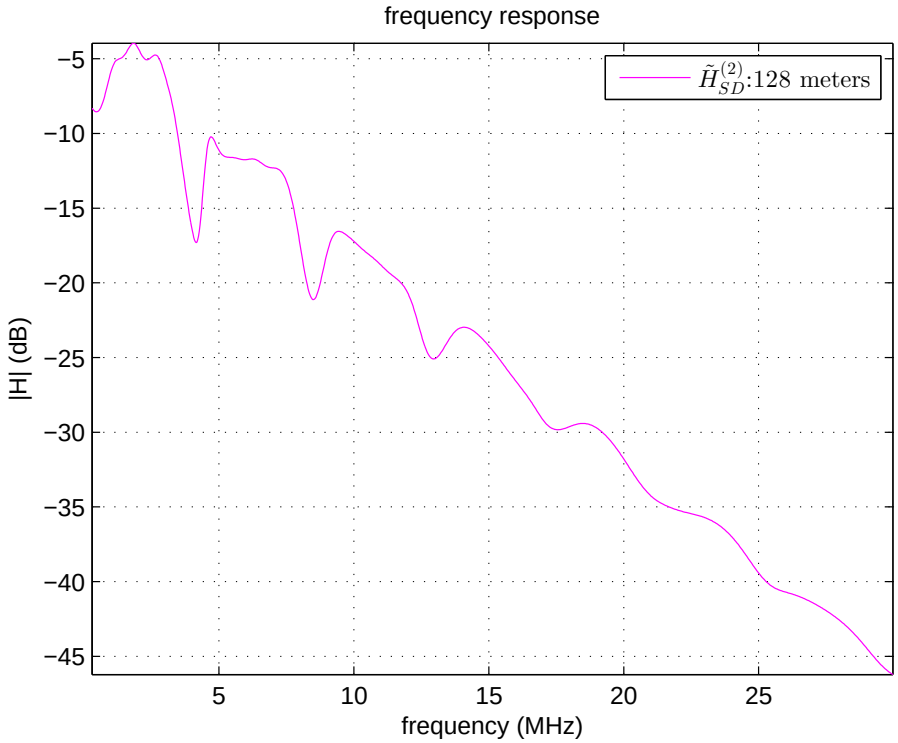

Figure 3.28: CTF result for the source-to-destination path in the second phase.

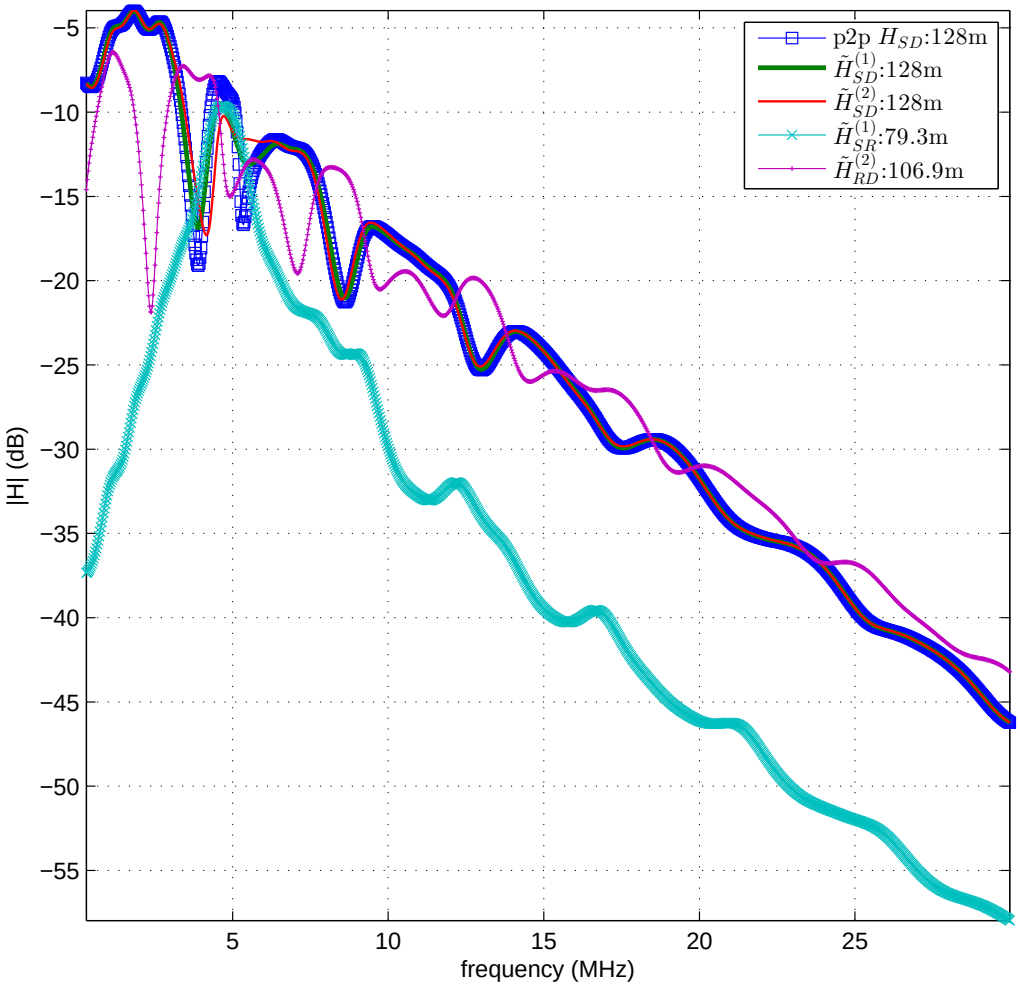

Figure 3.29: CTF comparison of different signaling path of the relay-involved PLC channel, where the P2P case is also given as a reference.

$$H_{SD} \neq \tilde{H}_{SD}^{(1)} \neq \tilde{H}_{SD}^{(2)} \tag{3.51}$$

and

$$\tilde{H}_{SD}^{(1)} \neq \tilde{H}_{SR}^{(1)} \tilde{H}_{RD}^{(2)} \tag{3.52}$$

$$\tilde{H}_{SD}^{(2)} \neq \tilde{H}_{SR}^{(1)} \tilde{H}_{RD}^{(2)}. \tag{3.53}$$

These results verified the conclusion we drawn in Section 3.2.

We point out that the above discussion is only concerned about the one-way (i.e. from the source node to the detonation node) transmission situation. We will consider the two-way information exchange PLC systems in Chapter 6, and its corresponding CTF of different paths will be derived then.

3.4 Chapter summary

Contrasted to the wireless relaying scenario, relay-involved PLC channel presents high correlation among different paths; appearing of any branched circuit connection (including the relay device itself) affects the channel transfer functions on each signaling path. Based on the transmission line theory analysis, we applied a general ABCD method to compute the CTF of the relay-involved PLC channel. With some strategical configuration, we developed a simple way to transform the relay-involved channel CTF generation problem into an equivalent P2P PLC channel case, which can be readily realized by applying the hybrid PLC channel model published in [32–34].

Simulation results verified our conclusion that, in general the CTF of relay-involved PLC channel cannot be obtained by simply multiplying several independent P2P PLC channels. As the simple CTF generation approach in this chapter is a direct application of the measurement verified Canate's model, our generated relay-involved channel samples establishes a realistic test platform for our relay schemes discussed in later chapters.

NOTE: Start from the next chapter, the remaining of this thesis is all about the relay-involved PLC channel condition. For notation convenience, we will use H_{SD}, H_{SR} and H_{RD} respectively to refer to $\tilde{H}_{SD}$, $\tilde{H}_{SR}$ and $\tilde{H}_{RD}$ shown in this chapter unless especially mentioned.

Chapter 4

Location of Relay Devices

In this chapter, we consider the situations where the power of the PLC devices have been fixed by the manufacturer, then the following questions need to be answered.

(1) Where are the best locations for the user to choose to implement their relay devices?

(2) How much benefit the system can get with the extra usage of relay devices under the same total power consumption?

As we are interested in the broadband PLC system, where multiple subcarriers has been used simultaneously, a criteria used to evaluate the best location choice need to be defined firstly. Apparently, several metrics can play this role. Ideally, we can define the criteria as to make every subcarrier signal obtain the best signal-to-noise ratio (SNR) at the same time. However, this is not feasible in general. On one hand, as the indoor PLC channel is highly frequency-selective, i.e. each PLC subchannel has a different attenuation level. On the other hand, the position change of one outlet (where the relay device is implemented) affects the channel attenuation of all subcarriers. Thus, this leads to the situation that for different subchannels, different locations should be chosen, which is obviously not physically possible for one relay device.

Hence as a practical solution, we can define the criteria as to make the most of the subcarriers obtain the best SNR, or as to make the system averaged receiving SNR to obtain the highest value. In this chapter, we adopt the latter approach. In other words, we analyze the best location choice for the relay nodes to implement in order to optimize the averaged performance among all subcarriers.

The reminder of this chapter is organized as follows. Section 4.1 gives a brief review of the related results both in theoretical research and industrial products. The single relay system is considered in Section 4.2, while Section 4.3 extends the discussion to the systems with multiple relay nodes. The comparison of the results with the conventional direct transmission (DT) system has be presented after these analysis in Section 4.4. Finally, we summarize this chapter by giving answers for the above proposed questions.

4.1 Literature review

There are surprisingly few published results on the selection of the relay location in the literature. In [41], the authors consider a special case, where the AF relay-assisted PLC system is used on the outdoor long distance middle voltage (MV) power lines. Under this special applicant scenario, it is common to use the relay device to recover the power of the attenuated communication signal, i.e. set the relay power to be equal to the source transmission power. As there is no tap-branches on MV power cable, the best location choice for relay device to deploy is at the *middle point* of the MV cable, which makes the attenuation of the signaling paths of source-to-relay and relay-to-destination equal. However, this conclusion does not hold for the indoor relay-assisted PLC system due to the following two reasons: (1) Unlike the outdoor MV cable case, there are only limited number of preexisting outlet locations which can be chosen to deploy the relay devices. (2) Different types of branches exist on the backbone of the indoor PLC cabling topology as we showed in Chapter 3.

On the other hand, on the market there are already some indoor PLC adapters which provide a kind of "self-assisting" feature to help the users to decide the best location choice for their PLC transceivers. As an example shown in Fig. 4.1, this PLC modem is equipped a "link quality" LED indicator using different color lighting to show the users an approximate idea about the data speed of link under the current implementation[42]. For the users who want to measure the exact real-time transmitting and receiving throughput of the system, a software application called "Powerline Utility" is also available as shown in Fig. 4.2. Although currently these functions are only available for the transceivers on the market, the same solution can be applied on PLC relay devices.

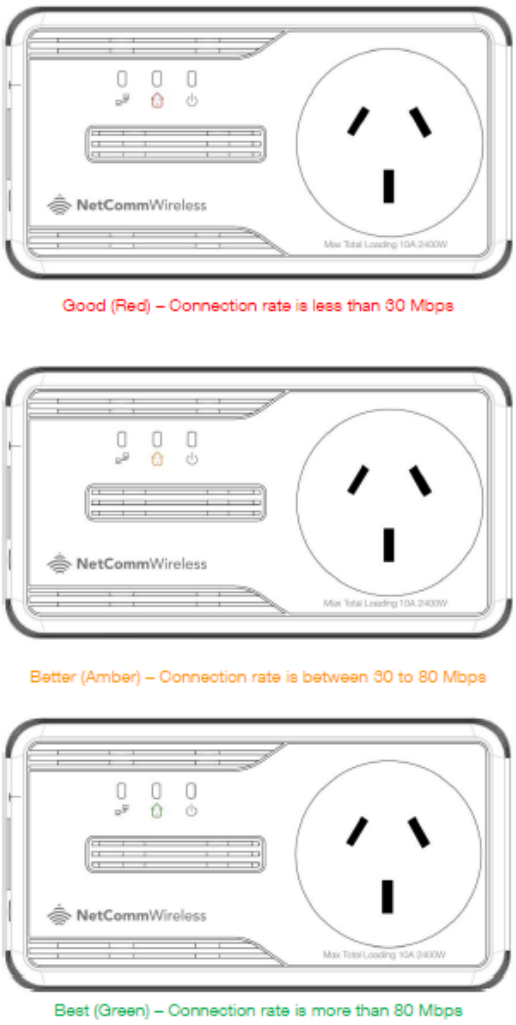

Figure 4.1: Each color of the “link quality” LED represents a connection rating.

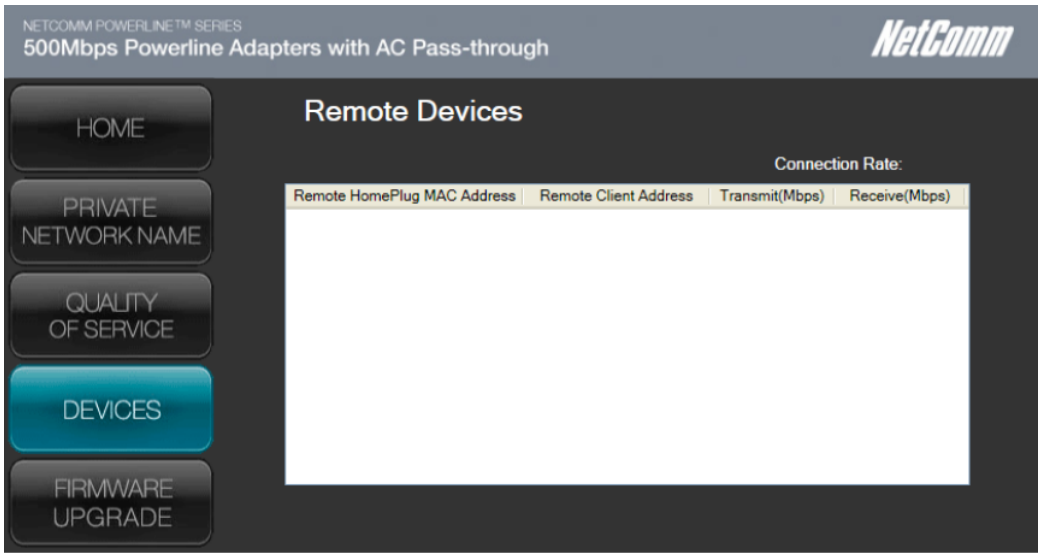

Figure 4.2: User interface displays the current link speed.

4.2 Location selection for single relay device

Let us consider an indoor PLC transmission scenario, where a source outlet S needs to send messages to a destination outlet D through a PLC network Φ_T between them, as shown in Fig. 4.3. Note here the PLC network Φ_T consists of three segments, namely (1) the backbone segment Φ_{SP} between the source outlet and the break point P; (2) the backbone segment Φ_{PD} between the destination outlet and the point P; and (3) the branch segment Φ_{PR}. It is often possible for the users to find another outlet R, on the backbone or on a branch, which located somewhere in the middle of the source and the destination nodes. Without losing generality, let us assume this relay outlet is located on the terminal of the branch segment Φ_{PR}, and the situation that the relay outlet is located on backbone can be treated as a special case in which the ABCD matrix of the branch segment

$$\Phi_{PR} = \begin{bmatrix} 1 & 0 \\ 0 & 1 \end{bmatrix}. \tag{4.1}$$

With this relay outlet, a relay device can be easily introduced and we refer to it as the relay node in the following. Using the CTF calculation method we developed in Chapter 3, we can obtain the CFT of the different signaling paths in this relay-involved PLC channel, i.e. $h_{SD}(f)$, $h_{SR}(f)$ and $h_{RD}(f)$ for the source-to-destination path, the source-to-relay path and

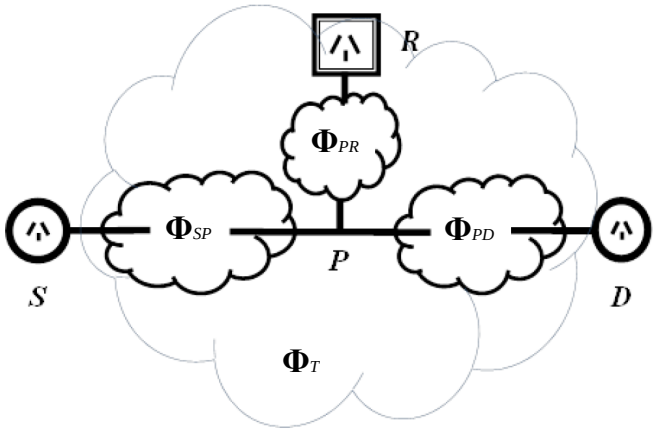

Figure 4.3: An indoor PLC transmission scenario.

the relay-to-destination path, respectively, where f means the frequency. Also we denote $\alpha_{SD}(f)$, $\alpha_{SR}(f)$ and $\alpha_{RD}(f)$ as the power attenuation density (PAD) of these three signaling paths respectively, then we can write

$$\alpha_{SD}(f) = |h_{SD}(f)|^2 \tag{4.2}$$

$$\alpha_{SR}(f) = |h_{SR}(f)|^2 \tag{4.3}$$

$$\alpha_{RD}(f) = |h_{RD}(f)|^2 \tag{4.4}$$

where the path PAD $\alpha_{L_1L_2}(f)$ (where $L_1 \in \{S,R\}$ and $L_2 \in \{R,D\}$) are frequency-selective and, obviously, depend on the location choice of the relay outlet R.

Based on these configuration, the block diagram of a relay-assisted broadband PLC system can be proposed as shown in Fig. 4.4, which consists of three nodes, i.e. the source node (S), the destination node (D) and the relay node (R). Let us denote the transmit power spectrum density (PSD) of the source node as $p_S(f)$, so that the signaling power from the source node is

$$P_S = \int_{f_0}^{f_1} p_S(f)df \tag{4.5}$$

where f_0 and f_1 are the lower and upper bonds of the system bandwidth. On the other

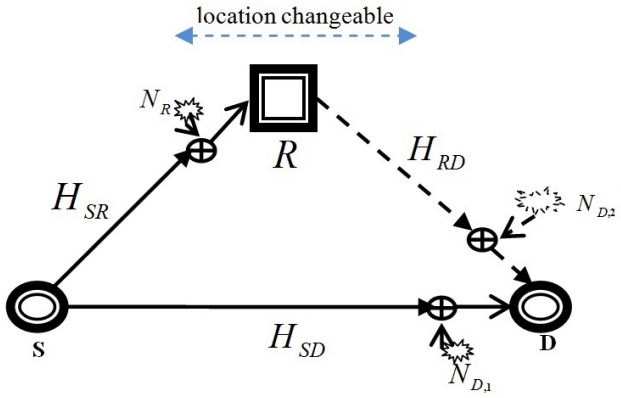

Figure 4.4: A relay-assisted broadband PLC system, where the dash line indicates the second signaling phase.

hand, the corresponding receiving PSD at the detonation node, denoted by $q_D(f)$, can be expressed as

$$q_D(f) = \alpha_{SD}(f) p_S(f). \tag{4.6}$$

Thus the receiving power at the end of the source-to-destination path, denoted as P_D, can be written as

$$\begin{aligned} P_D &= \int_{f_0}^{f_1} q_D(f) df \\ &= \int_{f_0}^{f_1} \alpha_{SD}(f) p_S(f) df \\ &= \alpha_{SD}(\Theta) \int_{f_0}^{f_1} p_S(f) df, \; f_0 < \Theta < f_1 \\ &= \alpha_{SD}(\Theta) P_S, \; f_0 < \Theta < f_1. \end{aligned} \tag{4.7}$$

Note we used the *first mean value theorem for integration* in the derivation of (4.7).

Actually, $|\alpha_{SD}(\Theta)|$ in (4.7) is a metric for the *average power attenuation* (APA) of the source-to-destination path, and in the following we will simply denote it as α_{SD}. Similarly we can define the APA of the relay-to-destination path and the source-to-relay path, respectively, as α_{RD} and α_{SR}.

We assume that coherent signal combination is used at the receiver, and the relay node works with AF signal processing mode while time-division duplexing (TDD) is assumed to satisfy

the half-duplexing constraint of the relay device.Thus the relay-assisted data transmission system works in two stages as illustrated in Fig. 4.4.

In the first stage, the source node broadcasts message signal $X(f)$ with power P_S. The relay node and the destination node receive this signal with different channel attenuation and noises. In the frequency domain, they can be written as

$$Y_R(f) = h_{SR}(f)X(f) + N_R(f) \tag{4.8}$$

$$Y_{D,1}(f) = h_{SD}(f)X(f) + N_{D,1}(f) \tag{4.9}$$

where $N_R(f)$ and $N_{D,1}(f)$ are the noise at relay node and destination node, respectively, in this stage.

It is easy to calculate the signal-to-noise ratio (SNR) in this stage at the destination as

$$SNR_{(1)} = \frac{\alpha_{SD}P_S}{W_{D,1}} \tag{4.10}$$

where $W_{D,1}$ is the noise power at destination in the first stage.

At the second stage, the relay node amplifies their received signal with power gain β, and forwards it to the destination with power P_R. Thus the received signal at the destination at this stage is written as

$$Y_{D,2}(f) = \sqrt{\beta}Y_R(f)h_{RD}(f) + N_{D,2}(f) \tag{4.11}$$

where $N_{D,2}(f)$ is the noise at the destination node in the second stage.

Substituting (4.8) into (4.11), we get

$$Y_{D,2}(f) = \sqrt{\beta}h_{SR}(f)h_{RD}(f)X(f) + \sqrt{\beta}h_{RD}(f)N_R(f) + N_{D,2}(f). \tag{4.12}$$

As the power of signal $Y_R(f)$ can be calculated as $P_S\alpha_{SR} + W_R$, we have

$$\beta = \frac{P_R}{P_S\alpha_{SR} + W_R} \tag{4.13}$$

where W_R is the noise power at the relay node. From (4.12), we can calculate the SNR at the destination node at this second phase as

$$SNR_{(2)} = \frac{\beta\alpha_{SR}\alpha_{RD}P_S}{P_R\beta\alpha_{RD} + W_{D,2}} \tag{4.14}$$

where $W_{D,2}$ is the noise power at destination in the second stage. For simplicity ,we assume $W_{D,1} = W_{D,2} = W_R = W$, i.e. the different node of the system share the same noise PSD, even though this is not always true as we discussed in Chapter 2.

Finally, the receiver combines the signals in (4.9) and (4.14) with the maximum ratio combing (MRC) technique, so that the effective SNR can be expressed as

$$\begin{aligned} SNR &= SNR_{(1)} + SNR_{(2)} \\ &= \frac{\alpha_{SD} P_S}{W} + \frac{\alpha_{SR}\alpha_{RD} P_S P_R}{P_S W \alpha_{SR} + W^2 + P_R W \alpha_{RD}}. \end{aligned} \tag{4.15}$$

4.2.1 Finite benefit from relay power

By observing (4.15), we can see that the higher relay power P_R used, the better SNR performance will be achieved. However, this trend will not last infinite, but converge to certain limitation. This can be shown as

$$\begin{aligned} &\lim_{P_R \to \infty} SNR \\ =&\lim_{P_R \to \infty} \left(\frac{\alpha_{SD} P_S}{W} + \frac{\alpha_{SR}\alpha_{RD} P_S P_R}{P_S W \alpha_{SR} + W^2 + P_R W \alpha_{RD}} \right) \\ =&\frac{P_S}{W} (\alpha_{SD} + \alpha_{SR}). \end{aligned} \tag{4.16}$$

An illustration of the convergence of AF relay power's benefit has been given in Fig. 4.5, where the convenient DT system's performance appears as a benchmark.

4.2.2 Optimal relay location

In practice, there are usually more than one outlet available between the transceivers. To benefit as much as possible from the relay power, we need to decide which outlet we should choose to deploy the relay device. Mathematically, for given P_S, P_R and W, this problem boils down to solve the optimization problem as

$$\max_{\alpha_{SR}} \frac{\alpha_{SD} P_S}{W} + \frac{\alpha_{SR}\alpha_{RD} P_S P_R}{P_S W \alpha_{SR} + W^2 + P_R W \alpha_{RD}} \tag{4.17}$$

$$s.t. \qquad 0 < \alpha_{SD} < \alpha_{SR} \leq 1. \tag{4.18}$$

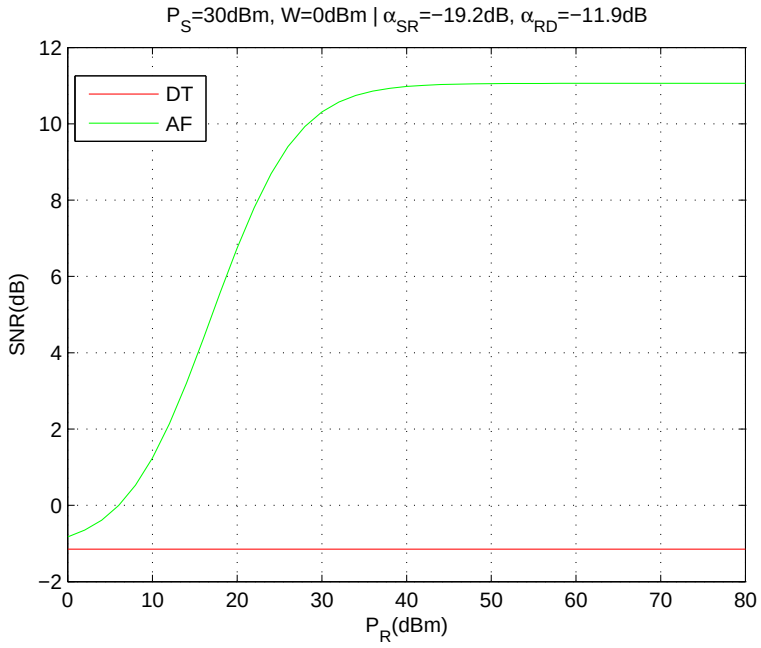

Figure 4.5: Convergence of the benefit from AF relay power, compared with the DT scheme which does not use any relay power.

Note in (4.17) the first term is constant. By using Cauchy-Schwartz inequality, it is easy to show that

$$\frac{P_S P_R \alpha_{SR} \alpha_{RD}}{P_S W \alpha_{SR} + W^2 + P_R W \alpha_{RD}} \leq \frac{P_S P_R \alpha_{SR} \alpha_{RD}}{W^2 + 2W\sqrt{P_R P_S \alpha_{SR} \alpha_{RD}}} \tag{4.19}$$

where the equality is only achieved when

$$P_S \alpha_{SR} = P_R \alpha_{RD}. \tag{4.20}$$

To better illustrate the physical meaning of result (4.20), we can rewrite it equivalently as

$$\frac{\alpha_{RD}}{\alpha_{SR}} = \frac{P_S}{P_R}. \tag{4.21}$$

Thus we find (4.21) is the condition for the optimal location of the relay node. It indicates that theoretically to get the most benefit from the relay power, the user of indoor PLC system should deploy the relay device at the outlet where the ratio of attenuation of the relay-to-destination channel and source-to-relay channel is equal to the ratio of the source and relay power. Obviously, conclusion (4.21) generalizes the result found for the MV outdoor relay-assisted PLC case in [41].

However, in a realistic indoor power line grid it is not always possible to find an outlet which satisfies the above condition. But, this gives us suggestion about the best-effort choice. In other words, if we have the attenuation information of the channels, we can use (4.21) as an ideal reference to decide the location choice of the relay node. We will examine more details about this with a numerical example in the next subsection.

Fig. 4.6 shows the comparison of SNR of the AF relay system with the DT system versus the difference between α_{RD} and α_{SR} in dB. Note that in the DT case, SNR does not change as there is no relay node introduced. In addition to illustrating the fact of (4.21), it also shows that for a given relay power P_R, as the transmit power P_S increases, the SNR improvement from AF relay scheme becomes less significant.

4.2.3 A practical example

To illustrate the optimal relay node location choosing method, let us consider a practical example as shown in Fig. 4.7. Between the source and destination nodes, there are two available outlets, namely A and B. It is easy to measure the channels' APA between locations S, A, B and D with a simple channel sounding technique. Thus we can use (4.21) as a criterion to decide which outlet we should choose to deploy the relay device for a better performance improvement.

Here, by assuming the source power and relay power are equally fixed by the manufacturer (i.e. $P_S = P_R$), we calculate as follows.

(1) If location A is chosen, then

$$\begin{aligned}\frac{\alpha_{AD}}{\alpha_{SA}} &= (-5.2dB - 13.6dB) - (-20.1dB) \\ &= 1.3dB. \end{aligned} \tag{4.22}$$

(2) If location B is chosen, then

$$\begin{aligned}\frac{\alpha_{BD}}{\alpha_{SB}} &= (-13.6dB) - (-20.1dB - 5.2dB) \\ &= 11.7dB. \end{aligned} \tag{4.23}$$

By comparing (4.22) and (4.23), we find that the value of (4.22) is more close to $\frac{P_S}{P_R} = 0$ dB. This means choosing outlet A can make the situation more close to the best condition.

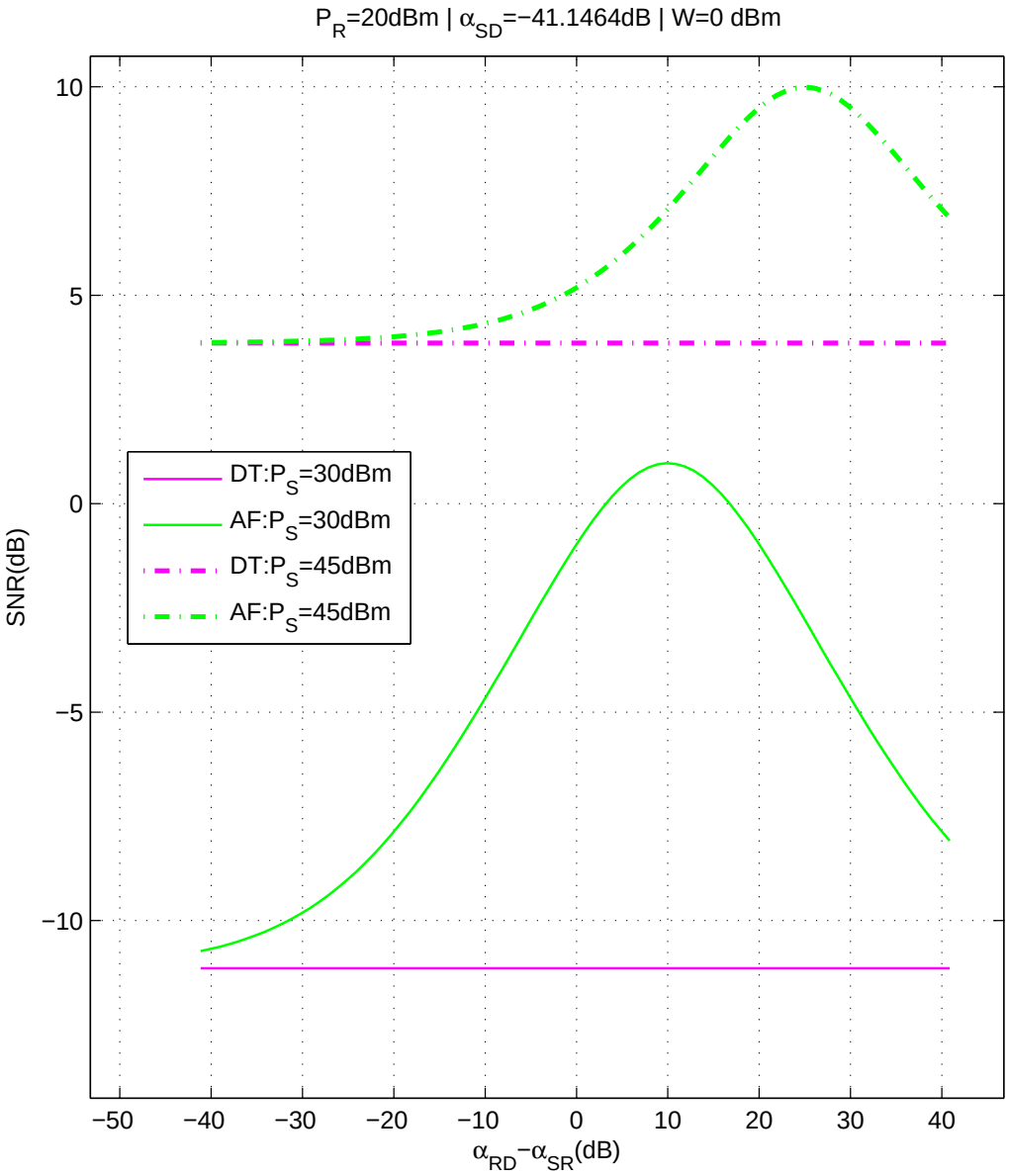

Figure 4.6: SNR of the AF relay scheme with varying ratio of path attenuation, which is decided by relay node's location, compared with the DT scheme.

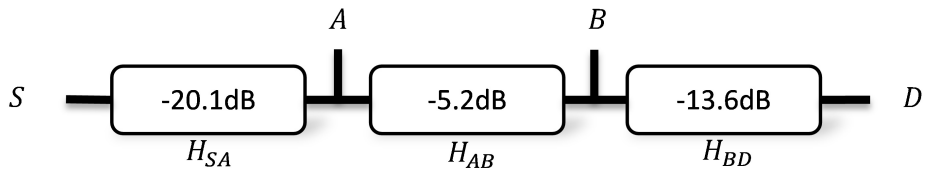

Figure 4.7: A practical example of relay location selection.

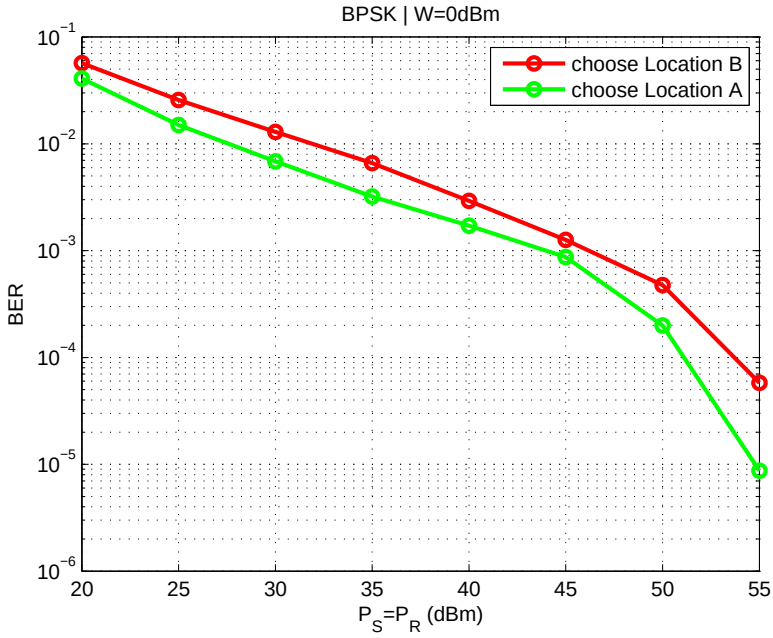

Figure 4.8: Simulation result for the practical example in Fig. 4.7.

In other words, outlet A is the best-effort choice here. This choice has been verified by numerical result as shown in Fig. 4.8, where the system simulation parameters, which follow the HomePlug AV specification[14], have been given in Table 4.1.

4.3 Location selection for multiple relay devices

In this section, we take a step further to generalize our discussion to the situation where N ($N \geq 2$) relay nodes simultaneously work to enhance the system performance. For simplicity,we firstly discuss the special case of two relay nodes involved (i.e. $N = 2$) in detail, then the generalization to the case of more than two relay devices introduced is straightforwardly given. Thus the system diagram can be given in Fig. 4.9. Let us denote the two relay nodes

Table 4.1: Parameters for simulation of example in Fig. 4.7

Frequency band		from 2MHz to 28MHz
OFDM	total subcarriers number	1156
	used subcarriers number	917
Modulation mode		fixed BPSK
The power of noise on channel		0dBm

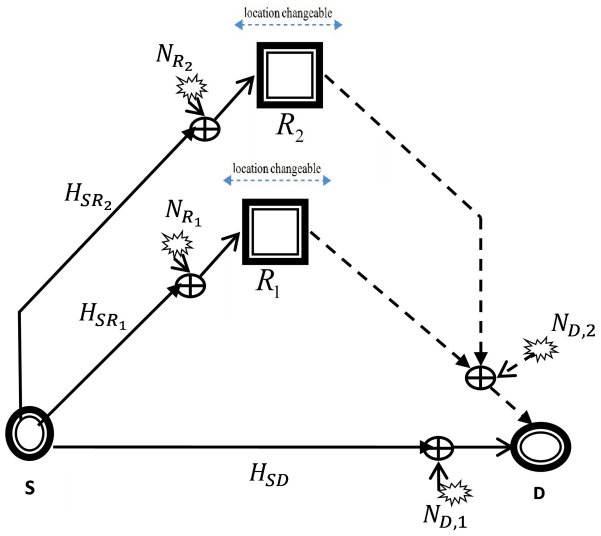

Figure 4.9: Diagram of the broadband PLC system, where source node (S) transmits information to the destination node (D) with the aid of two relay nodes (R_1 and R_2) simultaneously.

as R_1 and R_2 and use the notation system we defined in Section 4.2. Similar to the single relay case, the multiple relays assist data transmission in two stages as follows.

In the first stage, the source node broadcasts message signal $X(f)$ with power P_S. The two relay nodes (R_1 and R_2) and the destination node (D) receive this signal with different channel attenuation and noises. In the frequency domain, they can be written respectively

as

$$Y_{R_1}(f) = h_{SR_1}(f)X(f) + N_{R_1}(f) \tag{4.24}$$

$$Y_{R_2}(f) = h_{SR_2}(f)X(f) + N_{R_2}(f) \tag{4.25}$$

$$Y_{D,1}(f) = h_{SD}(f)X(f) + N_{D,1}(f) \tag{4.26}$$

where $N_{R_1}(f)$, $N_{R_2}(f)$ and $N_{D,1}(f)$ are the noise at relay node R_1 and R_2, and destination node D, respectively, in this stage.

It is easy to calculate the SNR in this stage at the destination as

$$SNR_{(1)} = \frac{\alpha_{SD}P_S}{W_{D,1}} \tag{4.27}$$

where $W_{D,1}$ is the noise power at destination in the first stage.

At the second stage, the two relay nodes amplify its received signal $Y_{R_1}(f)$ and $Y_{R_2}(f)$ with amplitude gain $\sqrt{\beta_1}\exp(j\theta_1)$ and $\sqrt{\beta_2}\exp(j\theta_2)$ respectively, and simultaneously forward it to the destination with power P_{R_1} and P_{R_2}. Thus the received signal at the destination at this stage is written as

$$\begin{aligned} Y_{D,2}(f) = &\sqrt{\beta_1}\exp(j\theta_1)Y_{R_1}(f)h_{R_1D}(f) \\ &+ \sqrt{\beta_2}\exp(j\theta_2)Y_{R_2}(f)h_{R_2D}(f) \\ &+ N_{D,2}(f) \end{aligned} \tag{4.28}$$

where $N_{D,2}(f)$ is the noise at the destination node in the second stage.

Substituting (4.24) and (4.25) into (4.28), we get

$$\begin{aligned} Y_{D,2}(f) = &\sqrt{\beta_1}\exp(j\theta_1)h_{SR_1}(f)h_{R_1D}(f)X(f) + \sqrt{\beta_2}\exp(j\theta_2)h_{SR_2}(f)h_{R_2D}(f)X(f) \\ &+ \sqrt{\beta_1}\exp(j\theta_1)N_{R_1}(f)h_{R_1D}(f) + \sqrt{\beta_2}\exp(j\theta_2)N_{R_2}(f)h_{R_2D}(f) \\ &+ N_{D,2}(f). \end{aligned} \tag{4.29}$$

Given the the channel state information (CSI) is known by the two relay nodes, by properly choosing the phase adjusters θ_1 and θ_2, these two signal components

$$\sqrt{\beta_1}\exp(j\theta_1)h_{SR_1}(f)h_{R_1D}(f)X(f)$$

and

$$\sqrt{\beta_2}\exp(j\theta_2)h_{SR_2}(f)h_{R_2D}(f)X(f)$$

in (4.29) can be made co-phase to each other. As the power of signal $Y_{R_1}(f)$ can be calculated as $P_S\alpha_{SR_1}+W_{R_1}$,while the power of signal $Y_{R_2}(f)$ can be calculated as $P_S\alpha_{SR_2}+W_{R_2}$, the power gain of relay node R_1 can be expressed as

$$\beta_1 = \frac{P_{R_1}}{P_S\alpha_{SR_1}+W_{R_1}} \tag{4.30}$$

and power gain of relay node R_2 as

$$\beta_2 = \frac{P_{R_2}}{P_S\alpha_{SR_2}+W_{R_2}} \tag{4.31}$$

where W_{R_1} and W_{R_2} are the powers of noise N_{R_1} and N_{R_2}, respectively. Noting the noise N_{R_1}, N_{R_2} and $N_{D,2}$ are assumed to be independent to each other, from (4.29) we can calculate the SNR at the destination node at the second phase as

$$SNR_{(2)} = \frac{(\beta_1\alpha_{SR_1}\alpha_{R_1D}+\beta_2\alpha_{SR_2}\alpha_{R_2D})P_S}{\beta_1\alpha_{R_1D}W_{R_1}+\beta_2\alpha_{R_2D}W_{R_2}+W_{D,2}} \tag{4.32}$$

where $W_{D,2}$ is the noise power at destination in the second stage. Again, for simplicity we assume $W_{D,1}=W_{D,2}=W_R=W$, i.e. the noise at different nodes of the system are i.i.d.

Finally, the receiver combines the signals in (4.26) and (4.28) with the MRC technique, so that the effective SNR can be expressed as

$$\begin{aligned} SNR &= SNR_{(1)}+SNR_{(2)} \\ &= \frac{\alpha_{SD}P_S}{W}+\frac{P_S}{W}\left(\frac{\frac{P_{R_1}\alpha_{SR_1}\alpha_{R_1D}}{\alpha_{SR_1}P_S+W}+\frac{P_{R_2}\alpha_{SR_2}\alpha_{R_2D}}{\alpha_{SR_2}P_S+W}}{1+\frac{\alpha_{R_1D}P_{R_1}}{\alpha_{SR_1}P_S+W}+\frac{\alpha_{R_2D}P_{R_2}}{\alpha_{SR_2}P_S+W}}\right). \end{aligned} \tag{4.33}$$

4.3.1 Optimal relay locations

In practice, between the transceivers there are usually more than two outlets available to introduce the two relay nodes. To benefit as much as possible from the relay powers, we need to decide which outlets we should choose to deploy the relay devices. Mathematically, for given noise power W, source power P_S, and relay powers $P_{R_1}$and P_R, the problem of best

locations choice boils down to solve the optimization problem formulated as

$$\max_{\alpha_{SR_1},\alpha_{SR_2}} \frac{\alpha_{SD}P_S}{W} + \frac{P_S}{W}\left(\frac{\frac{P_{R_1}\alpha_{SR_1}\alpha_{R_1D}}{\alpha_{SR_1}P_S+W} + \frac{P_{R_2}\alpha_{SR_2}\alpha_{R_2D}}{\alpha_{SR_2}P_S+W}}{1+\frac{\alpha_{R_1D}P_{R_1}}{\alpha_{SR_1}P_S+W}+\frac{\alpha_{R_2D}P_{R_2}}{\alpha_{SR_2}P_S+W}}\right) \tag{4.34}$$

$$s.t. \qquad 0 < \alpha_{SD} < \alpha_{SR_1}, \alpha_{SR_2} < 1. \tag{4.35}$$

As in (4.34) the first term and the first factor of the second term are constant, the remaining part can be equally written as

$$\frac{\frac{P_{R_1}\alpha_{SR_1}\alpha_{R_1D}}{\alpha_{SR_1}P_S+W}}{1+\frac{\alpha_{R_1D}P_{R_1}}{\alpha_{SR_1}P_S+W}+\frac{\alpha_{R_2D}P_{R_2}}{\alpha_{SR_2}P_S+W}} + \frac{\frac{P_{R_2}\alpha_{SR_2}\alpha_{R_2D}}{\alpha_{SR_2}P_S+W}}{1+\frac{\alpha_{R_1D}P_{R_1}}{\alpha_{SR_1}P_S+W}+\frac{\alpha_{R_2D}P_{R_2}}{\alpha_{SR_2}P_S+W}}. \tag{4.36}$$

Note we can write

$$(4.36) \leq \frac{\frac{P_{R_1}\alpha_{SR_1}\alpha_{R_1D}}{\alpha_{SR_1}P_S+W}}{1+\frac{\alpha_{R_1D}P_{R_1}}{\alpha_{SR_1}P_S+W}} + \frac{\frac{P_{R_2}\alpha_{SR_2}\alpha_{R_2D}}{\alpha_{SR_2}P_S+W}}{1+\frac{\alpha_{R_2D}P_{R_2}}{\alpha_{SR_2}P_S+W}} \tag{4.37}$$

$$= \frac{P_{R_1}\alpha_{SR_1}\alpha_{R_1D}}{\alpha_{SR_1}P_S+\alpha_{R_1D}P_{R_1}+W} + \frac{P_{R_2}\alpha_{SR_2}\alpha_{R_2D}}{\alpha_{SR_2}P_S+\alpha_{R_2D}P_{R_2}+W} \tag{4.38}$$

$$\leq \frac{P_{R_1}\alpha_{SR_1}\alpha_{R_1D}}{2\sqrt{P_SP_{R_1}\alpha_{SR_1}\alpha_{R_1D}}+W} + \frac{P_{R_2}\alpha_{SR_2}\alpha_{R_2D}}{2\sqrt{P_SP_{R_2}\alpha_{SR_2}\alpha_{R_2D}}+W} \tag{4.39}$$

where, as a result of the Cauchy-Schwartz inequality, the equality in (4.39) can be achieved only when

$$\begin{cases} \frac{\alpha_{R_1D}}{\alpha_{SR_1}} = \frac{P_S}{P_{R_1}} \\ \frac{\alpha_{R_2D}}{\alpha_{SR_2}} = \frac{P_S}{P_{R_2}} \end{cases} \tag{4.40}$$

Thus we find (4.40) is the condition for the optimal locations of the relay nodes. Interestingly, this indicates that when two relay nodes are introduced, the problem of simultaneous best location selection for the relay devices can be separately dealt one by one, i.e. each individual choice (for R_1 or R_2) subjects to one node best location condition (4.21) respectively. In other words, the best location choice condition for R_1 and R_2 are independent to each other.

In addition to illustrating the fact of (4.40), Fig. 4.10 shows SNR of the relay scheme when different location chosen for the two relay nodes, compared with the DT system. Note that in the DT case, SNR does not change as there is no relay node introduced.

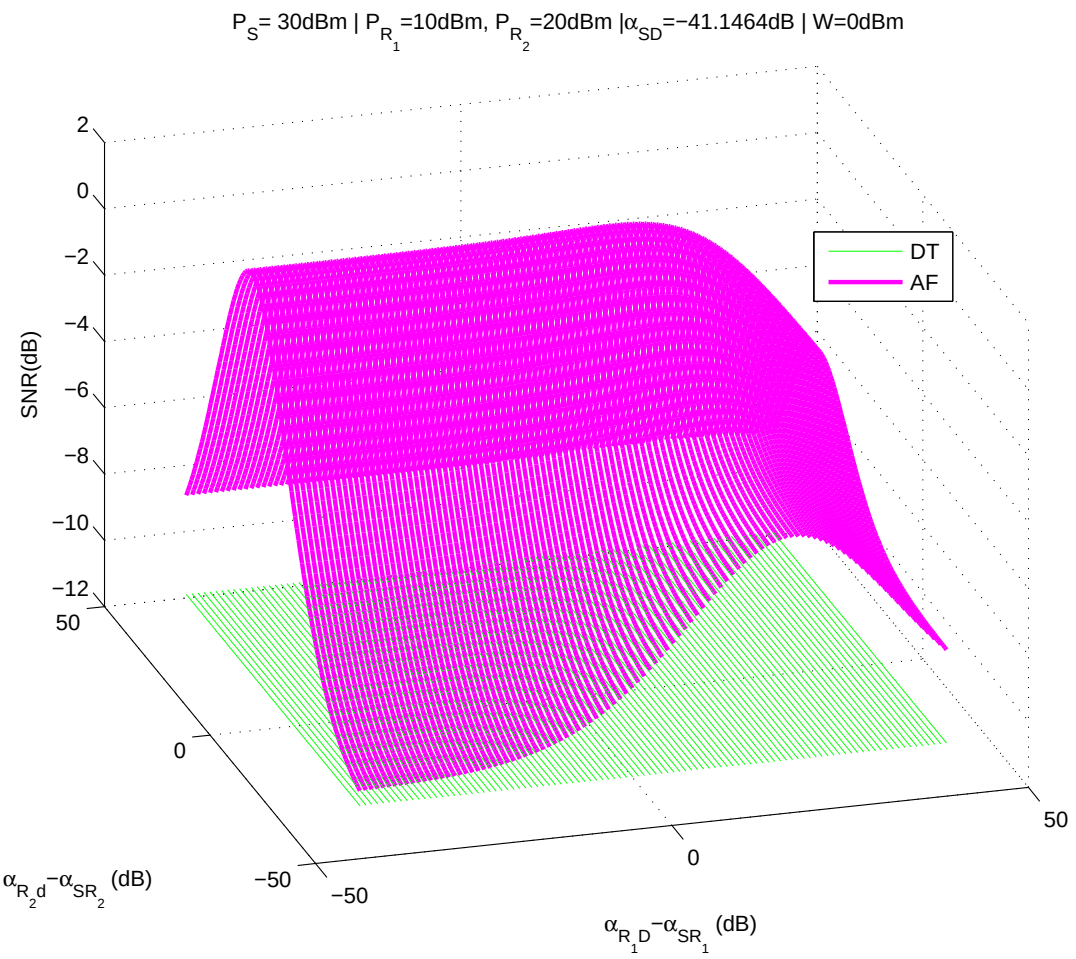

Figure 4.10: SNR of the two relay scheme with varying ratio of attenuation, compared with the DT scheme.

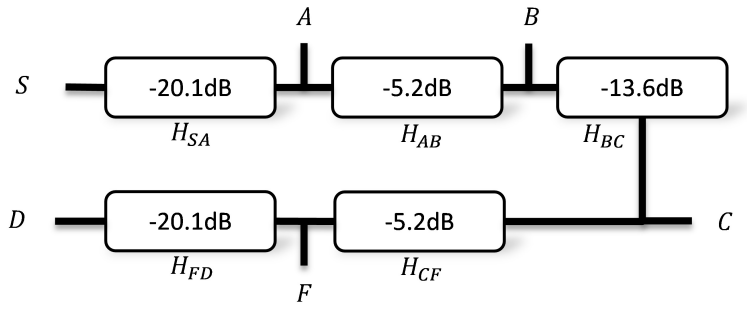

Figure 4.11: A practical example for multiple relays location selection.

4.3.2 A practical example

To illustrate the optimal relay node location selection method for the multiple relay nodes case, let us also consider a practical example as shown in Fig. 4.11. Between the source and destination nodes, there are four available outlets, namely A, B, C and F. Assuming that two relay devices need to be deployed at two locations, then the user needs to decide from the following location combinations:

$$(A,B),(A,C),(A,F),(B,C),(B,F),(C,F) \tag{4.41}$$

It is easy to measure the the channels' average power attenuation between each pair of outlets with a simple channel sounding technique. Thus we can use (4.40) as a criterion to decide which outlet we should choose to deploy the relay device for a better performance improvement.

Here, we assume the source power and relay power are equally fixed by the manufacturer as $P_S = \frac{1}{8}P_{R_1} = \frac{1}{8}P_{R_2}$, i.e.

$$\frac{P_S}{P_{R_1}} + \frac{P_S}{P_{R_2}} = -6dB, \tag{4.42}$$

we calculate as follows.

(1) If combination (A,B) is chosen, then

$$\begin{aligned}\frac{\alpha_{AD}}{\alpha_{SA}}+\frac{\alpha_{BD}}{\alpha_{SB}} &= -24dB-13.6dB \\ &= -37.6dB. \end{aligned} \tag{4.43}$$

(2) If combination (A,C) is chosen, then

$$\begin{aligned}\frac{\alpha_{AD}}{\alpha_{SA}}+\frac{\alpha_{CD}}{\alpha_{SC}} &= -24dB+13.6dB \\ &= -10.4dB. \end{aligned} \tag{4.44}$$

(3) If combination (A,F) is chosen, then

$$\begin{aligned}\frac{\alpha_{AD}}{\alpha_{SA}}+\frac{\alpha_{FD}}{\alpha_{SF}} &= -24dB+24dB \\ &= 0dB. \end{aligned} \tag{4.45}$$

(4) If combination (B,C) is chosen, then

$$\begin{aligned}\frac{\alpha_{BD}}{\alpha_{SB}}+\frac{\alpha_{CD}}{\alpha_{SC}} &= -13.6dB+13.6dB \\ &= 0dB. \end{aligned} \tag{4.46}$$

(5) If combination (B,F) is chosen, then

$$\begin{aligned}\frac{\alpha_{BD}}{\alpha_{SB}}+\frac{\alpha_{FD}}{\alpha_{SF}} &= -13.6dB+24dB \\ &= 10.4dB. \end{aligned} \tag{4.47}$$

(6) If combination (C,F) is chosen, then

$$\begin{aligned}\frac{\alpha_{CD}}{\alpha_{SC}}+\frac{\alpha_{FD}}{\alpha_{SF}} &= 13.6dB+24dB \\ &= 37.6dB. \end{aligned} \tag{4.48}$$

By comparing (4.43)-(4.48) with (4.42), we find that the value of (4.44) is most close to -6dB. This means choosing outlets A and C can make the situation more close to the best

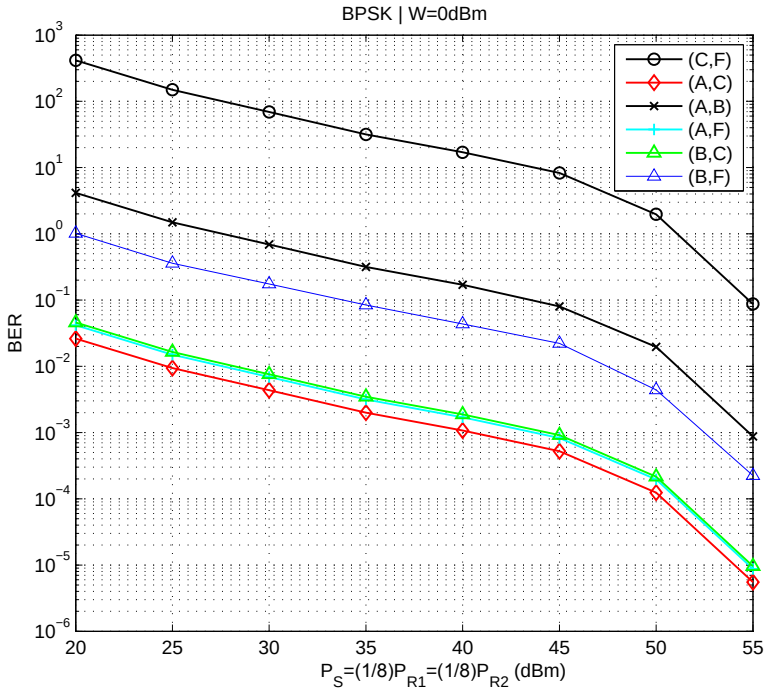

Figure 4.12: Simulation result for the practical example in Fig. 4.11.

condition. In other words, outlets combination (A,C) is the best-effort choice here. This choice has been verified by numerical simulation result as shown in Fig. 4.12. The simulation parameters are still set as in Table 4.1.

4.3.3 Generalization to the N relay devices case

From the discussion in the last two subsections, we can readily extend our conclusion (4.21) and (4.40) to the general case, where N ($N \geq 2$) relay nodes simultaneously work to enhance the system performance. We propose this conclusion as the following proposition.

IDEAL LOCATIONS CONDITION: For a relay-assisted PLC system, given its noise power W, source power P_S, and relay powers P_{R_i} ($i = 1,2,...,N$), if there are N outlets R_i ($i = 1,2,...,N$) are available between the transceivers, then the condition for the best location choice of the N relay devices expressed as set

$$\left\{ \frac{\alpha_{R_iD}}{\alpha_{SR_i}} = \frac{P_S}{P_{R_i}}, i = 1,2,...,N \right\}$$

where α_{R_iD} is the channel attenuation between outlet R_i and D, and α_{SR_i} for S and R_i.

Table 4.2: Parameters for performance simulation

Frequency band		from 2MHz to 28MHz
OFDM	total subcarriers number	1156
	used subcarriers number	917
Modulation mode on each subcarrier		fixed BPSK
Power allocation on each subcarrier		evenly distributed
Throughput	DT system	20.6246Mbps
	AF relay scheme	10.3123Mbps
Source-to-relay path	Backbone length / APA	17.6m / -19.2126dB
Relay-to-destination path	Backbone length / APA	46.5m / -21.9342dB
Source-to-destination path	Backbone length / APA	64.2m / -39.0858dB
The power of noise on channel		0dBm

As in the practical indoor PLC scenario, it is not always possible to find the outlets which meet the above ideal condition. We give the best-effort choice criterion for the user as

$$\min\left(\sum_{i=1}^{N}\frac{\alpha_{R_iD}}{\alpha_{SR_i}}-\sum_{i=1}^{N}\frac{P_S}{P_{R_i}}\right), i=1,2,...,N.$$

Thus with the knowledge about the power of source and relay nodes, along with the attention information of the different signaling paths, one can easily predict which outlets are the best locations chosen to deploy the relay devices.

4.4 Performance simulation

Given a proper location chosen for the relay devices, to demonstrate the performance improvement of the relay scheme, we compare the bit error rate (BER) performance of the one relay AF scheme with respect to the conventional DT system by simulation. To make our simulation close to the realistic situation, we refer to the HomePlug AV specification [14, 43] and set system parameters as in Table 4.2.

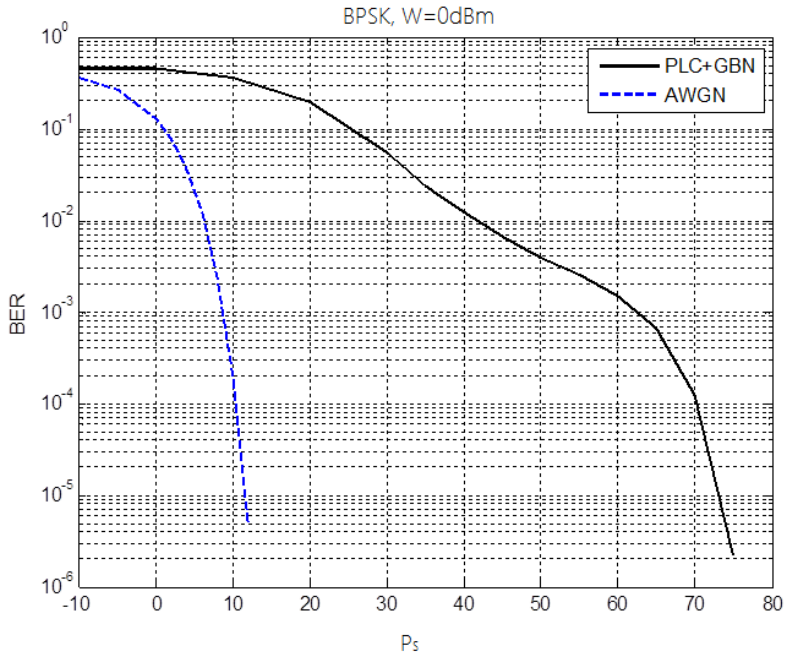

Figure 4.13: Performance of DT system working in a P2P PLC channel, compared with AWGN channel with the same noise power.

Direct transmission

To get insight about the distortion effect from the high attenuation and colored general background noise (GBN) of the PLC channel, we would like to firstly observe the different performance of a DT system, when it works in a point-to-point (P2P) PLC channel and an ideal additive white Gaussian noise (AWGN) channel, respectively. The comparison result is shown in Fig. 4.13.

By observing the significant change of performance curve, we can gain some insight of the heavy attenuation effect of the PLC channel. In addition, the different curve slopes reminds us the noise on PLC channel is not white.

AF relay scheme

Based on above result, now let us introduce a relay node into the system. Fixing the relay power P_R and setting source power P_S to different values, we observe a group of BER curves as shown in Fig. 4.14.

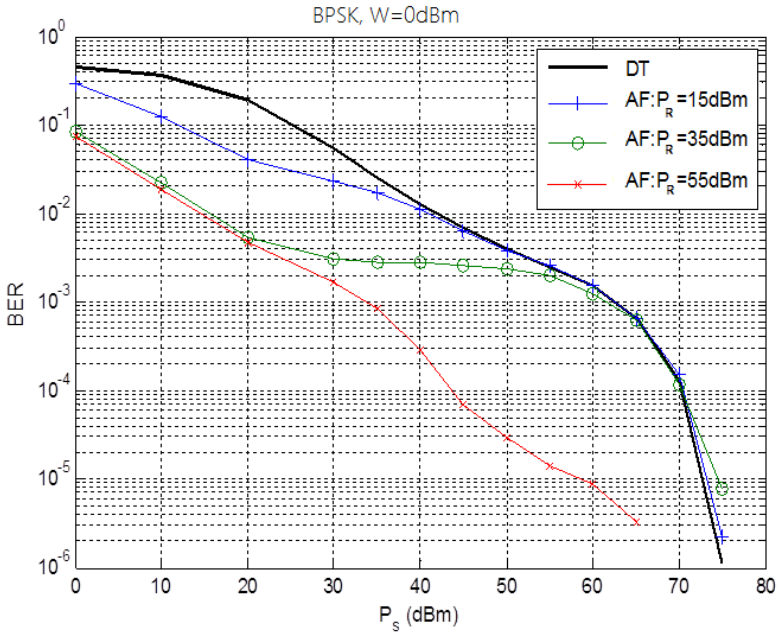

Figure 4.14: Performances of AF relay scheme, with different relay power.

From another angle of view, we could also set source power as constant, and observe the contribution from different level of relay powers as shown in Fig. 4.15.

Fig. 4.14 and Fig. 4.15 lead to the conclusion that source power is the fundamental factor of the system performance, while relay power is an enhancement. That is to say: (1) when P_S is too small, the contribution from the relay power is restricted; (2) With a proper source power amount, the more relay power P_R used, a better system performance can be achieved; (3) however, when the source power is high enough to afford a good SNR performance through the direct source-to-destination path, the relay scheme becomes unnecessary. The results from simulation verify our analysis in Section 4.3.

Finallly, we would like to motion that as in the above schemes the system total power is evenly allocated to each subcarrier, as shown in Table 4.2, the system performance has good potentiality to be further improved if the power allocation on each subcarrier can be optimized. We will address this topic in the next chapter.

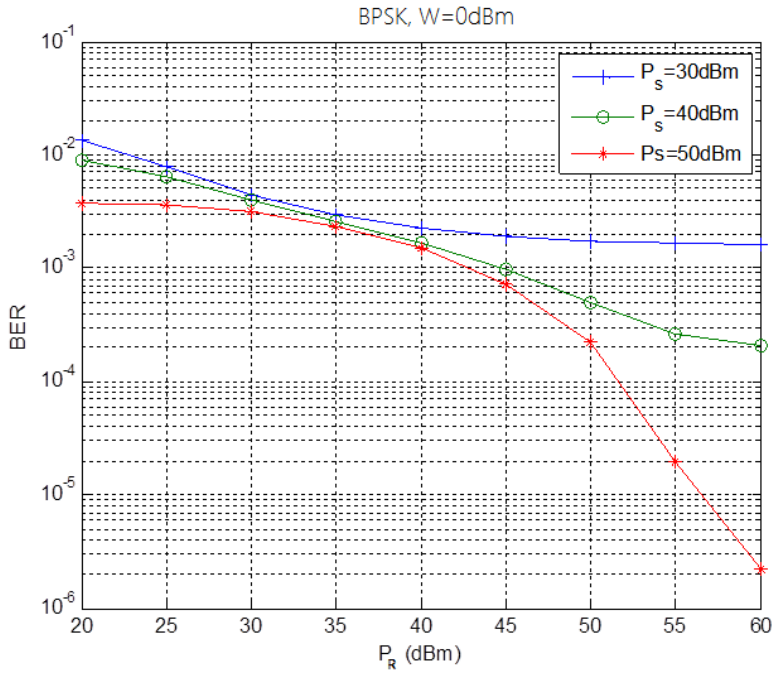

Figure 4.15: Performances of AF relay system, when source node uses different transmission power.

4.5 Chapter summary

Due to serious attenuation and frequency-selective distortion of its channel characteristics, the performance of indoor PLC systems is heavily influenced by the length and topology of the in-house power cable wiring. By exploiting the broadcast property of the indoor power grid to each outlet, in this chapter a simple but practical AF relay scheme is proposed to improve the system performance. The condition for the optimal location of the plug-in relay devices has been identified. As our example shows, this condition can be used as a criterion to guide the selection of the best-effort location to deploy the relay device for an indoor PLC system. Numerical simulation results[1] show that with the cost of extra relay device, more reliable performance can be obtained with respect to the conventional direct transmission scheme.

[1]Note in Fig. 4.5-4.6, Fig. 4.8, Fig. 4.10 and Fig. 4.12-4.15, for illustration clearlity, we used the assumption that the channel noise power is 0dBm. This leads to the result that the signal power is over 50dBm. In pracical enviorment, the noise power on a PLC channel is much lower, so that only a few Watts is needed for the proposed schemes.

Chapter 5

Optimal Power Allocation

The quality-of-service (QoS) criteria are very important to practical indoor PLC applications as they greatly affect the user experience. In this chapter, we adopt the general three-node/two-phase relay configuration, propose a non-regenerative multicarrier relay scheme for indoor broadband PLC networks, and investigate the joint source and relay power optimization of the non-regenerative relay systems used for indoor broadband PLC environment. Considering some applications require a minimum data rate support, we set the QoS criteria as the lower-bound of the capacity of the data-link from the source node to the destination node. As the QoS-constrained power allocation problem is highly non-convex, the globally optimal solution is computationally intractable to obtain. To overcome this challenge, we propose an alternating optimization (AO) method to decompose this problem into three convex sub-problems. Simulation results demonstrate the fast convergence and short delay of the proposed algorithm under realistic PLC test channels. In addition, compared with the two-hop and broadcast-and-forward relay systems, the general relay system can meet the same QoS requirement with less total network power. Note that in practical PLC systems, smaller transmission power leads to lower electromagnetic interference (EMI) to other communication systems.

The remainder of this chapter is organized as follows. A review of the existing non-generative relay schemes in the literature has been given in Section 5.1. Section 5.2 describes in detail the system model and problem formulation. The problem formulated is a joint optimization of relay and source power allocations over two phases subjecting to minimum link capacity requirement. The decomposed three sub-problems from Section 5.2 have been fully discussed in Sections 5.3 and 5.4. Based on these discussions, the overall AO algorithm has been presented in Section 5.5. Simulation examples are given in Section 5.6

to demonstrate the fast convergence and superior performance of the proposed algorithm. Finally, conclusions are followed.

5.1 Literature review

The non-regenerative relaying scheme has attracted much research interest recently. As this scheme only requires the relay node to amplify-and-forward (AF) signals, it has lower complexity, shorter processing delay and lower implementation cost. In [44] algorithms have been developed to maximize the relay system throughput by assuming that the relay node works in non-regenerative mode and the power at the source node and the relay node can be distributed over multiple sub-carriers. The communication process in [44] is completed in two successive phases. In the first phase, the source node transmits signal to the relay node. In the second phase, the relay node amplifies each sub-carrier component of the signal received from the source node, and forwards the amplified signal to the destination node. We call this *two-hop* relay scheme as there is no direct path between the source and destination nodes.

The effect of the direct path has been considered in [45, 46], where in the first phase the source node broadcasts signal to the relay and destination nodes. In the second phase, the relay node forwards its received signal to the destination node. As a result, the source node is always silent during the second phase. We call this *broadcast-and-forward* (BF) relay scheme.

The authors of [47] took a further step and proposed a relay scheme that allows the source node to transmit in both the first and second phases. In other words, when the relay node forwards its received signal, the source node repeats a transmission of the same information (as in the first phase) to the destination node in the second phase. We refer to this as *broadcast-and-multiaccess* (BMA) relay scheme. As a consequence of this configuration, the total network transmission power has been separated into the relay power and the source power, which in turn has been split into two parts (corresponding to two phases) for transmitting the same information twice. Obviously this is a very general case compared with the above two-hop and BF schemes.

The aim of [44]-[47] is to optimize a given objective function, for example signal-to-noise ratio (SNR), mutual information (MI) or system capacity, subjecting to the power constraints of the whole network or/and at each node. These problems belong to one group, i.e. the rate

maximization (RM) problems [48]. However, the QoS constrained problems, which belong to another group, i.e. margin maximization (MM) problems[48], are not often addressed in the literature. Note that in practical indoor PLC applications, such as HD video streaming, QoS criteria are very important as they greatly affect the user experience. On the other hand, in the conventional direct transmission (DT) system, the RM and MM problems are of duality to each other and admit a unique water-filling solution [48]. However, this fact does not hold when relay node has been introduced.

5.2 System model and problem formulation

The block diagram of the proposed general BMA relay system is shown in Fig. 5.1, which consists of three nodes, i.e. the source node (S), the destination node (D) and the relay node (R). We consider an orthogonal frequency-division multiplexing (OFDM) based mutlticarrier system. The whole system bandwidth is divided uniformly into K subcarriers, where the channel fading on each subcarrier is considered to be frequency-flat, i.e. it can be described as a channel coefficient. The channel response on the kth ($k = 1,2,\dots K$) subcarrier from node L_1 to node L_2 in the nth signaling path is denoted as $h_{L_1L_2}^{[k],(n)}$, where $L_1 \in \{S,R\}$, $L_2 \in \{R,D\}$and $n = 1,2$. By using the CTF generation method proposed in Chapter 3, discrete frequency responses for three different relay-involved PLC channel paths, namely the source-to-relay path $h_{SR}^{[k],(1)}$, the relay-to-detination path $h_{RD}^{[k],(2)}$ and the source-to-destination path in two phases $h_{SD}^{[k],(1)}$ and $h_{SD}^{[k],(2)}$, can be easily obtained.

Let us denote the transmit power on the kth subcarrier from the source node as $P_S^{[k]}$, and from the relay node as $P_R^{[k]}$. Furthermore, to distinguish the source power used in the first and second phase, we denote them as $P_{S,1}^{[k]}$ and $P_{S,2}^{[k]}$, respectively, i.e.

$$P_S^{[k]} = P_{S,1}^{[k]} + P_{S,2}^{[k]}. \tag{5.1}$$

Thus, the total network power P_Σ can be expressed as

$$\begin{aligned} P_\Sigma &= \sum_{k=1}^{K} P_S^{[k]} + \sum_{k=1}^{K} P_R^{[k]} \\ &= \sum_{k=1}^{K} P_{S,1}^{[k]} + \sum_{k=1}^{K} P_{S,2}^{[k]} + \sum_{k=1}^{K} P_R^{[k]}. \end{aligned} \tag{5.2}$$

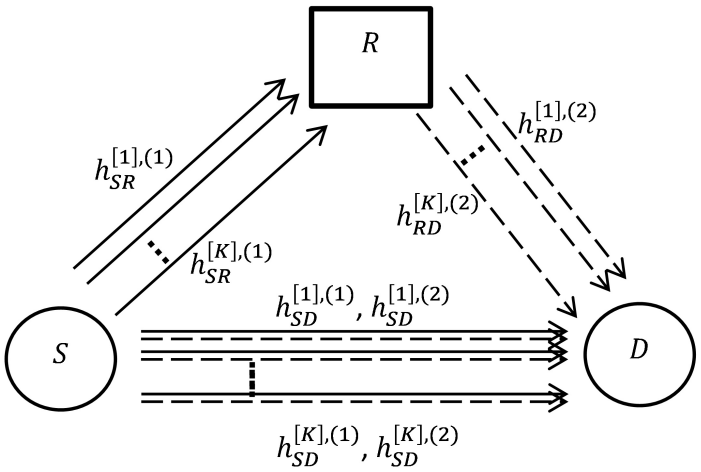

Figure 5.1: A multicarrier three-node relay system, where the solid-lines and dash-lines indicate phase 1 and 2, respectively. S, R and D stand for source node, relay node and destination node, respectively. Here $k = 1, \ldots, K$ is the index of subcarriers.

Following the OFDM principle, corresponding to the K subcarriers, each packet of information is encoded into K independent complex symbols $X^{[k]}$ $(k = 1, 2, \ldots K)$, of zero mean and unit variance. To complete a packet of information transmission from the source node to the destination node, the BAM relay scheme works according to the following two phases.

In the first phase, the source node broadcasts information signal $X^{[k]}$ $(k = 1, 2, \ldots K)$ over the kth subcarrier with the power $P_{S,1}^{[k]}$. Due to the broadcast nature of the indoor power grid, both the relay node and the destination node can receive this signal with different channel gain and noise disturbance, respectively

$$Y_{R,1}^{[k]} = h_{SR}^{[k],(1)} \sqrt{P_{S,1}^{[k]}} X^{[k]} + N_{R,1}^{[k]} \tag{5.3}$$

$$Y_{D,1}^{[k]} = h_{SD}^{[k],(1)} \sqrt{P_{S,1}^{[k]}} X^{[k]} + N_{D,1}^{[k]} \tag{5.4}$$

where $Y_{R,1}^{[k]}$ and $N_{R,1}^{[k]}$ denote the received kth subchannel signal and the subchannel noise, respectively, at the relay node; while $Y_{D,1}^{[k]}$ and $N_{D,1}^{[k]}$ denote the received kth subchannel signal and the subchannel noise, respectively, at the destination node in the first phase.

In the second phase, the relay amplifies its received signal on each sub-carrier with proper complex gain $g^{[k]} \exp(j\theta^{[k]})$, where $g^{[k]}$ is the amplitude gain and $\theta^{[k]}$ is the phase shift, and then forwards the amplified signal to the destination node with power $P_R^{[k]}$. At the meantime, the source node sends out another source message packet, this time with power $P_{S,2}^{[k]}$. Then

the received signal at the destination node in the second phase is

$$Y_{D,2}^{[k]} = h_{RD}^{[k],(2)} g^{[k]} \exp(j\theta^{[k]}) Y_{R,1}^{[k]} + h_{SD}^{[k],(2)} \sqrt{P_{S,2}^{[k]}} X^{[k]} + N_{D,2}^{[k]} \tag{5.5}$$

where $Y_{D,2}^{[k]}$and $N_{D,2}^{[k]}$ denote the received kth subchannel signal and the subchannel noise, respectively, at the destination node in the second phase.

Let us assume the noise PSD dose not change in two continuous signaling phases, and use $W_{L_2}^{[k]}$ to denote the power of noise at node L_2 in two phases. Thus we can write

$$g^{[k]} = \sqrt{\frac{P_R^{[k]}}{P_{S,1}^{[k]} |h_{SR}^{[k],(1)}|^2 + W_R^{[k]}}} \tag{5.6}$$

$$\theta^{[k]} = \angle h_{SD}^{[k],(2)} - \angle h_{SR}^{[k],(1)} - \angle h_{RD}^{[k],(2)}. \tag{5.7}$$

where $\angle(\cdot)$ stands for the angle of a complex number.

Actually the value of $\theta^{[k]}$ in (5.7) is a phase adjuster which makes the two signal components, in (5.5), from the direct path and the relay path, respectively, co-phase to each other. Finally, the destination node combines the two copies of received signal (5.4) and (5.5) over two phases by maximum ratio combining (MRC) processing with the knowledge of channel state information (CSI).

Let us denote the normalized signaling path gain from L_1 to L_2 in the nth ($n = 1, 2$) phase as

$$\gamma_{L_1 L_2}^{[k],(n)} = \frac{|h_{L_1 L_2}^{[k],(n)}|^2}{W_{L_2}^{[k]}} \tag{5.8}$$

and denote the SNR of the kth subcarrier at the destination node (D) in the nth phase as $SNR_{D,n}^{[k]}$, then from (5.3)-(5.7) we have

$$SNR_{D,1}^{[k]} = P_{S,1}^{[k]} \gamma_{SD}^{[k],1} \tag{5.9}$$

$$SNR_{D,2}^{[k]} = \frac{\left(\sqrt{P_{S,1}^{[k]} \gamma_{SR}^{[k],(1)} P_R^{[k]} \gamma_{RD}^{[k],(2)}} + \sqrt{\left(P_{S,1}^{[k]} \gamma_{SR}^{[k],(1)} + 1 \right) P_{S,2}^{[k]} \gamma_{SD}^{[k],(2)}} \right)^2}{1 + P_{S,1}^{[k]} \gamma_{SR}^{[k],(1)} + P_R^{[k]} \gamma_{RD}^{[k],(2)}} \tag{5.10}$$

Thus, we obtain the capacity (in bits/s/Hz) of the data-link from S to D as

$$C = \frac{1}{2}\sum_{k=1}^{K}\log_2\left(1+SNR_{D,1}^{[k]}+SNR_{D,2}^{[k]}\right) \tag{5.11}$$

where the factor 1/2 reflects the half-duplex constraint of the relay node.

We note that (5.11) is the capacity of a general three-node/two-phase AF relay system, which includes the following special cases:

(1) If $\gamma_{SD}^{[k],(n)} = 0$ where $n = 1,2$, the system becomes a two-hop relay system without the direct signaling path available. In PLC scenario this usually happens when the cable length between the source and the destination outlets is very long which makes the direct source-to-destination link very weak.

(2) If $P_{S,2}^{[k]} = 0$, it means the system becomes a BF relay system as we mentioned in Section 5.1.

(3) Interestingly, if $P_R^{[k]} = 0$, it means the relay node is not active, then the system become a *two-phase direct transmission system*, where the source transmits the same information packet twice independently in two phases to achieve time diversity.

(4) If $P_R^{[k]} = 0$ and $P_{S,2}^{[k]} = 0$, the scheme degrades to a conventional direct transmission (DT) system[1].

Without losing generality, we assume $\gamma_{L_1L_2}^{[k],(n)} > 0$ in the following. Setting QoS criteria as the lower-bound of the system capacity, to explore the most efficient utilization of the system power we propose the following optimization problem

$$\min_{P_{S,1}^{[k]},P_{S,2}^{[k]},P_R^{[k]}} P_\Sigma \tag{5.12}$$

$$s.t. C \geq q, \tag{5.13}$$

$$P_{S,1}^{[k]}, P_{S,2}^{[k]}, P_R^{[k]} \geq 0, \forall k \tag{5.14}$$

where (5.12) is the objective function of the total network transmission power, and $q \geq 0$ is the required minimum link capacity to support certain applications on the indoor PLC network, e.g. HDTV inter-room sharing service.

[1] In this case, the relay's half-duplex factor 1/2 does not exist.

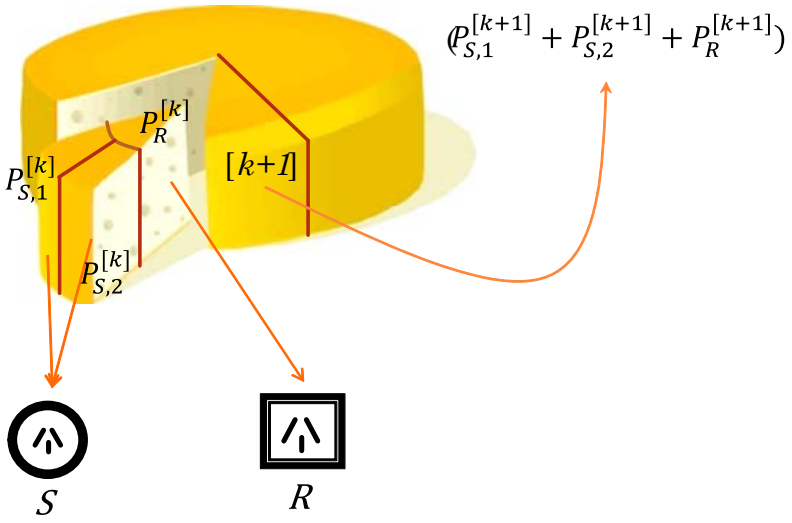

Figure 5.2: Illustration of power allocation problem.

To normalize the subcarrier number's effect on the system capacity, we can also define the averaged subchannel capacity (ASC) as

$$\bar{C} = \frac{C}{K} \tag{5.15}$$

which measured in bits/s/Hz/subcarrier, so that the capacity constraint (5.13) can be equally expressed as

$$\frac{C}{K} \geq \bar{q} \tag{5.16}$$

where

$$\bar{q} = \frac{q}{K} \tag{5.17}$$

is the minimal requirement of averaged capacity on each subcarrier.

Note the problem formulated in (5.12)-(5.14) has threefold tasks. On one hand, it should distribute the system total power optimally on each subcarrier; on the other hand, the power of each subcarrier need to be optimally allocated to the relay node and the source; for the power at the source node, it in turn needs to be split into two phases properly. This point has been illustrated in Fig. 5.2.

The exact solution to the problem (5.12)-(5.14) is difficult to obtain because the system

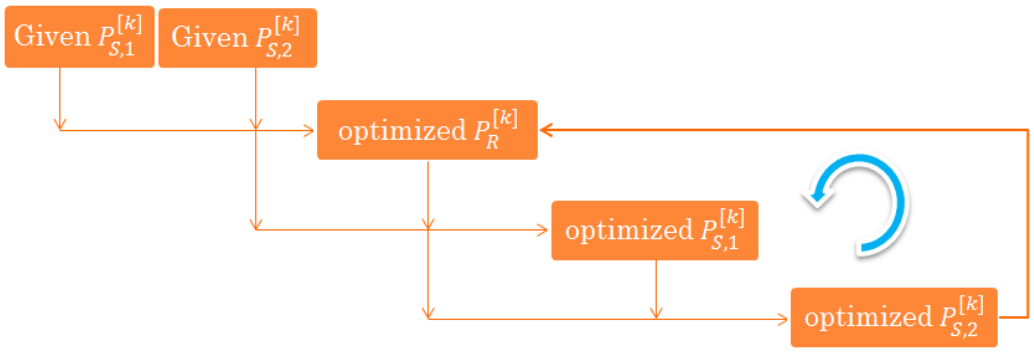

Figure 5.3: Illustration of the AO algorithm.

minimum capacity constraint in (5.13) is non-convex. In this chapter, we provide a locally optimal solution by adopting the AO approach from [49], where we first optimize $P_R^{[k]}$ with given $P_{S,1}^{[k]}$ and $P_{S,2}^{[k]}(k = 1,2,\ldots K)$; then optimize $P_{S,1}^{[k]}$ with given $P_{S,2}^{[k]}$ and previously optimized $P_R^{[k]}$; next we optimize $P_{S,2}^{[k]}$ with previously obtained $P_{S,1}^{[k]}$ and $P_R^{[k]}$. This process is repeated till convergence, i.e. the difference between the P_Σ obtained in two consecutive iterations is less than a preset threshold. This iterative process is illustrated in Fig. 5.3. For any two groups of fixed power allocation parameters, the resulted sub-problem becomes convex or can be approximated as convex. Based on this method, we will develop the overall algorithm to solve the problem (5.12)-(5.14). We discuss these issues in detail in the following sections.

5.3 Optimal relay power allocation with given source power allocations

Let x_k stand for $P_R^{[k]}(k = 1,2,\ldots K)$. For fixed $P_{S,1}^{[k]}$ and $P_{S,2}^{[k]}$, problem (5.12)-(5.14) becomes

$$\min_{x_k} \sum_{k=1}^{K} x_k \tag{5.18}$$

$$s.t. \quad 2q - \sum_{k=1}^{K} \log_2 \left(A_k + \frac{D_k + E_k\sqrt{x_k}}{B_k + C_k x_k} \right) \leq 0 \tag{5.19}$$

$$x_k \geq 0, \forall k \tag{5.20}$$

where

$$A_k = 1 + P_{S,1}^{[k]} \gamma_{SD}^{[k],(1)} + P_{S,1}^{[k]} \gamma_{SR}^{[k],(1)} \tag{5.21}$$

$$B_k = 1 + P_{S,1}^{[k]} \gamma_{SR}^{[k],(1)} \tag{5.22}$$

$$C_k = \gamma_{RD}^{[k],(2)} \tag{5.23}$$

$$D_k = \left(1 + P_{S,1}^{[k]} \gamma_{SR}^{[k],(1)}\right) \left(P_{S,2}^{[k]} \gamma_{SD}^{[k],(2)} - P_{S,1}^{[k]} \gamma_{SR}^{[k],(1)}\right) \tag{5.24}$$

$$E_k = 2\sqrt{P_{S,1}^{[k]} \gamma_{SR}^{[k],(1)} P_{S,2}^{[k]} \gamma_{SD}^{[k],(2)} \gamma_{RD}^{[k],(2)} \left(1 + P_{S,1}^{[k]} \gamma_{SR}^{[k],(1)}\right)}. \tag{5.25}$$

Let us write down the Karush-Kuhn-Tucker (KKT) conditions [50] to the problem (5.18)-(5.20) as, for $\forall k$,

$$\lambda \frac{C_k E_k x_k + 2C_k D_k \sqrt{x_k} - B_x E_x}{2\ln 2 \sqrt{x_k}(B_k + C_k x_k)(E_k \sqrt{x_k} + A_k B_k + D_k + A_k C_k x_k)} + 1 = 0 \tag{5.26}$$

$$\lambda \left[2q - \sum_{k=1}^{K} \log_2 \left(A_k + \frac{D_k + E_k \sqrt{x_k}}{B_k + C_k x_k}\right)\right] = 0 \tag{5.27}$$

$$\lambda \geq 0 \tag{5.28}$$

$$x_k \geq 0. \tag{5.29}$$

The problem (5.18)-(5.20) is not convex on $\{x_k \mid x_k \geq 0, k = 1, 2, \ldots K\}$,however its globally optimal solution is always located on a subset of it. To illustrate this point, an example of $F(x_k) = \log_2 \left(A_k + \frac{D_k + E_k \sqrt{x_k}}{B_k + C_k x_k}\right)$ (when $K = 1$) is shown in Fig. 5.4.

PROPOSITION 5.1: The problem (5.18)-(5.20) is convex on

$$\mathscr{X} = \left\{ x_k \mid 0 \leq x_k \leq x_{0,k}, x_{0,k} = \frac{(1 + \frac{2}{3}\sqrt{3}) B_k}{C_k}, k = 1, 2, \ldots K \right\}.$$

For fixed $\lambda > 0$, the left-hand-side (LHS) of (5.26) is monotone to x_k on $\mathscr{X}$. And the LHS of (5.27) is a piecewise monotone functions of x_k on $\mathscr{X}$.

PROOF: See Appendix A.1 at the end of this thesis.

From Proposition 5.1, a bisection search algorithm can be employed to solve the KKT conditions (5.26)-(5.29) on $\mathscr{X}$, which leads to the globally optimal solution of the problem (5.18)-(5.20).

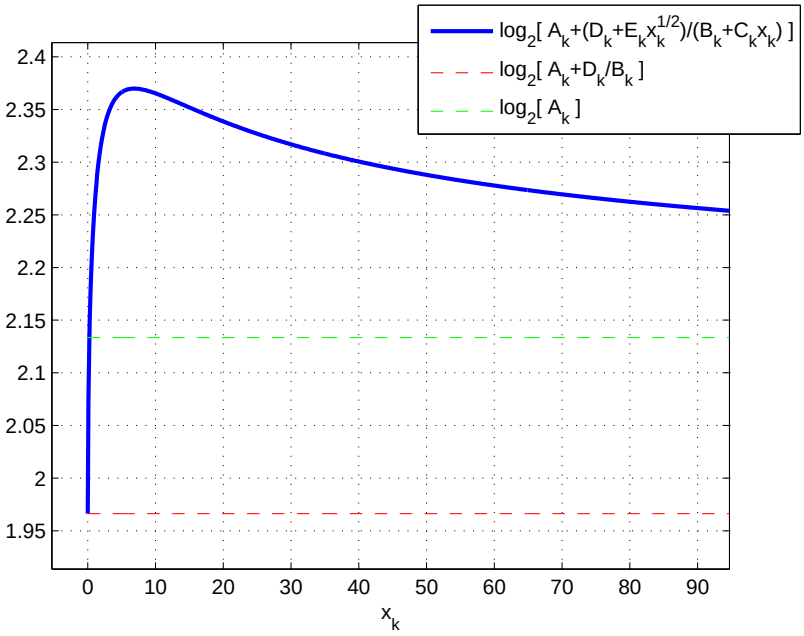

Figure 5.4: Example plot of $F(x_k)$ versus x_k, when $K = 1$.

5.4 Optimal source power allocations with given relay power allocation

Under a given relay power allocation $P_R^{[k]}$, the problem (5.12)-(5.14) is still a non-convex problem. Again we apply the approach of AO and decompose this problem into two sub-problem as shown in the following two subsections.

5.4.1 Optimal first-phase source power allocation with given second-phase power and relay power allocations

Let y_k stand for $P_{S,1}^{[k]}(k = 1,2,\ldots K)$, then for given $P_{S,2}^{[k]}$ and $P_R^{[k]}$ we now consider the optimization of the source power allocation in the first phase by solving the problem of

$$\min_{y_k} \sum_{k=1}^{K} y_k \tag{5.30}$$

$$s.t. \quad 2q - \sum_{k=1}^{K} \log_2 \left(F + G_k y_k + \frac{H_k + R_k \sqrt{y_k(1+L_k y_k)}}{L_k y_k + M_k} \right) \leq 0 \tag{5.31}$$

$$y_k \geq 0, \forall k \tag{5.32}$$

where

$$F_k = 1 + P_R^{[k]} \gamma_{RD}^{[k],(2)} + P_{S,2}^{[k]} \gamma_{SD}^{[k],(2)} \tag{5.33}$$

$$G_k = \gamma_{SD}^{[k],(1)} \tag{5.34}$$

$$H_k = -P_R^{[k]} \gamma_{RD}^{[k],(2)} \left(1 + P_R^{[k]} \gamma_{RD}^{[k],(2)} + P_{S,2}^{[k]} \gamma_{SD}^{[k],(2)}\right) \tag{5.35}$$

$$L_k = \gamma_{SR}^{[k],(1)} \tag{5.36}$$

$$M_k = 1 + P_R^{[k]} \gamma_{RD}^{[k],(2)} \tag{5.37}$$

$$R_k = 2\sqrt{\gamma_{SR}^{[k],(1)} P_{S,2}^{[k]} \gamma_{SD}^{[k],(2)} P_R^{[k]} \gamma_{RD}^{[k],(2)}}. \tag{5.38}$$

Let us write down the KKT condition to the problem (5.30)-(5.32) as, for $\forall k$,

$$\ln 2 \left(F + Gy + \frac{H + R\sqrt{Ly^2 + y}}{M + Ly}\right) = \mu \left[G - \frac{L\left(H + R\sqrt{Ly^2 + y}\right)}{(M + Ly)^2} + \frac{R(2Ly + 1)}{(2Ly + 2M)\sqrt{Ly^2 + y}}\right] \tag{5.39}$$

$$\mu \left[2q - \sum_{k=1}^{K} \log_2 \left(F + G_k y_k + \frac{H_k + R_k \sqrt{y_k(1 + L_k y_k)}}{L_k y_k + M_k}\right)\right] = 0 \tag{5.40}$$

$$\mu \geq 0 \tag{5.41}$$

$$y_k \geq 0. \tag{5.42}$$

PROPOSITION 5.2: The problem (5.30)-(5.32) is convex on $\{y_k \mid y_k \geq 0, k = 1, 2, \ldots K\}$. And for fixed $\mu > 0$, both the LHS of (5.39) and (5.40) are monotone functions of y_k.

PROOF: See Appendix A.2 at the end of this thesis.

Based on Proposition 5.2, the solution to the problem (5.30)-(5.32) can be obtained by using a bisection search algorithm.

5.4.2 Optimal second-phase source power allocation with given first-phase power and relay power allocations

Similarly, based on the optimized $P_{S,1}^{[k]}$ and $P_R^{[k]}$ from above, we now denote $P_{S,2}^{[k]}$ as z_k and consider the optimization of the source power allocation in the second phase by solving the problem of

$$\min_{z_k} \sum_{k=1}^{K} z_k \tag{5.43}$$

$$s.t. \quad 2q - \sum_{k=1}^{K} \log_2 \left(S_k + T_k z_k + U_k \sqrt{z_k}\right) \leq 0 \tag{5.44}$$

$$z_k \geq 0, \forall k \tag{5.45}$$

where

$$S_k = 1 + P_{S,1}^{[k]} \gamma_{SD}^{[k],(1)} + \frac{P_{S,1}^{[k]} \gamma_{SR}^{[k],(1)} P_R^{[k]} \gamma_{RD}^{[k],(2)}}{1 + P_{S,1}^{[k]} \gamma_{SR}^{[k],(1)} + P_R^{[k]} \gamma_{RD}^{[k],(1)}} \tag{5.46}$$

$$T_k = \frac{\left(P_{S,1}^{[k]} \gamma_{SR}^{[k],(1)} + 1\right) \gamma_{SD}^{[k],(2)}}{1 + P_{S,1}^{[k]} \gamma_{SR}^{[k],(2)} + P_R^{[k]} \gamma_{RD}^{[k],(2)}} \tag{5.47}$$

$$U_k = \frac{2\sqrt{P_{S,1}^{[k]} \gamma_{SR}^{[k],(1)} \gamma_{SD}^{[k],(2)} P_R^{[k]} \gamma_{RD}^{[k],(2)} \left(1 + P_{S,1}^{[k]} \gamma_{SR}^{[k],(1)}\right)}}{1 + P_{S,1}^{[k]} \gamma_{SR}^{[k],(1)} + P_R^{[k]} \gamma_{RD}^{[k],(2)}}. \tag{5.48}$$

The KKT conditions to the problem (5.43)-(5.45) are, for $\forall k$,

$$1 - \delta \frac{T_k + \frac{U_k}{2\sqrt{z_k}}}{\ln 2 \left(S_k + T_k z_k + U_k \sqrt{z_k}\right)} = 0 \tag{5.49}$$

$$\delta \left[2q - \sum_{k=1}^{K} \log_2 \left(S_k + T_k z_k + U_k \sqrt{z_k}\right)\right] = 0 \tag{5.50}$$

$$\delta \geq 0 \tag{5.51}$$

$$z_k \geq 0. \tag{5.52}$$

PROPOSITION 5.3: The problem (5.43)-(5.45) is convex on $\{z_k \mid z_k \geq 0, k = 1, 2, \ldots K\}$. And For fixed $\delta > 0$, the LHS of (5.49) and (5.50) are monotonically changing with z_k.

Algorithm 5.1 AO algorithm for solving the problem (5.12)-(5.14)

1) Initialize $P_{S,1}^{[1]} = p_{s1}$ while $P_{S,1}^{[k]} = 0$ $(k = 2,3,\ldots,K)$; $P_{S,2}^{[1]} = p_{s2}$ while $P_{S,2}^{[k]} = 0$ $(k = 2,3,\ldots,K)$; and $P_R^{[1]} = p_r$ while $P_R^{[k]} = 0$ $(k = 2,3,\ldots,K)$. Here the scalars p_{s1}, p_{s2} and p_r are positive numbers which satisfy (5.13) and (5.14).
2) Use bi-section algorithm with preselected (newly obtained) $P_{S,1}^{[k]}$ and $P_{S,2}^{[k]}$ to solve (5.26)-(5.29) to find a new set of $P_R^{[k]}$.
3) Use bi-section algorithm with the preselected (newly obtained) $P_{S,2}^{[k]}$ and $P_R^{[k]}$ to solve (5.39)-(5.42) to find a new set of $P_{S,1}^{[k]}$.
4) Use bi-section algorithm with newly obtained $P_R^{[k]}$ and $P_{S,1}^{[k]}$ to solve (5.49)-(5.52) to find a new set of $P_{S,2}^{[k]}$.
5) Calculate the total power value (5.2) with the obtained power allocation values from 2)-4).
6) If the difference of the value of (5.2) in two successive iterations is less than a preset threshold σ, then stop; otherwise, go to step 2).

PROOF: See Appendix A.3 at the end of this thesis.

Again, the solution to the problem (5.43)-(5.45) can be obtained by using a standard bisection algorithm.

5.5 Proposed iterative algorithm

Based on the discussion in Sections 5.3 and 5.4, we summarize the proposed AO algorithm for solving the problem (5.12)-(5.14). This is shown in Algorithm 5.1.

In general, the alternating optimization method cannot guarantee to converge to the globally optimal solution. However, since we obtain the global optimum for each subproblem, the proposed AO algorithm converges to a stationary point of the objective function (5.12). This will be verified by simulation examples in the next section.

5.6 Numerical examples

In this section we present simulation results based on a simple testing relay-involved PLC channel. Its topology is given in Fig. 5.5, where different types of cables have been used for

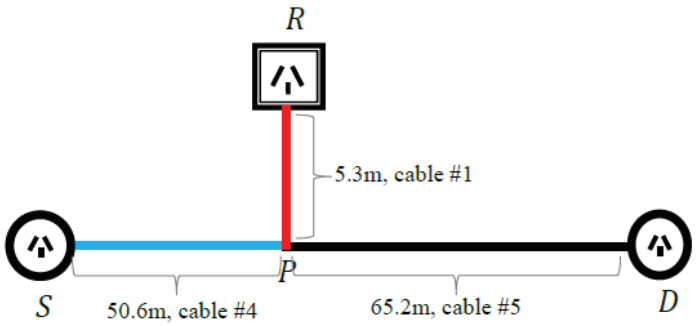

Figure 5.5: Topology of the testing channel.

different segments of the network. The parameters for each type of cable can be found in [32]. Moreover, the physical (PHY) layer specification of the HomePlug AV protocol [14] has been referred to set the simulation parameters.

(1) For simplicity, we assume the noise on different nodes of the network are independent and identically distributed (i.i.d.) and share the common PSD as shown in Fig. 5.6, where $k = 1, 2, ..., 1024$ is the subcarrier index.

(2) Let us set the source node's inner impedance as $Z_s = 50\Omega$ and the receiving impedance of the destination node as $Z_l = 150\Omega$. For the relay node, when it works in the Tx mode, it has an inner impedance $Z_{sR} = 50\Omega$, while in the Rx mode, it has a loading impedance $Z_{lR} = 150\Omega$.

(3) A preexisting load Z_b has been deployed on the outlet where the relay device is plugged in. The frequency response of Zb is given in Fig. 5.7.

(4)With the approach presented in Chapter 3, each signalling path in the relay-involved channel can be treated as an equivalent P2P channel, and the latter one can be easily realized by using Canete's PLC channel simulator [32]. By configuring the parameters used for this P2P channel as shown in Table 5.1-5.4, a group of correlated path gains ($h_{SD}^{[k],(1)}$, $h_{SR}^{[k],(1)}$,$h_{RD}^{[k],(2)}$,$h_{SD}^{[k],(2)}$) can be generated as shown in Fig. 5.8. Note in Fig. 14 the P2P channel gain $\tilde{h}_{SD}^{[k]}$ is also given, which corresponds to the situation where the relay device is unplugged from the grid.

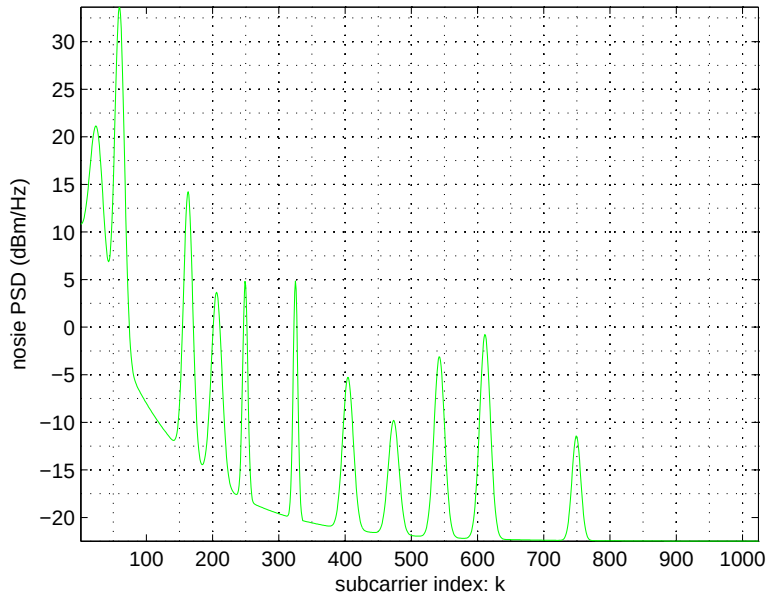

Figure 5.6: Common testing noise PSD on every node of the PLC network.

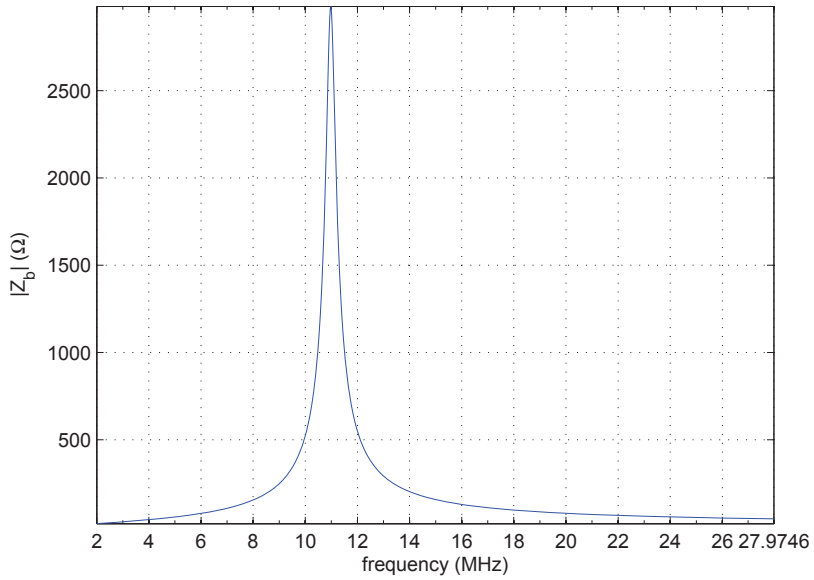

Figure 5.7: Frequency response of preexisting load Z_b.

Table 5.1: Parameters for gernerating $h_{SD}^{[k],(1)}$

line section name	length	cable type	terminated load
backbone 1	L_1=*50.6m*	n_{L1}=*4*	*N/A*
branch-tap 1	S_1=5.3m	n_{S1}=1	$Z_b//Z_{lR}$
backbone 2	L_2=*65.2m*	n_{L2}=*5*	*N/A*
branch-tap 2	S_2=0	n_{S_2}=N/A	Z_2=∞
backbone 3	L_3=*0*	n_{L_3}=*N/A*	*N/A*
branch-tap 3	S_3=0	n_{S_3}=N/A	Z_3=∞
backbone 4	L_4=*0*	n_{L_4}=*N/A*	*N/A*
Transmitting inner impedance:			Z_s=50Ω
Receiving load impedance:			Z_l=150Ω

Table 5.2: Parameters for gernerating $h_{SR}^{[k],(1)}$

line section name	length	cable type	terminated load
backbone 1	L_1=*50.6m*	n_{L1}=*4*	*N/A*
branch-tap 1	S_1=65.2m	n_{S1}=5	Z_l=150Ω
backbone 2	L_2=*5.3m*	n_{L2}=*1*	*N/A*
branch-tap 2	S_2=0	n_{S_2}=N/A	Z_2=∞
backbone 3	L_3=*0*	n_{L_3}=*N/A*	*N/A*
branch-tap 3	S_3=0	n_{S_3}=N/A	Z_3=∞
backbone 4	L_4=*0*	n_{L_4}=*N/A*	*N/A*
Transmitting inner impedance:			Z_s=50Ω
Receiving load impedance:			$Z_b//Z_{lR}$

Table 5.3: Parameters for gernerating $h_{RD}^{[k],(2)}$

line section name	length	cable type	terminated load
backbone 1	L_1=*0*	n_{L1}=*N/A*	*N/A*
branch-tap 1	S_1=0	n_{S1}=N/A	Z_b
backbone 2	L_2=*5.3m*	n_{L2}=*1*	*N/A*
branch-tap 2	S_2=50.6m	n_{S_2}=4	Z_2=∞
backbone 3	L_3=*65.2m*	n_{L_3}=*5*	*N/A*
branch-tap 3	S_3=0	n_{S_3}=N/A	Z_3=∞
backbone 4	L_4=*0*	n_{L_4}=*N/A*	*N/A*
Transmitting inner impedance:			Z_{sR}=50Ω
Receiving load impedance:			Z_l=150Ω

Table 5.4: Parameters for gernerating $h_{SD}^{[k],(2)}$

line section name	length	cable type	terminated load
backbone 1	L_1=*50.6m*	n_{L1}=*4*	*N/A*
branch-tap 1	S_1=5.3m	n_{S1}=1	$Z_b//Z_{sR}$
backbone 2	L_2=*65.2m*	n_{L2}=*5*	*N/A*
branch-tap 2	S_2=0	n_{S_2}=N/A	Z_2=∞
backbone 3	L_3=*0*	n_{L_3}=*N/A*	*N/A*
branch-tap 3	S_3=0	n_{S_3}=N/A	Z_3=∞
backbone 4	L_4=*0*	n_{L_4}=*N/A*	*N/A*
Transmitting inner impedance:			Z_s=50Ω
Receiving load impedance:			Z_l=150Ω

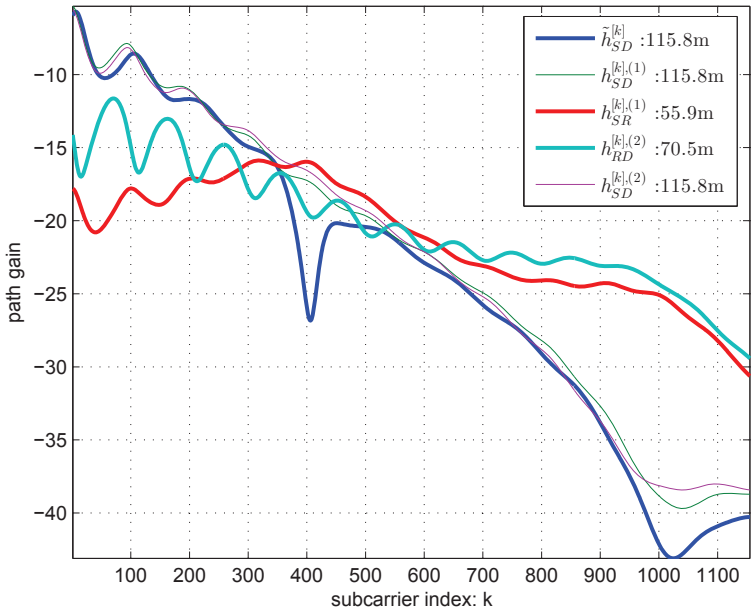

Figure 5.8: Different path gains existing in the testing relay-involved channel where the P2P channel gain has also been given.

(5) Using (5.8), the normalized path gains ($\gamma_{SD}^{[k],(1)}$,$\gamma_{SR}^{[k],(1)}$, $\gamma_{RD}^{[k],(2)}$ and $\gamma_{SD}^{[k],(2)}$) on each subcarrier can be calculated. The results are shown in Fig. 5.9.

The parameters used for simulation are summarized in Table 5.5. In addition, for the proposed iterative algorithm we specify the convergence condition as the difference between the total power obtained in two consecutive iterations less than 10^{-5}.

As an example to demonstrate the convergence speed of the overall AO algorithm, Fig. 5.10 shows the total transmission power $P_{\sum}$ versus the number of iterations, when the minimal ASC requirment $\bar{q}$ in (5.17) is set to five different values, from 1.0 to 3.0 bits/s/Hz/subcarrier,

Table 5.5: System parameters used for simulation

Frequency band	from 2MHz to 30MHz
OFDM total subcarriers number	K=1155
Signaling path gains $h^{[k],(n)}$	see Fig. 5.8
General background noise $N^{[k],(n)}$	see Fig. 5.6
Normalized path gains $\gamma^{[k],(n)}$	see Fig. 5.9

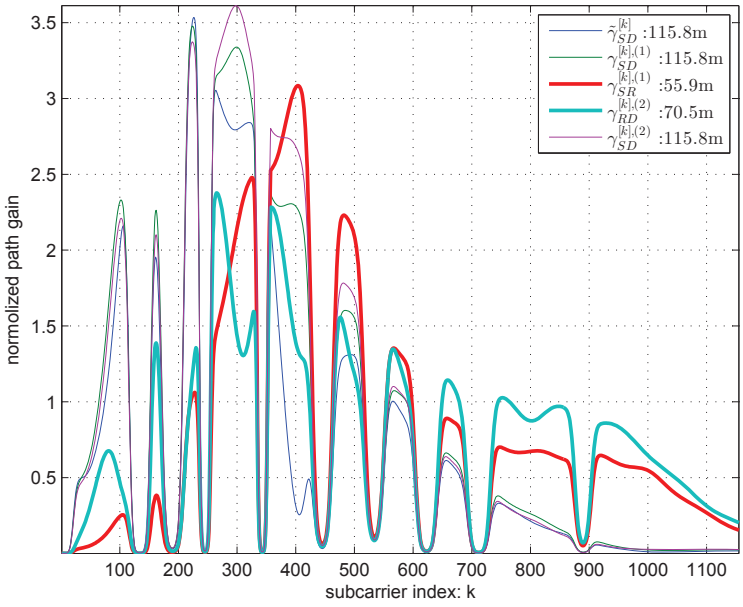

Figure 5.9: Normalized path gains, where the P2P channel's normalized path gain has also been given.

respectively. It can be seen that the proposed AO algorithm converges typically within six iterations. Specifically, the decreasing of the total power after four iterations is very small. Thus only a few iterations are required to achieve a good performance. This also indicates that the AO algorithm has a short processing delay, which is important for practical PLC relay systems. It can also be observed from Fig. 5.10 that with the increasing of required ASC, more transmission power is needed to meet the stricter QoS constraint, which reflects the typical QoS-cost trade-off in communication systems.

Next, we compare the proposed general BMA relay scheme (which is optimized by the AO power allocation algorithm) with the two-hop relay system (as proposed in [44]) and the BF relay system under the same testing channel condition. We can see from Fig. 5.11 that the BF scheme has a better performance than the two-hop system, while the AO algorithm enables the BAM system meet the requirement with the least power consumption. This is because with respect to the two-hop system, the BF scheme obtains spatial diversity from the direct link, while the general BMA system benefits from both the spatial diversity and the time diversity from the time-varying relaying channel condition.

As an example to show the power allocation on each subcarrier for the two-hop, BF and BMA relay systems, powers on one hundred subchannels (from 701 to 800) are shown in

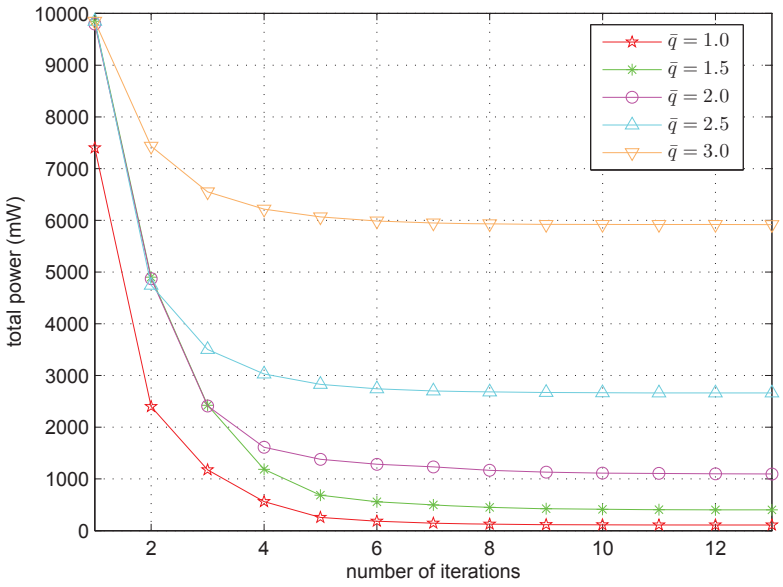

Figure 5.10: Total power versus number of iterations.

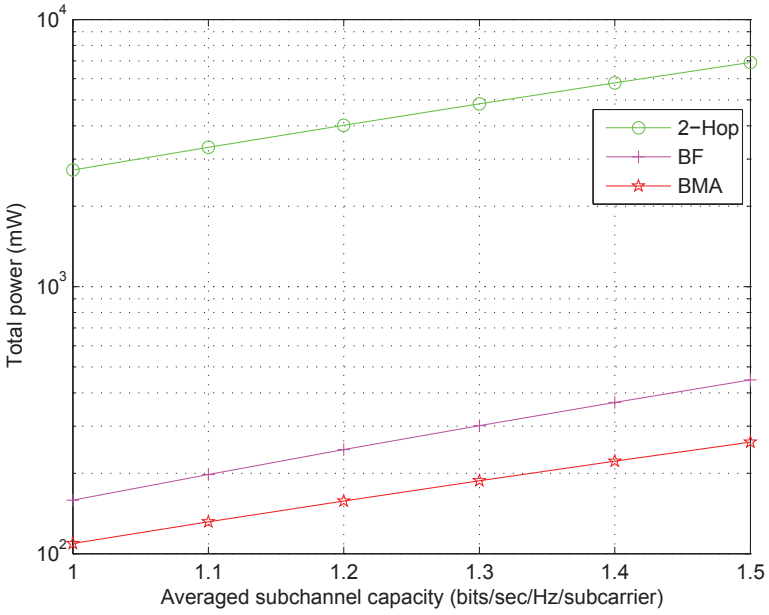

Figure 5.11: Total power versus minimal ASC requirement.

Fig. 5.12, where the common minimal requirement of ASC is set to 3.5 bits/s/Hz/subcarrier. The corresponding normalized channel gain on these subcarriers of the three systems can be found in Fig. 5.13. Considering the possible EMI from PLC systems to radio systems, we hope this power saving property can relieve this issue to some extent.

5.7 Chapter summary

We have developed an iterative algorithm to jointly optimize the source power and relay power allocations for the general three-node/two-phase AF relay system, where the source transmits in both time-phases. Specifically, we examined the minimization of the total transmission power when there is a minimal channel capacity requirement for PLC applications. Simulation results show that with respect to the two-hop and BF relay systems, the proposed algorithm can make the general BMA relay system attain the same QoS requirement with less total transmission power.

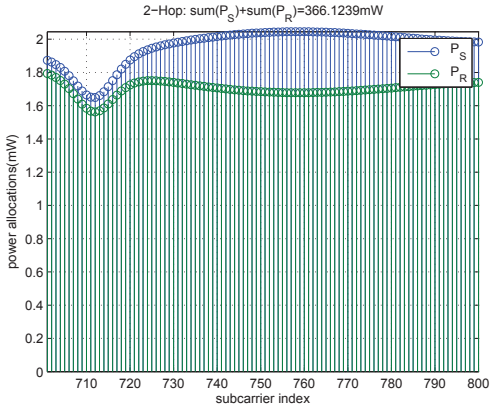

(a) Two-hop relay

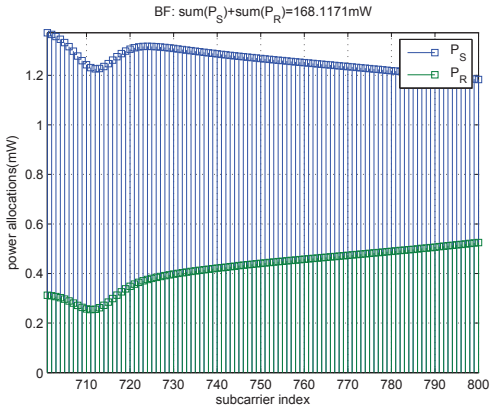

(b) Broadcast-and-forward (BF) relay

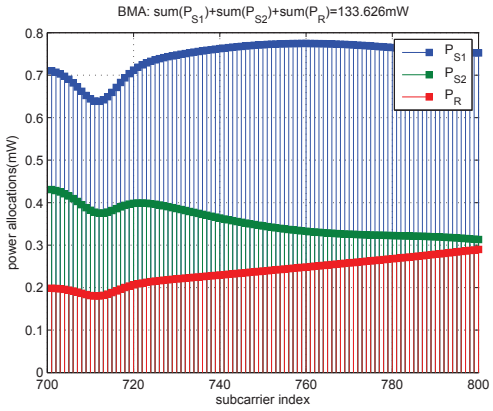

(c) broadcast-and-multiaccess (BMA) relay

Figure 5.12: Power allocations on each subchannel of the three relay schemes under common QoS requirement.

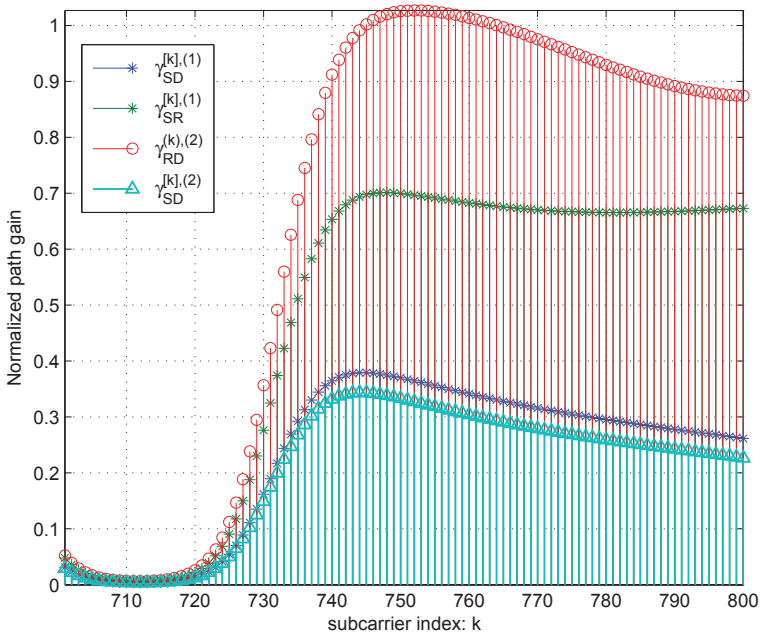

Figure 5.13: Normalized channel gain on the subcarriers 701-800.

Chapter 6

Two-Way Information Exchange in PLC Networks

Network coding as an emerging technology was firstly proposed in [51]. For its great improvement to network throughput and performance, it is expected to be one of the most critical technologies for networks of the future. In traditional networks, independent information streams are kept separate, such as routing, data storage, error control and so on. However, with network coding, where the network nodes not only simply forward but also process the incoming independent information flows. In other words, data streams that are independently produced and consumed do not necessarily need to be kept separate when they are transported throughout the network because there are ways to combine and later extract independent information. Note this kind of combining independent data streams allows to better tailor the information flow to the network environment and accommodate the demands of specific traffic patterns[52].

Under an indoor PLC application environment, it is often to find such a scenario where two PLC terminal nodes need to exchange information with the aid of a third node (we refer to as the relay node in the following) which locates in the middle of the two terminals. Actually, this scenario forms a very simple network structure (i.e. only three nodes in total) and can benefit from the application of the network coding at the relay node. When this configuration has been implemented in an indoor PLC network, it can be illustrated in Fig. 6.1. Under this configuration, in this chapter we would like to investigate the joint terminals and relay power optimization problem, given the special indoor relay-involved PLC channel conditions. With practical consideration, we set the relay node work in the AF mode and an

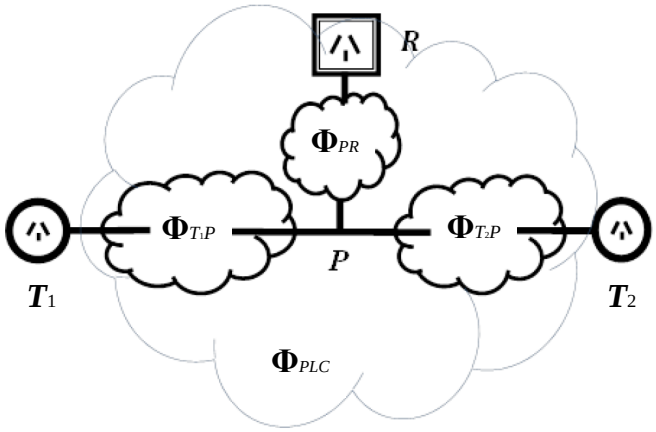

Figure 6.1: Outline of the simple three-node PLC network, where two terminal nodes (T_1 and T_2) exchange information with the aid of a relay node (R).

orthogonal frequency-division multiplexing (OFDM) based multicarrier modulation is used to satisfy the broadband data exchange requirement.

The remainder of this chapter is organized as follows. A brief review of the related works in the literature is given in Section 6.1. Details of the system model and problem formulation are discussed in Section 6.2. The problem formulated is a joint optimization of relay and source power allocations over two phases subjecting to minimum data rate requirement on each traffic direction. We decompose this non-convex problem into three sub-problems in Sections 6.3, 6.4 and 6.5. Based on these discussions, the overall AO algorithm to solve the formulated problem in 6.2 is presented in Section 6.6. As a fundamental requirement of simulation, Section 6.7 describes the approach we proposed to generate the frequency response for the different signaling paths of this relay-involved two-way PLC channel, which has not been addressed in the literature before. Simulation examples are then followed in Section 6.8 to demonstrate the fast convergence and superior performance of the proposed network coding system, compared with the conventional half-duplex information exchange systems. Finally, we conclude this chapter.

6.1 Literature review

Since the pioneering work of [51], network coding has become an active research topic in wireless networks to increase the transmission throughput [53, 54]. In network coding, the intermediate nodes may transmit not only the copy of received information bits, but also the combination of received messages. Such kinds of linear or nonlinear processing in the intermit nodes is called network coding. Consequently, the traditional role (i.e., store and forward) of intermit nodes becomes a special case of network coding, where the processing is to reproduce what they have received. By applying the max-flow min-cut theories, the achievable information rate region was discussed in [51] for single source multicast networks and in [55] for multisource multicast networks.

As firstly pointed out in [56, 57], due to the half-duplex constraint of the relay nodes, both the conventional AF and DF relay systems suffer from a reduced system capacity because of the pre-log factor $1/2$ as shown in (5.11) . To overcome this problem, the authors in [58] proposed the two-way relay system, which firstly has been investigated under wireless environments. In fact, it is a simple form of application of the network coding in the wireless relay systems. The authors of [59] considers an AF scheme for two-way relaying over OFDM, in which two terminals exchange information via a relay node. They perform power allocation at the relay and both terminals, as well as tone permutation at the relay node, so as to maximize the sum capacity. The authors of [60] introduce the idea of two-way relay scheme into PLC scenario, and this scheme has been addressed in detail in a recent work [61]. In [61] the authors consider that a relay device, working in the AF mode, is used to assist the data exchange of two terminals in an indoor PLC network, and find that the AF two-way system can increase the achievable data exchange rate.

In the conventional direct transmission (DT) system, the rate maximization (RM) and margin maximization (MM) problems are of duality to each other and admit a unique water-filling solution [48]. However this fact does not hold when relay nodes have been introduced. The aim of [58]-[61] is to maximize a given objective function, for example signal-to-noise ratio (SNR), mutual information (MI) or system capacity, subject to the power constraints of the whole network or/and at each node; however, the quality-of-service (QoS) constraints are still not addressed. Note that in practical indoor PLC applications, such as HD video streaming, QoS criteria are very important as they greatly affect the user experience.

In this chapter, we adopt the two-way AF multicarrier relay scheme, where a simple form of network coding is used at the relay node, for indoor PLC networks with QoS considerations.

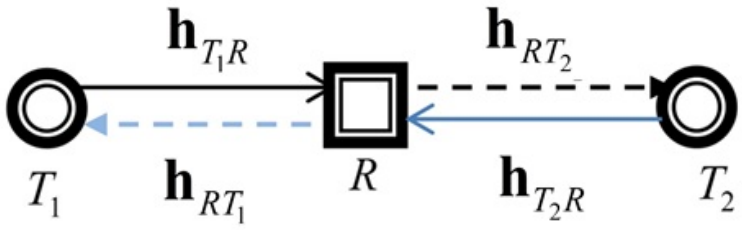

Figure 6.2: A multicarrier two-way information exchange system, where the solid-lines and dash-lines indicate phase 1 and 2 respectively. T_1, T_2 and R stand for the first terminal, the second terminal and the relay node respectively.

Specifically, we consider the joint optimization of the power allocation of two terminals and a relay node to minimize the network total transmission power consumption subject to QoS requirements. Particularly, we set the directional QoS criteria as the lower-bound of the data rate, sent from one terminal to the other. We mention that in practical PLC systems, smaller transmission power leads to lower electromagnetic interference (EMI) to other nearby communication systems.

6.2 System model and problem formulation

The block diagram of the proposed two-way PLC information exchange system is shown in Fig. 6.2 which consists of three nodes: two information terminals (T_1 and T_2) which need to exchange data with each other, and a relay node (R) between them. As mentioned earlier, we consider an OFDM-based mutlticarrier system, where the whole system bandwidth B is divided uniformly into K subcarriers. Given K is a large integer, on each subcarrier, the PLC channel fading can be considered to be frequency-flat. Thus the channel response on the kth ($k = 1,2,\ldots K$) subcarrier from node L_1 to node L_2 is denoted as $h_{L_1L_2}^{[k],(n)}$, where nodes $L_1, L_2 \in \{T_1, T_2, R\}$ and $n = 1,2$ is the index of signaling phase.

Let us denote the transmission power on the kth subcarrier from T_1 as $P_{T_1}^{[k]}$, from T_2as $P_{T_2}^{[k]}$, and from the relay node as $P_R^{[k]}$, respectively. Thus, the total network power P_Σ can be expressed as

$$P_\Sigma = \sum_{k=1}^{K} P_{T_1}^{[k]} + \sum_{k=1}^{K} P_{T_2}^{[k]} + \sum_{k=1}^{K} P_R^{[k]}. \tag{6.1}$$

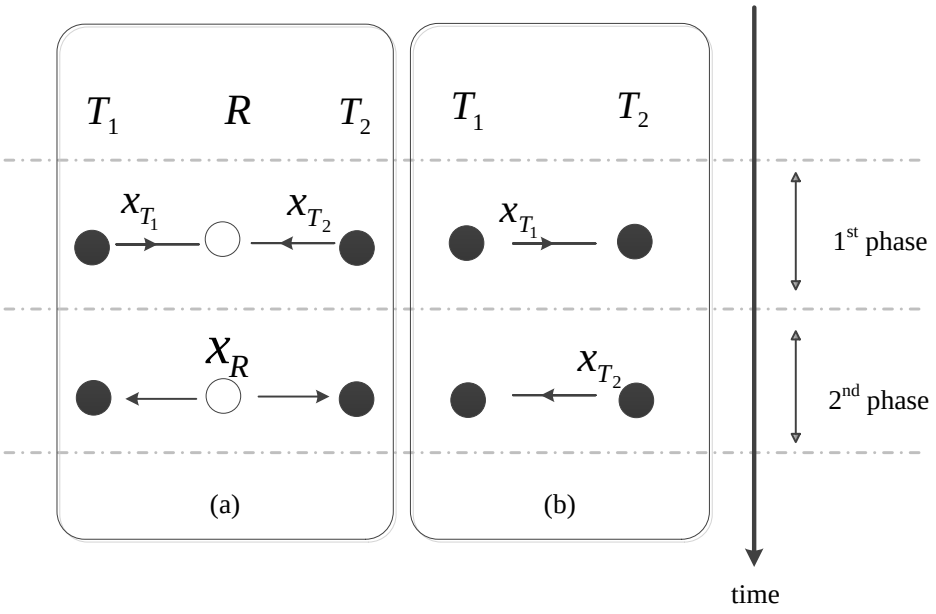

Figure 6.3: (a)Two-phase information exchange procedure illustration. (b) Conventional bidirectional DT system.

Following the OFDM principle, each packet of information from T_1 and T_2 is encoded into K independent complex symbols $X_1^{[k]}$ and $X_2^{[k]}$ ($k = 1,2,\ldots K$) of zero mean and unit variance, respectively. To complete two packets of data exchange between two terminals, this two-way relay scheme works in two phases as illustrated in Fig. 6.3a.

In the first phase, the terminal T_1 sends information signal $X_1^{[k]}$ ($k = 1,2,\ldots K$) over the kth subcarrier with power $P_{T_1}^{[k]}$, at the meantime, the terminal T_2 sends information signal $X_2^{[k]}$ ($k = 1,2,\ldots K$) over the same subcarrier with power $P_{T_2}^{[k]}$. Thus the received signal $Y_{R,1}^{[k]}$ at the relay node can be written as

$$Y_{R,1}^{[k]} = h_{T_1R}^{[k],(1)}\sqrt{P_{T_1}^{[k]}}X_1^{[k]} + h_{T_2R}^{[k],(1)}\sqrt{P_{T_2}^{[k]}}X_2^{[k]} + N_{R,1}^{[k]} \tag{6.2}$$

where the notation $N_{R,1}^{[k]}$ denotes the kth subchannel noise at the relay node in the first phase.

In the second phase, the relay node amplifies its received sum signal on each sub-carrier with proper amplitude gain $g^{[k]}$, then broadcasts the amplified signal to the terminals T_1 and T_2 with power $P_R^{[k]}$. Thus the received signals at the two terminals in the second phase are,

respectively,

$$Y_{T_1,2}^{[k]} = h_{RT_1}^{[k],(2)} g^{[k]} Y_{R,1}^{[k]} + N_{T_1,2}^{[k]} \tag{6.3}$$

$$Y_{T_2,2}^{[k]} = h_{RT_2}^{[k],(2)} g^{[k]} Y_{R,1}^{[k]} + N_{T_2,2}^{[k]} \tag{6.4}$$

where $N_{T_1,2}^{[k]}$ and $N_{T_2,2}^{[k]}$ denote the kth subchannel noise at the terminal T_1 and T_2, respectively in the second phase, and

$$g^{[k]} = \sqrt{\frac{P_R^{[k]}}{P_{T_1}^{[k]} |h_{T_1R}^{[k],(1)}|^2 + P_{T_2}^{[k]} |h_{T_2R}^{[k],(1)}|^2 + W_R^{[k]}}}. \tag{6.5}$$

Given the PSD of the noise does not change in two successive time-phase, we can denote the power of noise $N_{L_2,n}^{[k]}$ $(n = 1,2)$ at node L_2 in two phases as $W_{L_2}^{[k]}$, such as the notation $W_R^{[k]}$ appeared in (6.5). Substituting (6.2) and (6.5) into (6.3) and (6.4) leads to

$$\begin{aligned} Y_{T_1,2}^{[k]} = {} & h_{T_1R}^{[k],(1)} h_{RT_1}^{[k],(2)} \sqrt{\frac{P_R^{[k]} P_{T_1}^{[k]}}{P_{T_1}^{[k]} |h_{T_1R}^{[k],(1)}|^2 + P_{T_2}^{[k]} |h_{T_2R}^{[k],(1)}|^2 + W_R^{[k]}}} X_1^{[k]} \\ & + h_{T_2R}^{[k],(1)} h_{RT_1}^{[k],(2)} \sqrt{\frac{P_R^{[k]} P_{T_2}^{[k]}}{P_{T_1}^{[k]} |h_{T_1R}^{[k],(1)}|^2 + P_{T_2}^{[k]} |h_{T_2R}^{[k],(1)}|^2 + W_R^{[k]}}} X_2^{[k]} \\ & + h_{RT_1}^{[k],(2)} \sqrt{\frac{P_R^{[k]}}{P_{T_1}^{[k]} |h_{T_1R}^{[k],(1)}|^2 + P_{T_2}^{[k]} |h_{T_2R}^{[k],(1)}|^2 + W_R^{[k]}}} N_{R,1}^{[k]} \\ & + N_{T_1,2}^{[k]} \end{aligned} \tag{6.6}$$

$$\begin{aligned} Y_{T_2,2}^{[k]} = {} & h_{T_2R}^{[k],(1)} h_{RT_2}^{[k],(2)} \sqrt{\frac{P_R^{[k]} P_{T_2}^{[k]}}{P_{T_1}^{[k]} |h_{T_1R}^{[k],(1)}|^2 + P_{T_2}^{[k]} |h_{T_2R}^{[k],(1)}|^2 + W_R^{[k]}}} X_2^{[k]} \\ & + h_{T_1R}^{[k],(1)} h_{RT_2}^{[k],(2)} \sqrt{\frac{P_R^{[k]} P_{T_1}^{[k]}}{P_{T_1}^{[k]} |h_{T_1R}^{[k],(1)}|^2 + P_{T_2}^{[k]} |h_{T_2R}^{[k],(1)}|^2 + W_R^{[k]}}} X_1^{[k]} \\ & + h_{RT_2}^{[k],(2)} \sqrt{\frac{P_R^{[k]}}{P_{T_1}^{[k]} |h_{T_1R}^{[k],(1)}|^2 + P_{T_2}^{[k]} |h_{T_2R}^{[k],(1)}|^2 + W_R^{[k]}}} N_{R,1}^{[k]} \\ & + N_{T_2,2}^{[k]}. \end{aligned} \tag{6.7}$$

We assume all the channel state information (CSI) are known by the two terminals. Fur-

thermore, as T_1 have full knowledge of $X_1^{[k]}$, the first term in (6.6) can be readily eliminated and the remainder is used to decode the information beard by signal $X_2^{[k]}$. Similar extraction process is applied in (6.7). Let us denote the SNR of the kth subcarrier at the terminals T_1 as $SNR_{T_1}^{[k]}$, and terminal T_2 as $SNR_{T_2}^{[k]}$, and we can calculate

$$SNR_{T_1}^{[k]} = \frac{P_R^{[k]}|h_{T_2R}^{[k],(1)}|^2 P_{T_2}^{[k]}|h_{RT_1}^{[k],(2)}|^2}{W_{T_1}^{[k]}W_R^{[k]} + P_R^{[k]}|h_{RT_1}^{[k]}|^2 W_R^{[k]} + P_{T_1}^{[k]}|h_{T_1R}^{[k]}|^2 W_{T_1}^{[k]} + P_{T_2}^{[k]}|h_{T_2R}^{[k]}|^2 W_{T_1}^{[k]}} \tag{6.8}$$

$$SNR_{T_2}^{[k]} = \frac{P_R^{[k]}|h_{T_1R}^{[k],(1)}|^2 P_{T_1}^{[k]}|h_{RT_2}^{[k],(2)}|^2}{W_{T_2}^{[k]}W_R^{[k]} + P_R^{[k]}|h_{RT_2}^{[k],(2)}|^2 W_R^{[k]} + P_{T_1}^{[k]}|h_{T_1R}^{[k],(1)}|^2 W_{T_2}^{[k]} + P_{T_2}^{[k]}|h_{T_2R}^{[k],(1)}|^2 W_{T_2}^{[k]}}. \tag{6.9}$$

Let us introduce the notation *normalized path gain* $\gamma_{L_1L_2}^{[k],(n)}$ of subchannel $h_{L_1L_2}^{[k],(n)}$ as

$$\gamma_{L_1L_2}^{[k],(n)} = \frac{|h_{L_1L_2}^{[k],(n)}|^2}{W_{L_2}^{[k]}}, \tag{6.10}$$

so that (6.8) and (6.9) can be rewritten in a compact form as

$$SNR_{T_1}^{[k]} = \frac{P_R^{[k]}\gamma_{T_2R}^{[k],(1)} P_{T_2}^{[k]}\gamma_{RT_1}^{[k],(2)}}{1 + P_R^{[k]}\gamma_{RT_1}^{[k],(2)} + P_{T_1}^{[k]}\gamma_{T_1R}^{[k],(1)} + P_{T_2}^{[k]}\gamma_{T_2R}^{[k],(1)}} \tag{6.11}$$

$$SNR_{T_2}^{[k]} = \frac{P_R^{[k]}\gamma_{T_1R}^{[k],(1)} P_{T_1}^{[k]}\gamma_{RT_2}^{[k],(2)}}{1 + P_R^{[k]}\gamma_{RT_2}^{[k],(2)} + P_{T_1}^{[k]}\gamma_{T_1R}^{[k],(1)} + P_{T_2}^{[k]}\gamma_{T_2R}^{[k],(1)}}. \tag{6.12}$$

Thus, we can obtain the averaged sub-channel capacity (ASC) of the data traffic on the direction from T_2 to T_1 as

$$\bar{C}_1 = \frac{1}{2K}\sum_{k=1}^{K}\log_2\left(1 + \frac{P_R^{[k]}\gamma_{T_2R}^{[k],(1)} P_{T_2}^{[k]}\gamma_{RT_1}^{[k],(2)}}{1 + P_R^{[k]}\gamma_{RT_1}^{[k],(2)} + P_{T_1}^{[k]}\gamma_{T_1R}^{[k],(1)} + P_{T_2}^{[k]}\gamma_{T_2R}^{[k],(1)}}\right) \tag{6.13}$$

where the directional ASC (C_1) is measured in bits/s/Hz/subcarrier, and the factor $1/2$ indicate the two-phase characteristic of the system configuration. Similarly we can express the ASC of the data-link on the inverse traffic direction, namely from T_1 to T_2, as

$$\bar{C}_2 = \frac{1}{2K}\sum_{k=1}^{K}\log_2\left(1 + \frac{P_R^{[k]}\gamma_{T_1R}^{[k],(1)} P_{T_1}^{[k]}\gamma_{RT_2}^{[k],(2)}}{1 + P_R^{[k]}\gamma_{RT_2}^{[k],(2)} + P_{T_1}^{[k]}\gamma_{T_1R}^{[k],(1)} + P_{T_2}^{[k]}\gamma_{T_2R}^{[k],(1)}}\right). \tag{6.14}$$

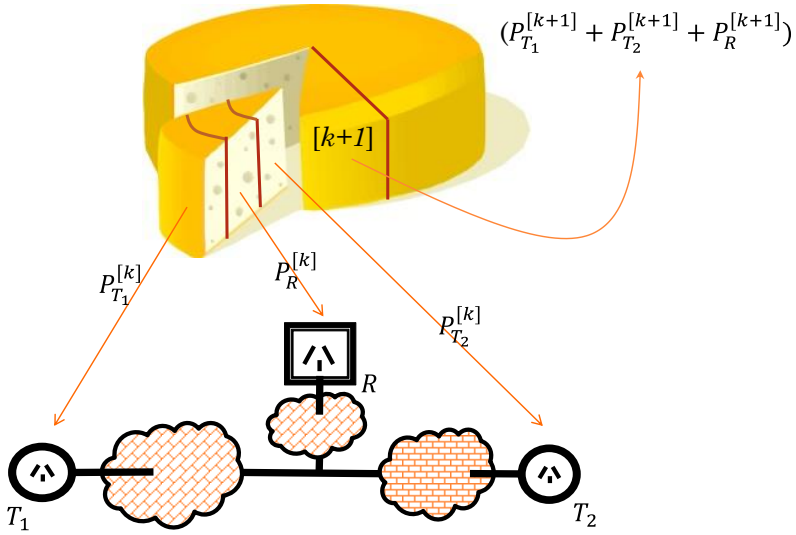

Figure 6.4: Illustration of power allocation problem.

With the QoS criteria as the lower-bounds of the ASC on two traffic directions, to make the most efficient utilization of the system total power we propose the following optimization problem

$$\min_{P_{T_1}^{[k]}, P_{T_2}^{[k]}, P_R^{[k]}} P_\Sigma \tag{6.15}$$

$$s.t. \bar{C}_1 \geq \bar{q}_1, \tag{6.16}$$

$$\bar{C}_2 \geq \bar{q}_2, \tag{6.17}$$

$$P_{T_1}^{[k]}, P_{T_2}^{[k]}, P_R^{[k]} \geq 0, \forall k \tag{6.18}$$

where (6.15) is the objective function of the total network transmission power, and $\bar{q}_1, \bar{q}_2 \geq 0$ are the required minimal ASC on each traffic direction to support certain applications.

Note the problem formulated in (6.15)-(6.18) has twofold tasks. On one hand, it should distribute the system total power optimally on each subcarrier. On the other hand, the power of each subcarrier needs to be optimally allocated to the two terminal nodes and the relay node. This point has been illustrated in Fig. 6.4. As the relay-involved PLC channel is naturally time-varying as we discussed in Chapter 3, this problem cannot be solved by a two-layered approach, such as used in [45].

We mention in the problem (6.15)-(6.18), $\bar{q}_1$ does not have to be equal to $\bar{q}_2$. For example, most of the time in PLC networks down-link QoS is more critical than the up-link one with regard to the user experience. For some scenarios where the QoS requirements do not need to be specified on each individual traffic direction, we can also define the system information exchange capacity (in bits/s/Hz) as

$$C_\varepsilon = K\left(\bar{C}_1 + \bar{C}_2\right). \tag{6.19}$$

So that from (6.16) and (6.17) we can write

$$C_\varepsilon \geq q_\varepsilon \tag{6.20}$$

where the minimal exchange data rate $q_\varepsilon = K\left(\bar{q}_1 + \bar{q}_2\right)$. Note (6.20) is the necessary, but not sufficient condition for (6.16) and (6.17), thus the problem

$$\min_{P_{T_1}^{[k]}, P_{T_2}^{[k]}, P_R^{[k]}} P_\Sigma \tag{6.21}$$

$$s.t. C_\varepsilon \geq q_\varepsilon, \tag{6.22}$$

$$P_{T_1}^{[k]}, P_{T_2}^{[k]}, P_R^{[k]} \geq 0, \forall k \tag{6.23}$$

is a special case of the problem (6.15)-(6.18).

Like the one-way relay-assisted transmission system we discussed in Chapter 5, the exact solution to the problem (6.15)-(6.18) is difficult to obtain because the system minimal ASC constraints in (6.16) and (6.17) are non-convex. In this chapter, again we provide a local optimum solution by adopting the AO approach from [49], where we first optimize $P_R^{[k]}$ with previously given $P_{T_1}^{[k]}$ and $P_{T_2}^{[k]} (k = 1, 2, \ldots K)$; then optimize $P_{T_1}^{[k]}$ with previously optimized $P_R^{[k]}$ and given $P_{T_2}^{[k]}$; next we optimize $P_{T_2}^{[k]}$ with previously optimized $P_R^{[k]}$ and $P_{T_1}^{[k]}$. Repeat this process until convergence, i.e. the difference between the total system power P_Σ obtained in two consecutive iterations is less than a preset threshold. For any two groups of fixed power allocation parameters, the resulted sub-problem becomes convex or quasi-convex. This procedure has been illustrated in Fig. 6.5. Based on this method, we will develop the overall algorithm to solve the original problem (6.15)-(6.18). We discuss these issues in detail from Section 6.3 to Section 6.5.

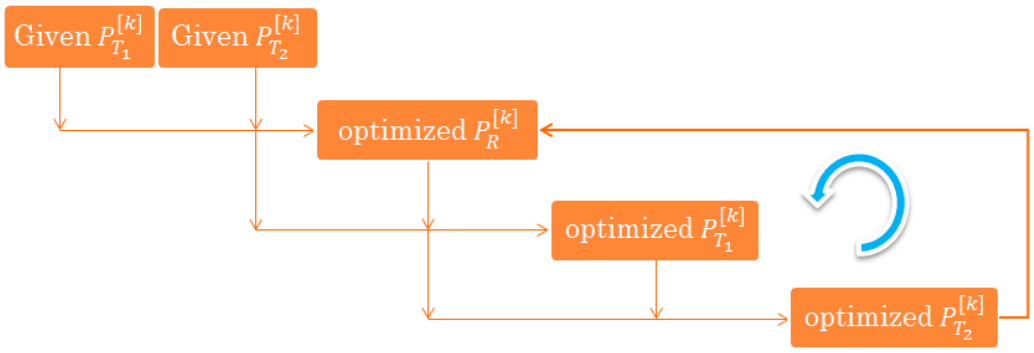

Figure 6.5: Illustration of the AO algorithm for two-way information exchange system.

6.3 Optimal relay power allocation with given terminal power allocations

Let x_k stand for $P_R^{[k]}$ $(k = 1,2,\ldots K)$. For fixed $P_{T_1}^{[k]}$ and $P_{T_2}^{[k]}$, the problem (6.15)-(6.18) becomes

$$\min_{x_k} \sum_{k=1}^{K} x_k \tag{6.24}$$

$$s.t. \quad 2K\bar{q}_1 - \sum_{k=1}^{K} \log_2\left(A_k - \frac{B_k}{C_k x_k + D_k}\right) \leq 0 \tag{6.25}$$

$$2K\bar{q}_2 - \sum_{k=1}^{K} \log_2\left(E_k - \frac{F_k}{G_k x_k + D_k}\right) \leq 0 \tag{6.26}$$

$$x_k \geq 0, \forall k \tag{6.27}$$

where

$$A_k = 1 + P_{T_2}^{[k]} \gamma_{T_2R}^{[k],(1)} \tag{6.28}$$

$$B_k = P_{T_2}^{[k]} \gamma_{T_2R}^{[k],(1)} \left(1 + P_{T_1}^{[k]} \gamma_{T_1R}^{[k],(1)} + P_{T_2}^{[k]} \gamma_{T_2R}^{[k],(1)}\right) \tag{6.29}$$

$$C_k = \gamma_{RT_1}^{[k],(2)} \tag{6.30}$$

$$D_k = 1 + P_{T_1}^{[k]} \gamma_{T_1R}^{[k],(1)} + P_{T_2}^{[k]} \gamma_{T_2R}^{[k],(1)} \tag{6.31}$$

$$E_k = 1 + P_{T_1}^{[k]} \gamma_{T_1R}^{[k],(1)} \tag{6.32}$$

$$F_k = P_{T_1}^{[k]} \gamma_{T_1R}^{[k],(1)} \left(1 + P_{T_1}^{[k]} \gamma_{T_1R}^{[k],(1)} + P_{T_2}^{[k]} \gamma_{T_2R}^{[k],(1)}\right) \tag{6.33}$$

$$G_k = \gamma_{RT_2}^{[k],(2)}. \tag{6.34}$$

Let us write down the Karush-Kuhn-Tucker (KKT) conditions [50] to the problem (6.24)-(6.27) as, for $\forall k$,

$$1-\lambda_1\frac{B_kC_k}{\ln 2\left(A_k-\frac{B_k}{C_kx_k+D_k}\right)(C_kx_k+D_k)^2}-\lambda_2\frac{F_kG_k}{\ln 2\left(E_k-\frac{F_k}{G_kx_k+D_k}\right)(G_kx_k+D_k)^2}=0 \quad (6.35)$$

$$\lambda_1\left[2K\bar{q}_1-\sum_{k=1}^{K}\log_2\left(A_k-\frac{B_k}{C_kx_k+D_k}\right)\right]=0 \quad (6.36)$$

$$\lambda_2\left[2K\bar{q}_2-\sum_{k=1}^{K}\log_2\left(E_k-\frac{F_k}{G_kx_k+D_k}\right)\right]=0 \quad (6.37)$$

$$\lambda_1,\lambda_2\geq 0 \quad (6.38)$$

$$x_k\geq 0. \quad (6.39)$$

PROPOSITION 6.1: The problem (6.24)-(6.27) is convex on $\{x_k \mid x_k\geq 0, k=1,2,\ldots K\}$. For fixed $\lambda_1,\lambda_2>0$, the left-hand-side (LHS) of (6.35)-(6.37) are all monotone functions of x_k.

PROOF: See Appendix B.1 at the end of this thesis.

Form Proposition 6.1, a bisection search algorithm can be employed to solve the KKT conditions (6.35)-(6.39), which leads to the optimal solution of the problem (6.24)-(6.27).

6.4 Optimal first terminal power allocation with given second terminal and relay power allocations

Let y_k stand for $P_{T_1}^{[k]}$ $(k = 1, 2, \ldots K)$, then for given $P_R^{[k]}$ and $P_{T_2}^{[k]}$ we now consider the optimal power allocation of the first terminal by solving the problem of

$$\min_{y_k} \sum_{k=1}^{K} y_k \tag{6.40}$$

$$s.t. \quad 2K\bar{q}_1 - \sum_{k=1}^{K} \log_2 \left(1 + \frac{H_k}{J_k y_k + L_k}\right) \leq 0 \tag{6.41}$$

$$2K\bar{q}_2 - \sum_{k=1}^{K} \log_2 \left(M_k - \frac{O_k}{J_k y_k + P_k}\right) \leq 0 \tag{6.42}$$

$$y_k \geq 0, \forall k \tag{6.43}$$

where

$$H_k = P_R^{[k]} \gamma_{T_2R}^{[k],(1)} P_{T_2}^{[k]} \gamma_{RT_1}^{[k],(2)} \tag{6.44}$$

$$J_k = \gamma_{T_1R}^{[k],(1)} \tag{6.45}$$

$$L_k = 1 + P_R^{[k]} \gamma_{RT_1}^{[k],(2)} + P_{T_2}^{[k]} \gamma_{T_2R}^{[k],(1)} \tag{6.46}$$

$$M_k = 1 + P_R^{[k]} \gamma_{RT_2}^{[k],(2)} \tag{6.47}$$

$$O_k = P_R^{[k]} \gamma_{RT_2}^{[k],(2)} \left(1 + P_R^{[k]} \gamma_{RT_2}^{[k],(2)} + P_{T_2}^{[k]} \gamma_{T_2R}^{[k],(1)}\right) \tag{6.48}$$

$$P_k = 1 + P_R^{[k]} \gamma_{RT_2}^{[k],(2)} + P_{T_2}^{[k]} \gamma_{T_2R}^{[k],(1)}. \tag{6.49}$$

Let us write down the KKT conditions to the problem (6.40)-(6.43) as, for $\forall k$,

$$1 - \mu_1 \frac{H_k J_k}{\ln 2 \left(-1 - \frac{H_k}{J_k y_k + L_k}\right) (J_k y_k + L_k)^2} - \mu_2 \frac{J_k O_k}{\ln 2 \left(M_k - \frac{O_k}{J_k y_k + P_k}\right) (J_k y_k + P_k)^2} = 0 \tag{6.50}$$

$$\mu_1 \left[2K\bar{q}_1 - \sum_{k=1}^{K} \log_2 \left(1 + \frac{H_k}{J_k y_k + L_k}\right)\right] = 0 \tag{6.51}$$

$$\mu_2 \left[2K\bar{q}_2 - \sum_{k=1}^{K} \log_2 \left(M_k - \frac{O_k}{J_k y_k + P_k}\right)\right] = 0 \tag{6.52}$$

$$\mu_1, \mu_2 \geq 0 \tag{6.53}$$

$$y_k \geq 0. \tag{6.54}$$

PROPOSITION 6.2: The problem (6.40)-(6.43) is quasi-convex on $\{y_k \mid y_k \geq 0, k = 1,2,\ldots K\}$. And for fixed $\mu_1, \mu_2 > 0$, the LHS of (6.50)-(6.52) are monotone functions of y_k.

PROOF: See Appendix B.2 at the end of this chapter.

Based on Proposition 6.2, the solution to the problem (6.40)-(6.43) can be obtained by using a bisection search algorithm.

6.5 Optimal second terminal power allocation with given first terminal and relay power allocations

Similarly, based on the optimized $P_{T_1}^{[k]}$ and $P_R^{[k]}$ from above, we now denote $P_{T_2}^{[k]}$ as z_k and consider the optimization of the second terminal's power allocation by solving the problem of

$$\min_{z_k} \sum_{k=1}^{K} z_k \tag{6.55}$$

$$s.t. \quad 2K\bar{q}_1 - \sum_{k=1}^{K} \log_2 \left(Q_k - \frac{R_k}{S_k z_k + T_k} \right) \leq 0 \tag{6.56}$$

$$2K\bar{q}_2 - \sum_{k=1}^{K} \log_2 \left(1 + \frac{U_k}{S_k z_k + V_k} \right) \leq 0 \tag{6.57}$$

$$z_k \geq 0, \forall k \tag{6.58}$$

where

$$Q_k = 1 + P_R^{[k]} \gamma_{RT_1}^{[k],(2)} \tag{6.59}$$

$$R_k = P_R^{[k]} \gamma_{RT_1}^{[k],(2)} \left(1 + P_R^{[k]} \gamma_{RT_1}^{[k],(2)} + P_{T_1}^{[k]} \gamma_{T_1R}^{[k],(1)} \right) \tag{6.60}$$

$$S_k = \gamma_{T_2R}^{[k],(1)} \tag{6.61}$$

$$T_k = 1 + P_R^{[k]} \gamma_{RT_1}^{[k],(2)} + P_{T_1}^{[k]} \gamma_{T_1R}^{[k],(1)} \tag{6.62}$$

$$U_k = P_R^{[k]} \gamma_{T_1R}^{[k],(1)} P_{T_1}^{[k]} \gamma_{RT_2}^{[k],(2)} \tag{6.63}$$

$$V_k = 1 + P_R^{[k]} \gamma_{RT_2}^{[k],(2)} + P_{T_1}^{[k]} \gamma_{T_1R}^{[k],(1)}. \tag{6.64}$$

The KKT conditions to the problem (6.55)-(6.58) are, for $\forall k$

$$1-\delta_1\frac{R_kS_k}{\ln 2\left(Q_k-\frac{R_k}{S_kz_k+T_k}\right)(S_kz_k+T_k)^2}-\delta_2\frac{S_kU_k}{\ln 2\left(-1-\frac{U_k}{S_kz_k+V_k}\right)(S_kz_k+V_k)^2}=0 \quad (6.65)$$

$$\delta_1\left[2K\bar{q}_1-\sum_{k=1}^{K}\log_2\left(Q_k-\frac{R_k}{S_kz_k+T_k}\right)\right]=0 \quad (6.66)$$

$$\delta_2\left[2K\bar{q}_2-\sum_{k=1}^{K}\log_2\left(1+\frac{U_k}{S_kz_k+V_k}\right)\right]=0 \quad (6.67)$$

$$\delta_1,\delta_2\geq 0 \quad (6.68)$$

$$z_k\geq 0. \quad (6.69)$$

PROPOSITION 6.3: The problem (6.55)-(6.58) is quasi-convex on $\{z_k \mid z_k \geq 0, k=1,2,\ldots K\}$. And for fixed $\delta_1,\delta_2>0$, the LHS of (6.65)-(6.67) are monotonically changing with z_k.

Note the structural similarity between the problem (6.40)-(6.43) and the problem (6.55)-(6.58). The proof of Proposition 6.3 is similar to the proof of Proposition 6.2 in Appendix B.2.

Again, the solution to the problem (6.55)-(6.58) can be obtained by using a conventional bisection algorithm.

6.6 Overall iterative algorithm

Based on the discussion from Section 6.3 to Section 6.5, we summarize the proposed AO algorithm for solving the problem (6.15)-(6.18). This is shown in Algorithm 6.1.

In general, the alternating optimization method cannot guarantee to converge to the globally optimal solution. However, since we obtain the global optimum for each subproblem, the proposed AO algorithm converges to a stationary point of the objective function (6.15). This will be verified by simulation examples in Section 6.8.

Algorithm 6.1 AO algorithm for solving the problem (6.15)-(6.18)

1) Initialize $P_{T_1}^{[1]} = p_{t1}$ while $P_{T_1}^{[k]} = 0$ $(k = 2,3,\ldots,K)$; $P_{T_2}^{[1]} = p_{t2}$ while $P_{T_2}^{[k]} = 0$ $(k = 2,3,\ldots,K)$; and $P_R^{[1]} = p_r$ while $P_R^{[k]} = 0$ $(k = 2,3,\ldots,K)$. Here the scalars p_{t1}, p_{t2} and p_r are positive numbers which satisfy (6.16) and (6.17).
2) Use bi-section algorithm with preselected (newly obtained) $P_{T_1}^{[k]}$ and $P_{T_2}^{[k]}$ to solve (6.35)-(6.39) to find a new set of $P_R^{[k]}$.
3) Use bi-section algorithm with the preselected (newly obtained) $P_{T_2}^{[k]}$ and $P_R^{[k]}$ to solve (6.50)-(6.54) to find a new set of $P_{T_1}^{[k]}$.
4) Use bi-section algorithm with newly obtained $P_R^{[k]}$ and $P_{T_1}^{[k]}$ to solve (6.65)-(6.69) to find a new set of $P_{T_2}^{[k]}$.
5) Calculate the total power value (6.1) with the obtained power allocation values from 2)-4).
6) If the difference of the value of (6.1) in two successive iterations is less than a preset threshold σ, then stop; otherwise, go to step 2).

6.7 CTF generation for two-way relay-involved PLC channels

As addressed in Chapter 3, given the topology of a power line network along with its load impedance information, we can use the ABCD theory to calculate its CTF. On the other hand, we can also use the simple approach we proposed to define a testing power line network and directly obtain a group of realistic signaling path gains from this testing relay-involved channel. Considering the two-way relay-involved PLC channel has different characteristics against the one-way transmission case, we address it in detail as follows.

For the convenience of discussion, we redraw the topology of Canate's hybrid point-to-point PLC channel model in Fig. 6.6. Based on this structure, let us construct a testing two-way relay-involved indoor PLC channel with the following two steps:

(1) Set the parameters of this hybrid model as in Table 6.1; this leads to a three-segment (i.e. backbone segments 1 and 2, and a branch segment) network structure.

(2) Introduce the relay device (R) on the only available branch, i.e. branch-tap 1, and implement the pair of data terminals (T_1 and T_2) on two end of the three-segment network. Note the terminal T_i $(i = 1,2)$ has two working modes, i.e. transmitting mode and receiving mode. For the former one, we can think it consists of an ideal voltage source V_{s_i} and inner impedance Z_{G_i}, while the latter case can be represented by a load impedance Z_{T_i}.

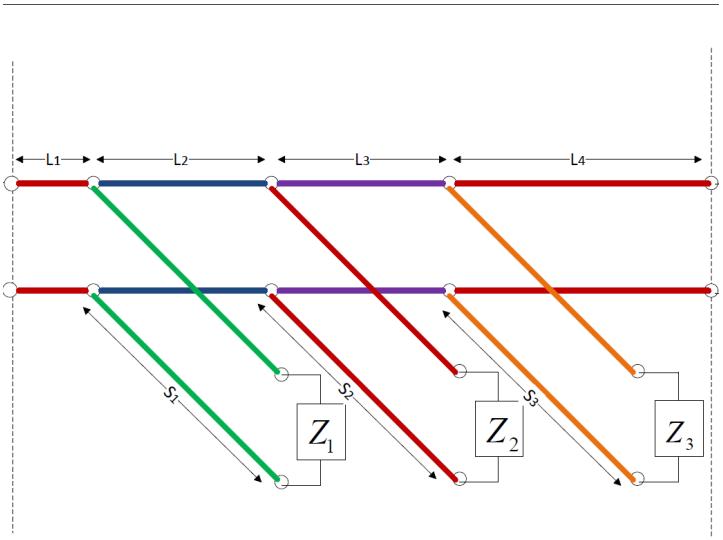

Figure 6.6: Network topology of Canate's PLC channel model.

Table 6.1: Parameters for the three-segment network realization

line section name	length	cable type	terminated load
backbone 1	L_1=*59.3m*	n_{L1}=*2*	*N/A*
branch-tap 1	S_1=11.4m	n_{S1}=1	Z_1 and relay device R
backbone 2	L_2=*48.7m*	n_{L2}=*3*	*N/A*
branch-tap 2	S_2=0	N/A	Z_2=∞
backbone 3	L_3=*0*	*N/A*	*N/A*
branch-tap 3	S_3=0	N/A	Z_3=∞
backbone 4	L_4=*0*	*N/A*	*N/A*
Data terminal at one end:			T_1
Data terminal at the other end:			T_2

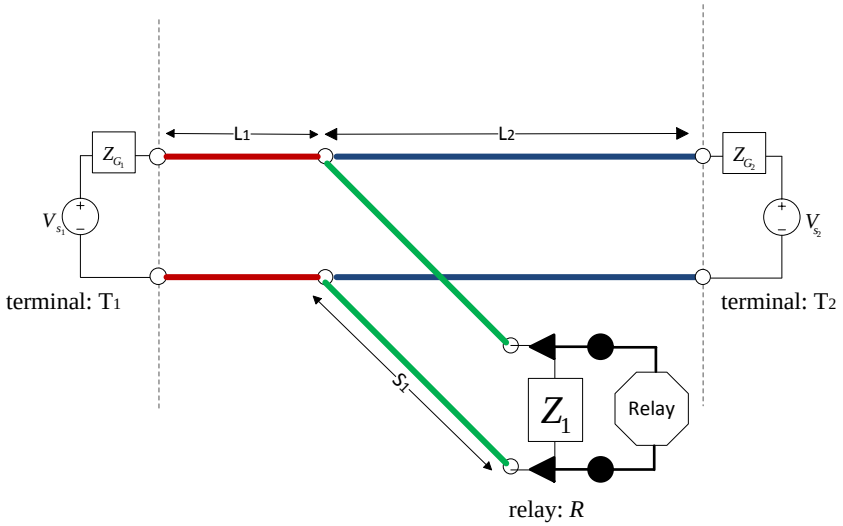

Figure 6.7: Network layout for the three-segment case.

The resulted structure has been shown in Fig. 6.7, where Z_1 is a preexisting load with its frequency response as shown in Fig. 6.8. We set $Z_{G_1} = Z_{G_2} = 5\Omega$, $Z_{T_1} = Z_{T_2} = 150\Omega$ and the total subcarrier number $K = 1024$ in the following.

Similar to the one-way transmission case, in different signaling phase, the network nodes work in different mode and have different electrical characteristics. Let us address them one by one.

Path gains $h_{T_1R}^{[k],(1)}$ and $h_{T_2R}^{[k],(1)}$

As in the first phase the relay node can be treated as a load with impedance $Z_{lR} = 150\Omega$, then the frequency response of the paths $h_{T_1R}^{[k],(1)}$ and $h_{T_2R}^{[k],(1)}$ can be generated from the equivalent network layout as illustrated in Fig. 6.9, Note the parallel equivalent impedance of Z_1 and Z_{lR} can be calculated by using (3.34).

(1) Treat the backbone segment 2 as a "branch" and $V_{s_2} \to 0$ (superposition theorem), we can directly obtain $h_{T_1R}^{[k],(1)}$ by setting the parameters of Canate's hybrid model (Fig. 6.6) as in Table 6.2.

(2) Similarly, treat the backbone segment 1 as a "branch" and $V_{s_1} \to 0$, we can obtain $h_{T_2R}^{[k],(1)}$ by setting the parameters of the hybrid model as in Table 6.3.

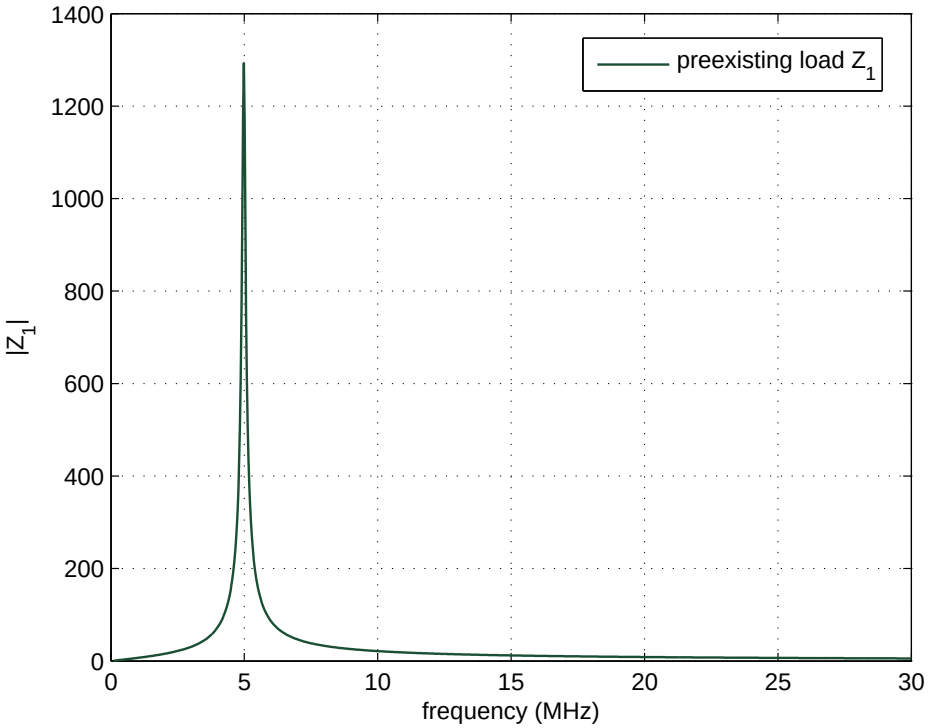

Figure 6.8: Frequency response of Z_1.

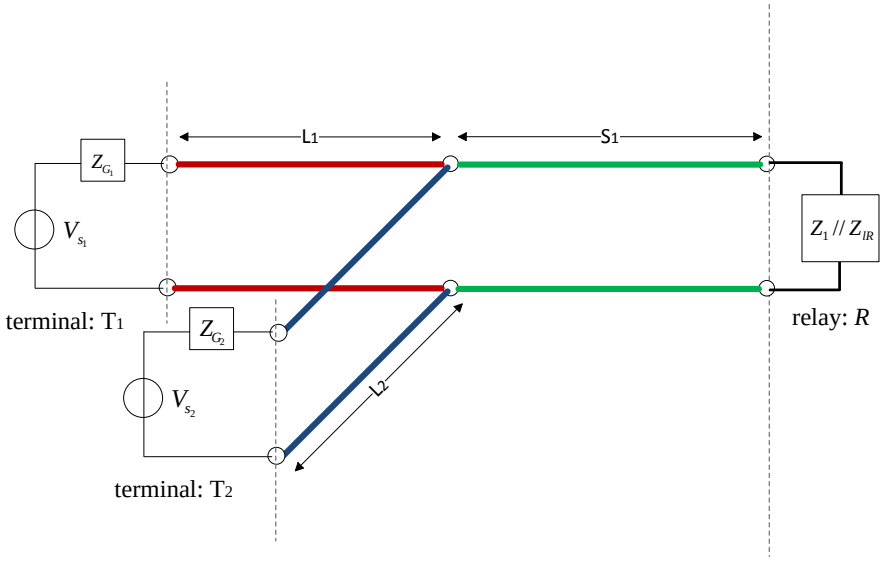

Figure 6.9: Equivalent network layout for the generation of $h_{T_1R}^{[k],(1)}$ and $h_{T_2R}^{[k],(1)}$.

Table 6.2: Parameters for generating path gain $h_{T_1R}^{[k],(1)}$

line section name	length	cable type	terminated load
backbone 1	L_1=*59.3m*	n_{L1}=*2*	*N/A*
branch-tap 1	L_2=48.7m	n_{L2}=3	Z_{G_2}=5Ω
backbone 2	S_1=*11.4m*	n_{S1}=*1*	*N/A*
branch-tap 2	S_2=0	N/A	Z_2=∞
backbone 3	L_3=*0*	*N/A*	*N/A*
branch-tap 3	S_3=0	N/A	Z_3=∞
backbone 4	L_4=*0*	*N/A*	*N/A*
	Transmitting inner impedance:		Z_{G_1}=5Ω
	Receiving load impedance:		$Z_1 /\!\!/ Z_{lR}$

Table 6.3: Parameters for generating path gain $h_{T_2R}^{[k],(1)}$

line section name	length	cable type	terminated load
backbone 1	L_2=48.7m	n_{L2}=3	*N/A*
branch-tap 1	L_1=*59.3m*	n_{L1}=*2*	Z_{G_1}=5Ω
backbone 2	S_1=*11.4m*	n_{S1}=*1*	*N/A*
branch-tap 2	S_2=0	N/A	Z_2=∞
backbone 3	L_3=*0*	*N/A*	*N/A*
branch-tap 3	S_3=0	N/A	Z_3=∞
backbone 4	L_4=*0*	*N/A*	*N/A*
	Transmitting inner impedance:		Z_{G_2}=5Ω
	Receiving load impedance:		$Z_1 /\!\!/ Z_{lR}$

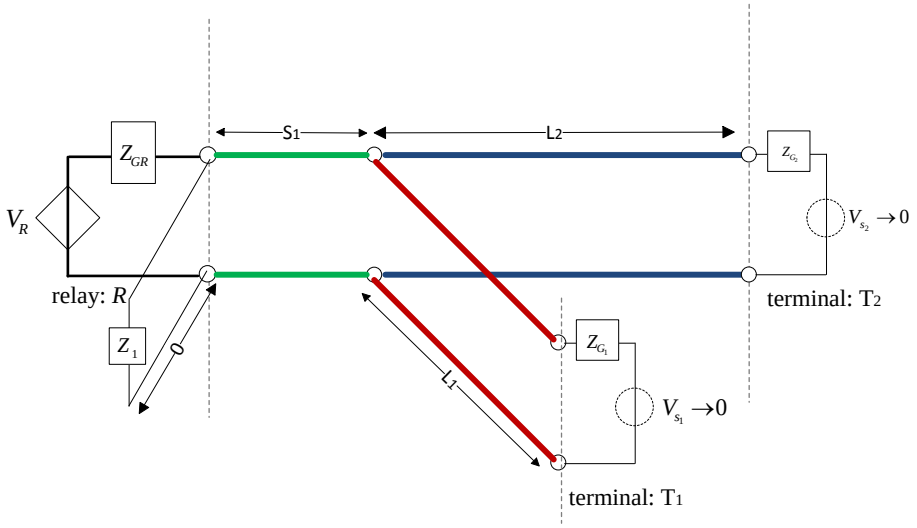

Figure 6.10: Equivalent network layout for CTF generation of source-to-destination path in the second phase.

Path gains $h_{RT_1}^{[k],(2)}$ and $h_{RT_2}^{[k],(2)}$

In the second phase, the relay node changes its working mode and act as a transmitter, which consists of an ideal voltage source V_R and inner impedance $Z_{GR} = 5\Omega$. It is necessary to reconstruct the equivalent network layout as given in Fig. 6.10. Following the superposition theorem, in the second phase we should set $V_{s_2} \to 0$ and $V_{s_1} \to 0$.

(1) Treat the backbone segment 2 as a "branch", we can obtain $h_{RT_1}^{[k],(2)}$ by setting the hybrid model parameter as in Table 6.4.

(2) Similarly, treat the backbone segment 1 as a "branch", $h_{RT_2}^{[k],(2)}$can be obtained by setting the hybrid model parameter as in Table 6.5.

The generated path gains are summarized in Fig. 6.11.

6.8 Numerical examples

In this section we present simulation results based on the same testing relay-involved channel condition generated in Section 5.5 of the last chapter. The parameters used for simulation has been summarized in Table 5.5.

Table 6.4: Parameters for generating path gain $h_{RT_1}^{[k],(2)}$

line section name	length	cable type	terminated load
backbone 1	L_0=*0m*	*N/A*	*N/A*
branch-tap 1	S_0=0m	N/A	Z_1
backbone 2	S_1=*11.4m*	n_{S1}=*1*	*N/A*
branch-tap 2	L_2=48.7m	n_{L2}=3	Z_{T_2}=150Ω
backbone 3	L_1=*59.3m*	n_{L1}=*2*	*N/A*
branch-tap 3	S_3=0	N/A	Z_3=∞
backbone 4	L_4=*0*	*N/A*	*N/A*
	Transmitting inner impedance:		Z_{GR}=5Ω
	Receiving load impedance:		Z_{T_1}=150Ω

Table 6.5: Parameters for generating path gain $h_{RT_2}^{[k],(2)}$

line section name	length	cable type	terminated load
backbone 1	L_0=*0m*	*N/A*	*N/A*
branch-tap 1	S_0=0m	N/A	Z_1
backbone 2	S_1=*11.4m*	n_{S1}=*1*	*N/A*
branch-tap 2	L_1=59.3m	n_{L1}=2	Z_{T_1}=150Ω
backbone 3	L_2=*48.7m*	n_{L2}=*3*	*N/A*
branch-tap 3	S_3=0	N/A	Z_3=∞
backbone 4	L_4=*0*	*N/A*	*N/A*
	Transmitting inner impedance:		Z_{GR}=5Ω
	Receiving load impedance:		Z_{T_2}=150Ω

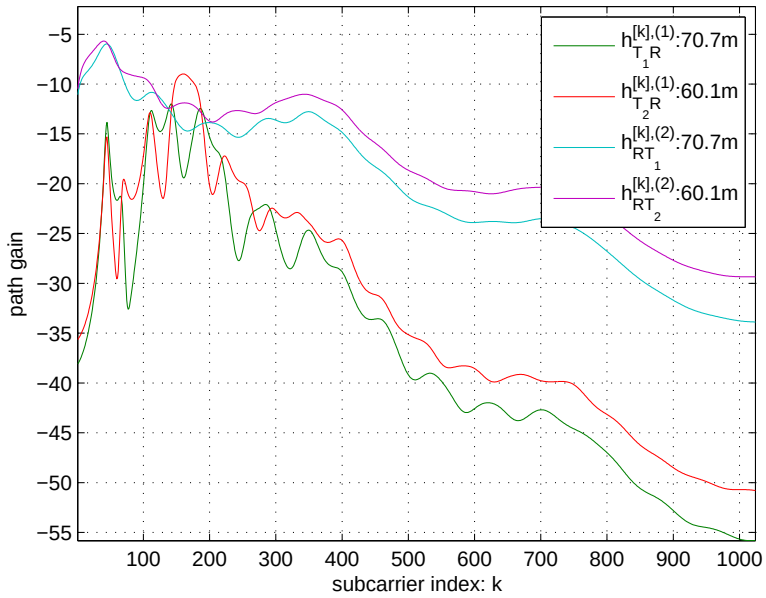

Figure 6.11: Generated testing path gains.

For the proposed iterative algorithm, we also set the convergence condition as the difference between the total power obtained in two consecutive iterations less than 10^{-5}.

For presentation simplicity, we refer to the two-way relay inforamtion exchange scheme as R2WX in the fowllowing. Under the same channel condition we compare the proposed R2WX scheme (which is optimzied by the AO power allocation algorithm) with the bidirectional direct transmission (BDT) system. To ensure a fair comparison, we configure the BDT system to work in the half-duplex mode as illustrated in Fig. 6.3b. From Fig. 6.3b we can see that in the first time-slot, terminal T_1 sends information signal $X_1^{[k]}$ $(k = 1,2,\ldots K)$ with power $D_{T_1}^{[k]}$ over the kth subcarrier to terminal T_2 subject to the directional QoS requirement (6.17). As reported in [48], to meet the ASC constraint on this traffic direction, the optimal power allocation for T_1 is the classical water-filling algorithm. In the second phase, the terminal T_2 replies information signal $X_2^{[k]}$ $(k = 1,2,\ldots K)$ with power $D_{T_2}^{[k]}$ to terminal T_1 subjecting to the QoS requirement on this traffic direction (6.16). Again the water-filling algorithm is used for the power allocation in T_2. Thus, the total network power of the BDT data exchange system is calculated

$$P_{DT} = \sum_{k=1}^{K} D_{T_1}^{[k]} + \sum_{k=1}^{K} D_{T_2}^{[k]}. \tag{6.70}$$

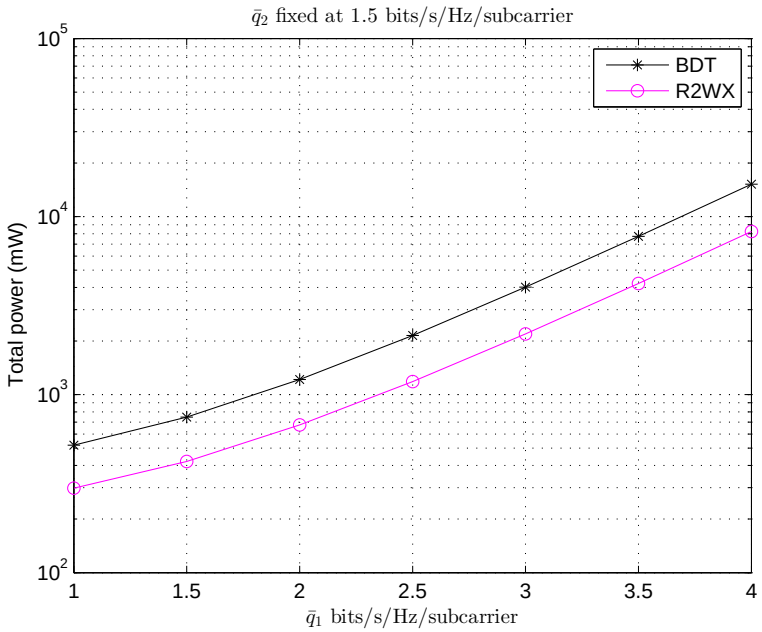

Figure 6.12: Total power versus one directional ASC.

The total network power versus the common QoS requirements curve for the BDT system and two-way relay systems is shown in Fig. 6.12, where we fix $\bar{q}_2$ at 1.5 bits/s/Hz/subcarrier, and increase $\bar{q}_1$ from 1 to 4 bits/s/Hz/subcarrier. We can see from Fig. 6.12 that with respect to the BDT system, the AO algorithm makes the R2WX system meet the QoS requirements with much less power consumption.

As an example to show the power allocation on each subcarrier for the BDT and R2WX systems, powers on seventy subchannels (from 631 to 700) are shown in Fig. 6.13, where the ASC on two traffic directions ($\bar{q}_1$ and $\bar{q}_2$) are set to 2.5 and 1.5 bits/s/Hz/subcarrier, respectively. In Fig. 6.13a, we can see that the terminal T_2 spends more power than T_1 on each subchannel, which is a result of the stricter QoS requirement $\bar{q}_1$ on this traffic direction. Despite this, the power allocations in both terminals follow a similar pattern, which reflect the characteristics of the water-filling algorithm. On the other hand, the power allocation for the R2WX system shown in Fig. 6.13b demonstrates that the AO algorithm not only concerns the direct path's characteristics, but also take the property of the terminal-to-relay links into account. This leads to a more energy-efficient performance of the R2WX system compared with the BDT system.

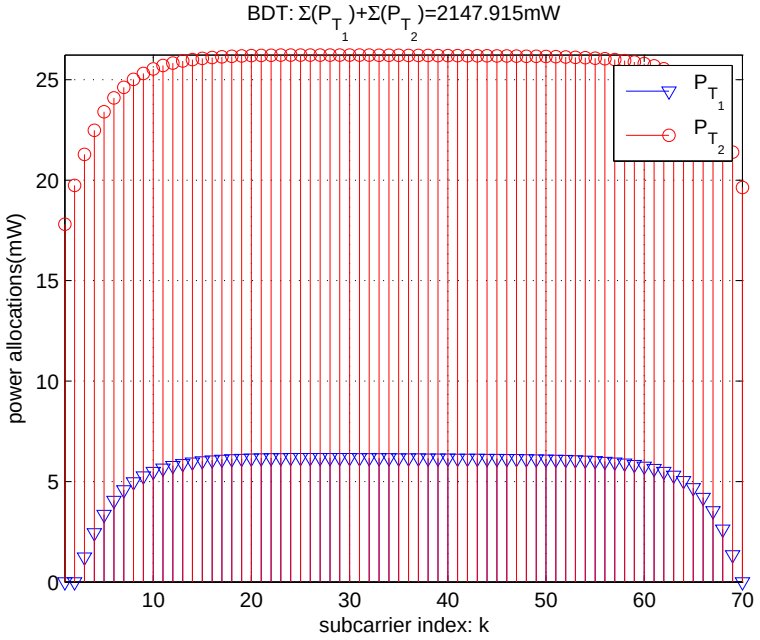

(a) BDT system

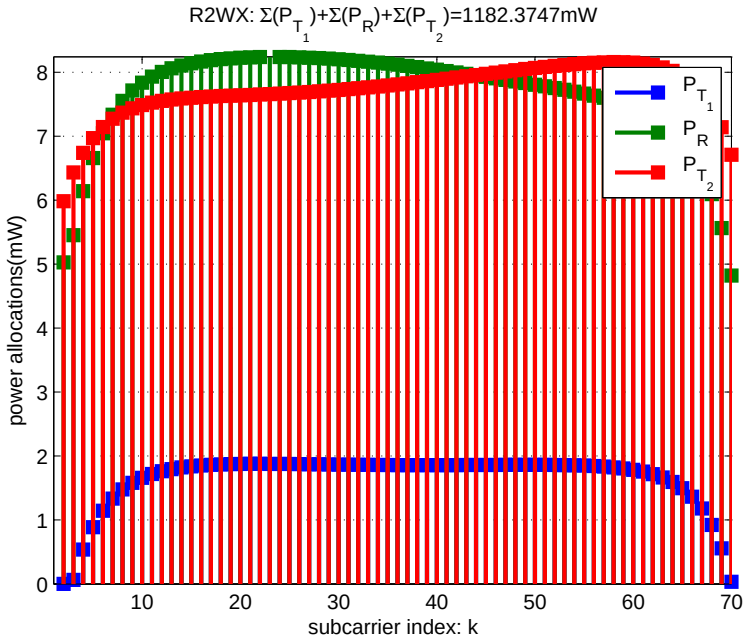

(b) R2WX system

Figure 6.13: Comparison of the power allocations on each subcarrier.

6.9 Chapter summary

Based on a two-way relay-involved PLC channel condition generation approach, we have developed an iterative algorithm to jointly optimize the power allocation between two terminals and one relay node for two-way multicarrier relay systems, where the two terminals exchange information in two time-phases. Specifically, we examined the minimization of the total transmission power when there are minimal ASC requirements on each traffic direction under the indoor PLC environment. Simulation results show that with respect to the conventional bidirectional two-terminal DT system, the proposed algorithm can make the two-way relay system attain the same QoS requirements with less total transmission power.

Chapter 7

Space-Time Coding in PLC Networks

A major challenge of indoor broadband power line communication (PLC) networks is how to provide robust and efficient communication performance under the hostile PLC channel conditions—highly frequency-selective attenuation and considerable noise level. To achieve this goal, in Chapter 6 we introduced the idea of network coding into relay-involved indoor PLC networks and showed its effectiveness. On the other hand, the space-time coding (STC) technology, which is firstly proposed for wireless communication systems, also attracted much interest in the PLC research community. While network coding provides better usage of the existing capacity, STC increases the link capacity among the networks.

Motivated by [62], in this chapter we introduce STC techniques based on the two-way information exchange PLC network, which we proposed in Chapter 6. This multi-relay involved network configuration has been shown in Fig. 7.1. By using the different locations of the multiple relay nodes and the time-varying characteristics of the relay-involved PLC channel, we explore the space-diversity and time-diversity of the indoor PLC network at the same time. Clearly, this an efficient approach which integrated the benefit from both the network coding and STC simultaneously.

The rest of this chapter is organized as follows. Section 7.1 gives a brief review about some related research results. In Section 7.2, a unified two-way traffic model based on practical indoor cabling typologies has be presented, and an adaptive space-time coding scheme for this model has been derived. Section 7.3 discusses the method to generate this multiple relay nodes involved two-way PLC channel. In Section 7.4 simulation results demonstrate that compared with the pure network coding two-way system (without STC processing) ,

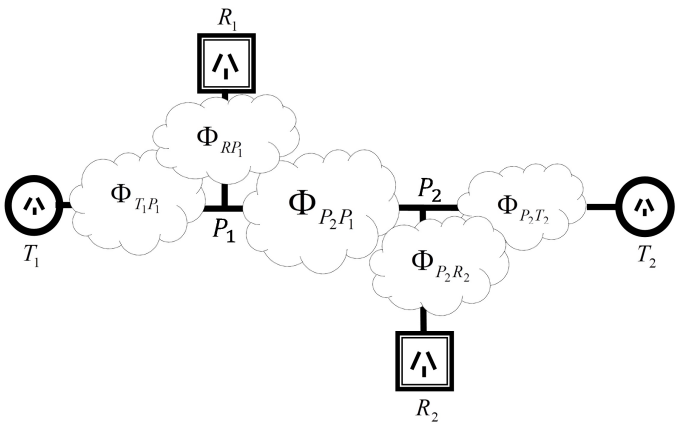

Figure 7.1: Two-way information exchange PLC network with multiple relay nodes.

the new adaptive system can improve the performance significantly. Finally, conclusions are given in Section 7.5.

7.1 Literature review

In wireless communications, when the network nodes share their antenna to transmit information, a virtual multiple-input and multiple-output (MIMO) system is formed to increase the channel capacity. This is usually referred to as cooperative communications. This problem was theoretically studied in [63]. The authors of [56] analyzed the distributed STC to exploit cooperative diversity in wireless networks. In terms of probability of outage and achievable rate region, a general framework of user cooperation was discussed in [64]. Both the cooperative communication and network coding adopt relay nodes; however, the roles of relay nodes in the two schemes are different. In the former one, the relay forwards the information in either AF or DF mode to achieve spatial diversity, while in network coding the relay combines the information from different sources and processes the received combined information before forwarding it out. In [62], the authors investigate how to combine these two schemes together under a wireless ad-hoc network environment.

On the other hand, many signal processing solutions, which were developed for wireless communications systems, now have been adopted into PLC systems, such as compressed sensing [15], cognitive radio [16], and MIMO techniques [17, 18]. In particular, based on the common broadcasting nature between the wireless signal propagation and the power-

cable guided signal transmission, research on the application of advanced relaying processing for PLC systems has become an attractive topic [15, 19, 24, 65, 66]. In [20], the author describes a relay-assisted PLC system based on single-frequency networking condition assumption. The authors of [2, 21, 22] have investigated the optimal time-slot duration allocation between the direct transmission phase and the relay phase, when there is only one relay node. Under the assumption that there are certain amount of outlets available and each outlet between the transceivers on the power grid is a potential relay node, [23] proposed a multi-hop transmission scheme combined with the application of distributed space-time block code (DSTBC) in PLC networks, where each relay node is assigned a unique signature vector which enables the destination node to successively combine the multiaccess received signal without the a priori knowledge about which relay nodes are active.

Due to the half-duplex constraint of the relay node, both the conventional AF and DF relay system suffer from a reduced capacity because the existing of the pre-log factor $1/2$ [56, 57]. To overcome this shortage, the authors of [60] introduce the idea of two-relay scheme into PLC scenario, and this scheme has been addressed in detail in a recent work [61]. In [61] the authors consider that a relay device, working in the AF mode, is used to assist the data exchange of two terminals in an indoor PLC network, and find that the AF two-way system can increase the achievable data exchange rate.

The relaying signal processing schemes in [15]-[23] can be categorized into one group, where relay node(s) enhance one-way data transmission with AF or DF relaying mode. While [60]-[61] belong to another group, in which a simple form of network coding has been realized to improve system capability. Note these two effective techniques are not exclusive to each other. Inspired by [62], in this chapter we propose a unified two-way traffic model for indoor PLC network, where multiple relay nodes work in AF mode. Depending on whether STC technique is applied at the relay nodes, this unified system can work adaptively in one of the following two schemes, namely cooperative STC and naive multiple amplify-and-foreword (MAF) schemes. Thus, the proposed adaptive cooperative space-time coding (ASTC) scheme exploits the benefit from both the cooperative diversity and network coding at the same time. Specifically, under the practical indoor PLC environments we investigate the performance improvement of the proposed ASTC system with respect to its non-adaptive counterparts, i.e. fixed STC and MAF schemes where no adaptive decision is used at the relay nodes.

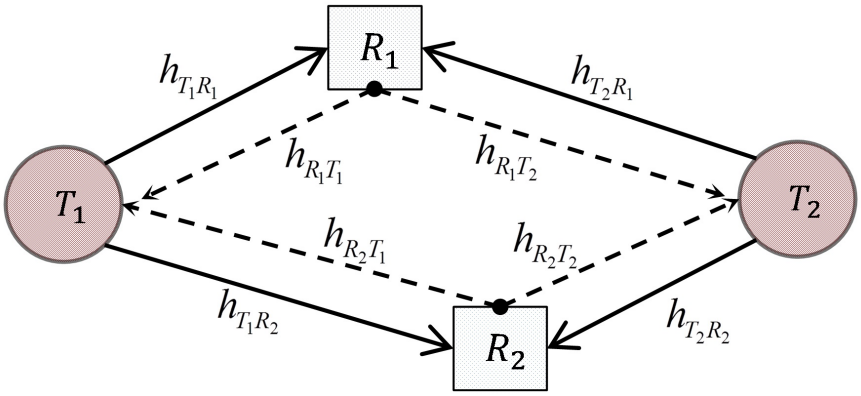

Figure 7.2: Unified two-way information exchange system, where the solid-lines and dash-lines indicate phase 1 and 2, respectively.

7.2 Unified two-way traffic model

The block diagram of the proposed unified two-way information exchange system is shown in Fig. 7.2, which consists of four nodes: two information terminals (T_1 and T_2) which need to exchange data with each other, and two relay nodes (R_1 and R_2) between them. Let us first analyze this unified system working in the cooperative space-time coding (STC) scheme.

7.2.1 STC scheme

To complete one round of data exchange between two terminals, the STC scheme works in two phases (phase 1 and 2), and each phase consists of two time-slots. This configuration is shown in Fig. 7.3a. With the quasi-stationary property of PLC channels[13], we can assume that the channel states do not change across two consecutive time-slots. In other words, the CTF between any two network nodes are stationary in phase 1 or 2.

We start our discussion by considering a narrow-band/single-carrier modulation system, where the channel fading is considered to be frequency-flat. Thus in phase i (i =1 and 2) the channel coefficient from node L_1 to node L_2 is denoted as $h^{(i)}_{L_1L_2}$. In every time-slot, one information package from T_1 and T_2 is encoded as complex symbols x_{T_1} and x_{T_2} of zero mean and variance p_{T_1} and p_{T_2}, respectively. As we consider the case where only two relay nodes are involved, we will use the classical Alamouti space-time coding scheme [67].

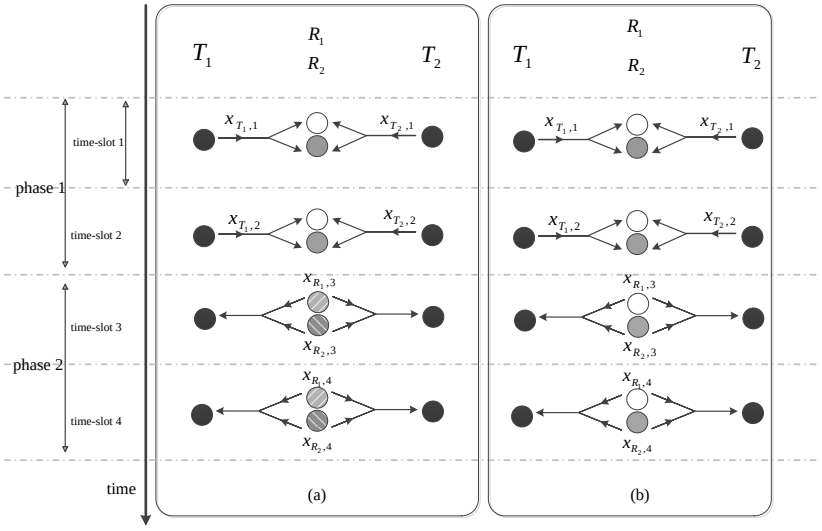

Figure 7.3: (a) STC scheme; (b) MAF scheme.

However, we mention with a more general STC design, such as [68]-[69], the analysis can be similarly done for the situations where more than two relay nodes are involved.

Phase 1: terminals-toward-relays in time-slots 1 and 2

In the first phase, the terminal T_1 sends out a data block $\mathbf{x}_{T_1}$, which consists of two sequential signals $x_{T_1,1}$ and $x_{T_1,2}$ over two consecutive time-slots (slot 1 and 2). We denote this as $\mathbf{x}_{T_1} = \begin{bmatrix} x_{T_1,1} & x_{T_1,2} \end{bmatrix}$. At the mean time, terminal T_2 send out another data block $\mathbf{x}_{T_2}$, which also consists of two sequential signals $x_{T_2,1}$ and $x_{T_2,2}$, i.e. $\mathbf{x}_{T_2} = \begin{bmatrix} x_{T_2,1} & x_{T_2,2} \end{bmatrix}$. Thus in Phase 1, the relay node R_1 receives multiaccess signal block as

$$\begin{aligned} \mathbf{y}_{R_1} &= \begin{bmatrix} y_{R_1,1} & y_{R_1,2} \end{bmatrix} \\ &= \begin{bmatrix} h^{(1)}_{T_1R_1} x_{T_1,1} + h^{(1)}_{T_2R_1} x_{T_2,1} + n_{R_1,1} \\ h^{(1)}_{T_1R_1} x_{T_1,2} + h^{(1)}_{T_2R_1} x_{T_2,2} + n_{R_1,2} \end{bmatrix}^T \\ &= h^{(1)}_{T_1R_1} \mathbf{x}_{T_1} + h^{(1)}_{T_2R_1} \mathbf{x}_{T_2} + \mathbf{n}_{R_1} \end{aligned} \tag{7.1}$$

where $\mathbf{n}_{R_1} = \begin{bmatrix} n_{R_1,1} & n_{R_1,2} \end{bmatrix}$ is the noise at R_1 over time-slots 1 and 2.

Similarly, at the relay node R_2, the received signal block is

$$\begin{aligned}\mathbf{y}_{R_2} &= \begin{bmatrix} y_{R_2,1} & y_{R_2,2} \end{bmatrix} \\ &= \begin{bmatrix} h^{(1)}_{T_1R_2} x_{T_1,1} + h^{(1)}_{T_2R_2} x_{T_2,1} + n_{R_1,1} \\ h^{(1)}_{T_1R_2} x_{T_1,2} + h^{(1)}_{T_2R_2} x_{T_2,2} + n_{R_2,2} \end{bmatrix} \\ &= h^{(1)}_{T_1R_2} \mathbf{x}_{T_1} + h^{(1)}_{T_2R_2} \mathbf{x}_{T_2} + \mathbf{n}_{R_2} \end{aligned} \tag{7.2}$$

where $\mathbf{n}_{R_2} = \begin{bmatrix} n_{R_2,1} & n_{R_2,2} \end{bmatrix}$ is the noise at R_2.

Cooperative STC at relay nodes

Firstly, we write the signal blocks at relay nodes R_1 and R_2 in matrix form as

$$\begin{bmatrix} \mathbf{y}_{R_1} \\ \mathbf{y}_{R_2} \end{bmatrix} = \begin{bmatrix} y_{R_1,1} & y_{R_1,2} \\ y_{R_2,1} & y_{R_2,2} \end{bmatrix}. \tag{7.3}$$

The cooperative STC processing has been done at the two relay nodes independently as follows. At relay node R_1, the second signal $y_{R_1,2}$ has been conjugated and negated. On the other hand, at relay node R_2, it first changes the time sequence between $y_{R_2,1}$ and $y_{R_2,2}$, and then take the conjugation over $y_{R_2,1}$. Thus after this STC processing, the signal blocks at relay nodes R_1 and R_2 can be written as

$$\begin{bmatrix} \mathbf{x}_{R_1} \\ \mathbf{x}_{R_2} \end{bmatrix} = \begin{bmatrix} y_{R_1,1} & -y^*_{R_1,2} \\ y_{R_2,2} & y^*_{R_2,1} \end{bmatrix}. \tag{7.4}$$

Note the signal blocks' power remains unchanged with this STC processing.

Substituting (7.1) and (7.2) into (7.4), we can rewrite $\mathbf{x}_{R_1}$ and $\mathbf{x}_{R_2}$ individually as

$$\begin{aligned}\mathbf{x}_{R_1} &= \begin{bmatrix} x_{R_1,3} & x_{R_1,4} \end{bmatrix} \\ &= \begin{bmatrix} y_{R_1,1} & -y^*_{R_1,2} \end{bmatrix} \\ &= \begin{bmatrix} h^{(1)}_{T_1R_1} x_{T_1,1} + h^{(1)}_{T_2R_1} x_{T_2,1} + n_{R_1,1} \\ -h^{(1)*}_{T_1R_1} x^*_{T_1,2} - h^{(1)*}_{T_2R_1} x^*_{T_2,2} - n^*_{R_1,2} \end{bmatrix}^T \\ &= \dot{\mathbf{x}}_{T_1} \dot{\mathbf{H}}^{(1)}_{T_1R_1} + \dot{\mathbf{x}}_{T_2} \dot{\mathbf{H}}^{(1)}_{T_2R_1} + \dot{\mathbf{n}}_{R_1} \end{aligned} \tag{7.5}$$

where $\dot{\mathbf{x}}_{T_1} = \begin{bmatrix} x_{T_1,1} & -x^*_{T_1,2} \end{bmatrix}$, $\dot{\mathbf{x}}_{T_2} = \begin{bmatrix} x_{T_2,1} & -x^*_{T_2,2} \end{bmatrix}$ while $\dot{\mathbf{H}}^{(1)}_{T_1R_1} = \begin{bmatrix} h^{(1)}_{T_1R_1} & 0 \\ 0 & h^{(1)*}_{T_1R_1} \end{bmatrix}$, $\dot{\mathbf{H}}^{(1)}_{T_2R_1} = \begin{bmatrix} h^{(1)}_{T_2R_1} & 0 \\ 0 & h^{(1)*}_{T_2R_1} \end{bmatrix}$ and $\dot{\mathbf{n}}_{R_1} = \begin{bmatrix} n_{R_1,1} & -n^*_{R_1,2} \end{bmatrix}$. And

$$\begin{aligned}\mathbf{x}_{R_2} &= \begin{bmatrix} x_{R_2,3} & x_{R_2,4} \end{bmatrix} \\ &= \begin{bmatrix} y_{R_2,2} & y^*_{R_2,1} \end{bmatrix} \\ &= \begin{bmatrix} h^{(1)}_{T_1R_2} x_{T_1,2} + h^{(1)}_{T_2R_2} x_{T_2,2} + n_{R_2,2} \\ h^{(1)*}_{T_1R_2} x^*_{T_1,1} + h^{(1)*}_{T_2R_2} x^*_{T_2,1} + n^*_{R_1,1} \end{bmatrix}^T \\ &= \ddot{\mathbf{x}}_{T_1} \ddot{\mathbf{H}}^{(1)}_{T_1R_2} + \ddot{\mathbf{x}}_{T_2} \ddot{\mathbf{H}}^{(1)}_{T_2R_2} + \ddot{\mathbf{n}}_{R_2} \end{aligned} \tag{7.6}$$

where $\ddot{\mathbf{x}}_{T_1} = \begin{bmatrix} x_{T_1,2} & x^*_{T_1,1} \end{bmatrix}$, $\ddot{\mathbf{x}}_{T_2} = \begin{bmatrix} x_{T_2,2} & x^*_{T_2,1} \end{bmatrix}$ while $\ddot{\mathbf{H}}^{(1)}_{T_1R_2} = \begin{bmatrix} h^{(1)}_{T_1R_2} & 0 \\ 0 & h^{(1)*}_{T_1R_2} \end{bmatrix}$, $\ddot{\mathbf{H}}^{(1)}_{T_2R_2} = \begin{bmatrix} h^{(1)}_{T_2R_2} & 0 \\ 0 & h^{(1)*}_{T_2R_2} \end{bmatrix}$ and $\ddot{\mathbf{n}}_{R_2} = \begin{bmatrix} n_{R_2,2} & n^*_{R_2,1} \end{bmatrix}$.

Phase 2: relays-toward-terminals in time-slots 3 and 4

In the second phase, the relay node R_1 amplifies its coded signal block $\mathbf{x}_{R_1}$ with gain g_{R_1}, then broadcasts the resulted signal block over two consecutive time-slots (slots 3 and 4). At the mean time, relay node R_2 amplifies its coded signal block $\mathbf{X}_{R_2}$ with gain g_{R_2} then broadcasts the amplified signals. Thus in phase 2, the received signal block at terminal T_1 can be written as

$$\begin{aligned}\mathbf{y}_{T_1} &= \begin{bmatrix} y_{T_1,3} & y_{T_1,4} \end{bmatrix} \\ &= h^{(2)}_{R_1T_1} g_{R_1} \mathbf{x}_{R_1} + h^{(2)}_{R_2T_1} g_{R_2} \mathbf{x}_{R_2} + \mathbf{n}_{T_1}\end{aligned} \tag{7.7}$$

where $\mathbf{n}_{T_1} = \begin{bmatrix} n_{T_1,3} & n_{T_1,4} \end{bmatrix}$ denotes the noise at T_1over time-slots 3 and 4.

Similarly at T_2, we have

$$\begin{aligned}\mathbf{y}_{T_2} &= \begin{bmatrix} y_{T_2,3} & y_{T_2,4} \end{bmatrix} \\ &= h^{(2)}_{R_1T_2} g_{R_1} \mathbf{x}_{R_1} + h^{(2)}_{R_2T_2} g_{R_2} \mathbf{x}_{R_2} + \mathbf{n}_{T_2}\end{aligned} \tag{7.8}$$

where $\mathbf{n}_{T_2} = \begin{bmatrix} n_{T_2,3} & n_{T_2,4} \end{bmatrix}$denotes the noise at T_2.

Extraction and combing scheme at terminals

We assume all the channel state information (CSI) are known by the two terminals. At terminal T_1, let us substitute (7.5) and (7.6) into (7.7) and we have

$$\begin{aligned}\mathbf{y}_{T_1} = &\left(\dot{\mathbf{x}}_{T_1} \dot{\mathbf{H}}^{(1)}_{T_1R_1} g_{R_1} h^{(2)}_{R_1T_1} + \ddot{\mathbf{x}}_{T_1} \ddot{\mathbf{H}}^{(1)}_{T_1R_2} g_{R_2} h^{(2)}_{R_2T_1}\right) \\ &+ \left(\dot{\mathbf{x}}_{T_2} \dot{\mathbf{H}}^{(1)}_{T_2R_1} g_{R_1} h^{(2)}_{R_1T_1} + \ddot{\mathbf{x}}_{T_2} \ddot{\mathbf{H}}^{(1)}_{T_2R_2} g_{R_2} h^{(2)}_{R_2T_1}\right) \\ &+ \left(g_{R_1} h^{(2)}_{R_1T_1} \dot{\mathbf{n}}_{R_1} + g_{R_2} h^{(2)}_{R_2T_1} \ddot{\mathbf{n}}_{R_2} + \mathbf{n}_{T_1}\right).\end{aligned} \tag{7.9}$$

As terminal T_1 has full knowledge of $\mathbf{x}_{T_1}$, the first term in (7.9) can be readily eliminated. The reminder, which are used to recover the information beard by $\mathbf{x}_{T_2}$, are written as

$$\begin{aligned}&\hat{\mathbf{y}}_{T_1} \\ &= \begin{bmatrix} \hat{y}_{T_1,3} & \hat{y}_{T_1,4} \end{bmatrix} \\ &= \begin{bmatrix} x_{T_2,1} h^{(1)}_{T_2R_1} g_{R_1} h^{(2)}_{R_1T_1} + x_{T_2,2} h^{(1)}_{T_2R_2} g_{R_2} h^{(2)}_{R_2T_1} + g_{R_1} h^{(2)}_{R_1T_1} n_{R_1,1} + g_{R_2} h^{(2)}_{R_2T_1} n_{R_2,2} + n_{T_1,3} \\ -x^*_{T_2,2} h^{(1)*}_{T_2R_1} g_{R_1} h^{(2)}_{R_1T_1} + x^*_{T_2,1} h^{(1)*}_{T_2R_2} g_{R_2} h^{(2)}_{R_2T_1} - g_{R_1} h^{(2)}_{R_1T_1} n^*_{R_1,2} + g_{R_2} h^{(2)}_{R_2T_1} n^*_{R_2,1} + n_{T_1,4} \end{bmatrix}^T.\end{aligned} \tag{7.10}$$

For the convenience of presentation, let us rewrite (7.10) as scalar form as

$$\hat{y}_{T_1,3} = x_{T_2,1}h_A + x_{T_2,2}h_B + n_a \tag{7.11}$$

$$\hat{y}_{T_1,4} = -x^*_{T_2,2}h_C + x^*_{T_2,1}h_D + n_b \tag{7.12}$$

where

$$h_A = h^{(1)}_{T_2R_1} g_{R_1} h^{(2)}_{R_1T_1} \tag{7.13}$$

$$h_B = h^{(1)}_{T_2R_2} g_{R_2} h^{(2)}_{R_2T_1} \tag{7.14}$$

$$n_a = g_{R_1} h^{(2)}_{R_1T_1} n_{R_1,1} + g_{R_2} h^{(2)}_{R_2T_1} n_{R_2,2} + n_{T_1,3} \tag{7.15}$$

$$h_C = h^{(1)*}_{T_2R_1} g_{R_1} h^{(2)}_{R_1T_1} \tag{7.16}$$

$$h_D = h^{(1)*}_{T_2R_2} g_{R_2} h^{(2)}_{R_2T_1} \tag{7.17}$$

$$n_b = -g_{R_1} h^{(2)}_{R_1T_1} n^*_{R_1,2} + g_{R_2} h^{(2)}_{R_2T_1} n^*_{R_2,1} + n_{T_1,4}. \tag{7.18}$$

Thus, we can construct the estimated information signals, $\widetilde{x}_{T_2,1}$ and $\widetilde{x}_{T_2,2}$, by the following combing scheme

$$\widetilde{x}_{T_2,1} = \frac{h^*_C \hat{y}_{T_1,3} + h_B \hat{y}^*_{T_1,4}}{h_A h^*_C + h_B h^*_D} \tag{7.19}$$

$$\widetilde{x}_{T_2,2} = \frac{h^*_D \hat{y}_{T_1,3} - h_A \hat{y}^*_{T_1,4}}{h_A h^*_C + h_B h^*_D}. \tag{7.20}$$

Substituting (7.11) and (7.12) into (7.19) and (7.20), we get

$$\widetilde{x}_{T_2,1} = x_{T_2,1} + \frac{h^*_C n_a + h_B n^*_b}{h_A h^*_C + h_B h^*_D} \tag{7.21}$$

$$\widetilde{x}_{T_2,2} = x_{T_2,2} + \frac{h^*_D n_a - h_A n^*_b}{h_A h^*_C + h_B h^*_D}. \tag{7.22}$$

Similarly, at terminal T_2, by substituting (7.5) and (7.6) into (7.8) we have

$$\begin{aligned}\mathbf{y}_{T_2} = &\left(\dot{\mathbf{x}}_{T_2}\dot{\mathbf{H}}^{(1)}_{T_2R_1} g_{R_1} h^{(2)}_{R_1T_2} + \ddot{\mathbf{x}}_{T_2}\ddot{\mathbf{H}}^{(1)}_{T_2R_2} g_{R_2} h^{(2)}_{R_2T_2}\right) \\ &+ \left(\dot{\mathbf{x}}_{T_1}\dot{\mathbf{H}}^{(1)}_{T_1R_1} g_{R_1} h^{(2)}_{R_1T_2} + \ddot{\mathbf{x}}_{T_1}\ddot{\mathbf{H}}^{(1)}_{T_1R_2} g_{R_2} h^{(2)}_{R_2T_2}\right) \\ &+ \left(g_{R_1} h^{(2)}_{R_1T_2}\dot{\mathbf{n}}_{R_1} + g_{R_2} h^{(2)}_{R_2T_2}\ddot{\mathbf{n}}_{R_2} + \mathbf{n}_{T_2}\right).\end{aligned} \tag{7.23}$$

After the extraction processing, we get

$$\begin{aligned}
&\hat{\mathbf{y}}_{T_2} \\
&= \left[\begin{array}{cc} \hat{y}_{T_2,3} & \hat{y}_{T_2,4} \end{array} \right] \\
&= \left[\begin{array}{c} x_{T_1,1} h^{(1)}_{T_1R_1} g_{R_1} h^{(2)}_{R_1T_2} + x_{T_1,2} h^{(1)}_{T_1R_2} g_{R_2} h^{(2)}_{R_2T_2} + g_{R_1} h^{(2)}_{R_1T_2} n_{R_1,1} + g_{R_2} h^{(2)}_{R_2T_2} n_{R_2,2} + n_{T_2,3} \\ -x^*_{T_1,2} h^{(1)*}_{T_1R_1} g_{R_1} h^{(2)}_{R_1T_2} + x^*_{T_1,1} h^{(1)*}_{T_1R_2} g_{R_2} h^{(2)}_{R_2T_2} - g_{R_1} h^{(2)}_{R_1T_2} n^*_{R_1,2} + g_{R_2} h^{(2)}_{R_2T_2} n^*_{R_2,1} + n_{T_2,4} \end{array} \right]^T .
\end{aligned} \tag{7.24}$$

Rewriting (7.24) as scalar form as

$$\hat{y}_{T_2,3} = x_{T_1,1} h_E + x_{T_1,2} h_F + n_c \tag{7.25}$$

$$\hat{y}_{T_2,4} = -x^*_{T_1,2} h_G + x^*_{T_1,1} h_M + n_d \tag{7.26}$$

where

$$h_E = h^{(1)}_{T_1R_1} g_{R_1} h^{(2)}_{R_1T_2} \tag{7.27}$$

$$h_F = h^{(1)}_{T_1R_2} g_{R_2} h^{(2)}_{R_2T_2} \tag{7.28}$$

$$n_c = g_{R_1} h^{(2)}_{R_1T_2} n_{R_1,1} + g_{R_2} h^{(2)}_{R_2T_2} n_{R_2,2} + n_{T_2,3} \tag{7.29}$$

$$h_G = h^{(1)*}_{T_1R_1} g_{R_1} h^{(2)}_{R_1T_2} \tag{7.30}$$

$$h_M = h^{(1)*}_{T_1R_2} g_{R_2} h^{(2)}_{R_2T_2} \tag{7.31}$$

$$n_d = -g_{R_1} h^{(2)}_{R_1T_2} n^*_{R_1,2} + g_{R_2} h^{(2)}_{R_2T_2} n^*_{R_2,1} + n_{T_2,4}. \tag{7.32}$$

Thus at terminal T_2 we can construct the estimated information signals $\widetilde{x}_{T_1,1}$ and $\widetilde{x}_{T_1,2}$ by

$$\widetilde{x}_{T_1,1} = \frac{h^*_G \hat{y}_{T_2,3} + h_F \hat{y}^*_{T_2,4}}{h_E h^*_G + h_F h^*_M} \tag{7.33}$$

$$\widetilde{x}_{T_1,2} = \frac{h^*_M \hat{y}_{T_2,3} - h_E \hat{y}^*_{T_2,4}}{h_E h^*_G + h_F h^*_M}. \tag{7.34}$$

Substituting (7.25) and (7.26) into (7.34) and (7.36), we get

$$\widetilde{x}_{T_1,1} = x_{T_1,1} + \frac{h^*_G n_c + h_F n^*_d}{h_E h^*_G + h_F h^*_M} \tag{7.35}$$

$$\widetilde{x}_{T_1,2} = x_{T_1,2} + \frac{h^*_M n_c - h_E n^*_d}{h_E h^*_G + h_F h^*_M}. \tag{7.36}$$

Finally the combined signals (7.21)-(7.22) in T_1, and (7.35)-(7.36) in T_2, are sent to the maximum likelihood (ML) detector for digital symbol decoding, respectively.

7.2.2 MAF scheme

Except that there is no STC processing involved at the relay nodes, similar signal propagation can be analyzed for the MAF scheme, which is shown in Fig. 7.3b, where the same notation system has been used. Thus, in phase 1 the relay nodes R_1 and R_2 receive multiaccess signal blocks respectively as

$$\mathbf{y}_{R_1} = h^{(1)}_{T_1R_1}\mathbf{x}_{T_1} + h^{(1)}_{T_2R_1}\mathbf{x}_{T_2} + \mathbf{n}_{R_1} \tag{7.37}$$

and

$$\mathbf{y}_{R_2} = h^{(1)}_{T_1R_2}\mathbf{x}_{T_1} + h^{(1)}_{T_2R_2}\mathbf{x}_{T_2} + \mathbf{n}_{R_2}. \tag{7.38}$$

Like in the STC scheme, the relay nodes R_1 amplifies its signal block $\mathbf{y}_{R_1}$ with gain g_{R_1}, then broadcasts the amplified signal block. At the mean time, relay node R_2 amplifies its signal block $\mathbf{y}_{R_2}$ with gain g_{R_2} then broadcasts the amplified signals. Thus in phase 2, the received signal block at terminal T_1 and T_2 can be written respectively as

$$\mathbf{y}_{T_1} = h^{(2)}_{R_1T_1}g_{R_1}\mathbf{y}_{R_1} + h^{(2)}_{R_2T_1}g_{R_2}\mathbf{y}_{R_2} + \mathbf{n}_{T_1} \tag{7.39}$$

and

$$\mathbf{y}_{T_2} = h^{(2)}_{R_1T_2}g_{R_1}\mathbf{y}_{R_1} + h^{(2)}_{R_2T_2}g_{R_2}\mathbf{y}_{R_2} + \mathbf{n}_{T_2}. \tag{7.40}$$

Finally after the known information $\mathbf{x}_{T_1}$ has been removed in the terminal T_1, by using (7.37)-(7.40), its decoding signal block is written as

$$\begin{bmatrix} \hat{y}_{T_1,3} \\ \hat{y}_{T_1,4} \end{bmatrix} = \begin{bmatrix} x_{T_2,1}\left(h^{(1)}_{T_2R_1}g_{R_1}h^{(2)}_{R_1T_1} + h^{(1)}_{T_2R_2}g_{R_2}h^{(2)}_{R_2T_1}\right) + g_{R_1}h^{(2)}_{R_1T_1}n_{R_1,1} + g_{R_2}h^{(2)}_{R_2T_1}n_{R_2,1} + n_{T_1,3} \\ x_{T_2,2}\left(h^{(1)}_{T_2R_1}g_{R_1}h^{(2)}_{R_1T_1} + h^{(1)}_{T_2R_2}g_{R_2}h^{(2)}_{R_2T_1}\right) + g_{R_1}h^{(2)}_{R_1T_1}n_{R_1,2} + g_{R_2}h^{(2)}_{R_2T_1}n_{R_2,2} + n_{T_1,4} \end{bmatrix}. \tag{7.41}$$

Similarly for terminal T_2, we have

$$\begin{bmatrix} \hat{y}_{T_2,3} \\ \hat{y}_{T_2,4} \end{bmatrix} = \begin{bmatrix} x_{T_1,1}\left(h^{(1)}_{T_1R_1}g_{R_1}h^{(2)}_{R_1T_2}+h^{(1)}_{T_1R_2}g_{R_2}h^{(2)}_{R_2T_2}\right)+g_{R_1}h^{(2)}_{R_1T_2}n_{R_1,1}+g_{R_2}h^{(2)}_{R_2T_2}n_{R_2,1}+n_{T_2,3} \\ x_{T_1,2}\left(h^{(1)}_{T_1R_1}g_{R_1}h^{(2)}_{R_1T_2}+h^{(1)}_{T_1R_2}g_{R_2}h^{(2)}_{R_2T_2}\right)+g_{R_1}h^{(2)}_{R_1T_2}n_{R_1,2}+g_{R_2}h^{(2)}_{R_2T_2}n_{R_2,2}+n_{T_2,4} \end{bmatrix}. \tag{7.42}$$

7.2.3 ASTC scheme

For simplicity we assumed that the noise at different nodes in different phase are i.i.d and share the same power w, i.e.

$$w^{(i)}_{R_1} = w^{(i)}_{R_2} = w^{(i)}_{T_1} = w^{(i)}_{T_2} = w \tag{7.43}$$

where the phase index $i = 1,2$.

As the information signals $x_{T_1,m}$ and $x_{T_2,m}$ $(m = 1,2)$ are with power p_{T_1} and p_{T_2} respectively, for the STC scheme, we can calculate the SNR corresponding to the combined signals (7.21)-(7.22) at T_1 as[1]

$$SNR^{STC}_{T_1} = \frac{p_{T_2}\left|(h^{(1)}_{T_2R_1}g_{R_1}|h^{(2)}_{R_1T_1}|)^2+(h^{(1)}_{T_2R_2}g_{R_2}|h^{(2)}_{R_2T_1}|)^2\right|^2}{w\left(|g_{R_1}h^{(2)}_{R_1T_1}|^2+|g_{R_2}h^{(2)}_{R_2T_1}|^2+1\right)\left(|h^{(1)}_{T_2R_1}g_{R_1}h^{(2)}_{R_1T_1}|^2+|h^{(1)}_{T_2R_2}g_{R_2}h^{(2)}_{R_2T_1}|^2\right)}. \tag{7.44}$$

Also, the SNR expression for the MAF scheme at T_1 is

$$SNR^{MAF}_{T_1} = \frac{p_{T_2}\left|h^{(1)}_{T_2R_1}g_{R_1}h^{(2)}_{R_1T_1}+h^{(1)}_{T_2R_2}g_{R_2}h^{(2)}_{R_2T_1}\right|^2}{w\left(|g_{R_1}h^{(2)}_{R_1T_1}|^2+|g_{R_2}h^{(2)}_{R_2T_1}|^2+1\right)}. \tag{7.45}$$

Let us denote the difference between the values (7.44) and (7.45) as

$$\Delta SNR_{T_1}\,(dB) = 10\log_{10}\frac{SNR^{STC}_{T_1}}{SNR^{MAF}_{T_1}}. \tag{7.46}$$

[1] As the channel conditions do not change over one phase, it is easy to see that the SNR in the two time-slots 3 and 4, within the phase 2, are the same, i.e. $SNR^{STC}_{T_1,3} = SNR^{STC}_{T_1,4} = SNR^{STC}_{T_1}$.

It can be seen that the sign of the value (7.46) depends on the channel conditions. Assuming the relay nodes have the CSI, then to maximize SNR at T_1 of the proposed unified two-way system, we can set the relay nodes work in the STC sheme if (7.46) is positive; otherwise we make the system work in the MAF scheme. We refer to this as the ASTC scheme and have

$$SNR_{T_1}^{ASTC} = \max\left\{SNR_{T_1}^{MAF}, SNR_{T_1}^{STC}\right\}. \tag{7.47}$$

In addition, the system total power can be expressed as

$$p_{sum} = 2\left(p_{T_1} + p_{T_2} + p_{R_1} + p_{R_2}\right) \tag{7.48}$$

where

$$p_{R_1} = g_{R_1}^2\left(|h_{T_1R_1}^{(1)}|^2 p_{T_1} + |h_{T_2R_1}^{(1)}|^2 p_{T_2} + w\right) \tag{7.49}$$

$$p_{R_2} = g_{R_2}^2\left(|h_{T_1R_2}^{(1)}|^2 p_{T_1} + |h_{T_2R_2}^{(1)}|^2 p_{T_2} + w\right). \tag{7.50}$$

Note similar analysis and results can be obtained for terminal T_2.

7.2.4 Multicarrier case

Based on the above single-carrier results, we now extend our discussion to the broadband/multicarrier modulation case. We consider an orthogonal frequency-division multiplexing (OFDM) based system, where the whole system bandwidth is divided uniformly into K subcarriers. On each subcarrier, the channel fading is considered to be frequency-flat. Thus in phase i (i =1 and 2) the channel coefficient on the kth ($k = 1,2,\ldots K$) subcarrier from node L_1 to node L_2 is denoted as $h_{L_1L_2}^{[k],(i)}$, where $L_1, L_2 \in \{T_1, T_2, R_1, R_2\}$. Following the OFDM principle, in every time-slot one information package from T_1 and T_2 is encoded into K independent complex symbols $x_{T_1}^{[k]}$ and $x_{T_2}^{[k]}$ ($k = 1,2,\ldots K$) of zero mean and variance $p_{T_1}^{[k]}$ and $p_{T_2}^{[k]}$, respectively. Let us denote in each time-slot the amplitude gain on the kth subcarrier at R_1 and R_2 as $g_{R_1}^{[k]}$ and $g_{R_2}^{[k]}$, while the relaying power as $p_{R_1}^{[k]}$ and $p_{R_2}^{[k]}$ respectively. Thus

we have

$$p_{R_1}^{[k]} = \left(g_{R_1}^{[k]}\right)^2 \left(|h_{T_1R_1}^{(1),[k]}|^2 p_{T_1}^{[k]} + |h_{T_2R_1}^{(1),[k]}|^2 p_{T_2}^{[k]} + w^{[k]}\right) \tag{7.51}$$

$$p_{R_2}^{[k]} = \left(g_{R_2}^{[k]}\right)^2 \left(|h_{T_1R_2}^{(1),[k]}|^2 p_{T_1}^{[k]} + |h_{T_2R_2}^{(1),[k]}|^2 p_{T_2}^{[k]} + w^{[k]}\right). \tag{7.52}$$

Thus, the total network power P_Σ can be expressed as

$$\begin{aligned} P_\Sigma &= \sum_{k=1}^{K} p_{sum}^{[k]} \\ &= 2\sum_{k=1}^{K} \left(p_{T_1}^{[k]} + p_{T_2}^{[k]} + p_{R_1}^{[k]} + p_{R_2}^{[k]}\right). \end{aligned} \tag{7.53}$$

And the SNR on the kth subcarrier from traffic directionT_2 to T_1 (we denote as $SNR_{T_1}^{ASTC,[k]}$), can be easily extended from the result (7.47). Furthermore, we can expresses the capacity (in bits/s/Hz) of the OFDM-based ASTC system on this traffic direction as

$$C_{T_1} = \frac{1}{2}\sum_{k=1}^{K} \log_2\left(1 + SNR_{T_1}^{ASTC,[k]}\right). \tag{7.54}$$

Again, similar results can be obtain for the other traffic direction from T_1 to T_2.

Based on these results, the power allocation problem for each subcarrier at each network nodes (i.e. T_1, T_2, R_1, R_2) can be formulated under different constraints. For example, the one-direction[2] rate maximization (RM) problem [48] can be written as

$$\max_{p_{T_1}^{[k]}, p_{T_2}^{[k]}, g_{R_1}^{[k]}, g_{R_2}^{[k]}} C_{T_1} \tag{7.55}$$

$$s.t. P_\Sigma \leq p \tag{7.56}$$

where p is the total budget available power. On the other hand, if we set the quality-of-service (QoS) criterion as the lower-bounds of the capacity on traffic direction T_2 to T_1, to explore the most efficient utilization of the system power we can propose the following

[2]Note the RM problem for the other traffic direction, or for the capacity sum of both directions, can be similarly formulated.

one-direction[3] margin maximization (MM) problem [48]

$$\min_{p_{T_1}^{[k]}, p_{T_2}^{[k]}, g_{R_1}^{[k]}, g_{R_2}^{[k]}} P_{\Sigma} \tag{7.57}$$

$$s.t. C_{T_1} \geq q_1 \tag{7.58}$$

where $q_1 \geq 0$ is the required minimum capacity on this traffic direction to support certain applications.

Compare (7.44) and (7.45) with the expressions (6.8) and (6.9), we can see they share the same mathematical structure characteristics. Thus the solutions to the above two power allocation problems can be found by adopting the same AO optimization method as we discussed in detail in Chapter 6.

7.3 Channel condition generation when multiple relay nodes involved

In this section let us use a example to show how to generate the relay-involved channel condition when multiple relay nodes are introduced. The network structure (in Fig. 7.1) and nodes working status are similar to the single relay node assisted two-way information exchange system as we proposed in Chapter 6, except the number of existing relay devices. With our simple relay-involved CTF generation approach and setting parameters as in Table 7.1, we can create a testing channel with a four-segment layout as shown in Fig. 7.4, where Z_1 and Z_2 are two preexisting load with their frequency response as shown in Fig. 7.5. Let us assume $Z_{G_1} = Z_{G_2} = Z_{GR_1} = Z_{GR_2} = 5\Omega$, where Z_{G_1}, Z_{G_2}, Z_{GR_1} and Z_{GR_2} are the inner impedance of T_1, T_2, R_1 and R_2 respectively; while $Z_{T_1} = Z_{T_2} = Z_{lR_1} = Z_{lR_2} = 150\Omega$, where Z_{T_1}, Z_{T_2}, Z_{lR_1} and Z_{lR_2} are the receiving impedance of T_1, T_2, R_1 and R_2 respectively.

Now, let us strategically set the testing network's parameters as in Tables 7.2-7.9 respectively, a group of realistic path gains (i.e. $h_{T_1R_1}^{[k],(1)}$, $h_{T_1R_2}^{[k],(1)}$, $h_{T_2R_1}^{[k],(1)}$, $h_{T_2R_2}^{[k],(1)}$, $h_{R_1T_1}^{[k],(2)}$, $h_{R_1T_2}^{[k],(2)}$, $h_{R_2T_1}^{[k],(2)}$, and $h_{R_2T_2}^{[k],(2)}$) can be generated. This is shown in Fig. 7.6, where $k = 1, 2, ..., 1024$ is the subcarrier index. It also can be seen from Fig. 7.6 that the relay-involved PLC channel paths are highly correlated.

[3]Note the MM problem with QoS constraint(s) on the other traffic direction, or on both directions simultaneously, can be similarly formulated.

Table 7.1: Parameters for the four-segment network realization.

line section name	length	cable type	terminated load
backbone 1	L_1=*10.6m*	n_{L1}=*5*	*N/A*
branch-tap 1	S_1=21.4m	n_{S1}=2	$Z_1$and relay device R_1
backbone 2	L_2=*0m*	*N/A*	*N/A*
branch-tap 2	S_2=10.2m	n_{S2}=2	$Z_2$and relay device R_2
backbone 3	L_3=*30.7m*	n_{L3}=*5*	*N/A*
branch-tap 3	S_3=0	N/A	Z_3=∞
backbone 4	L_4=*0*	*N/A*	*N/A*
Data terminal at one end:			T_1
Data terminal at the other end:			T_2

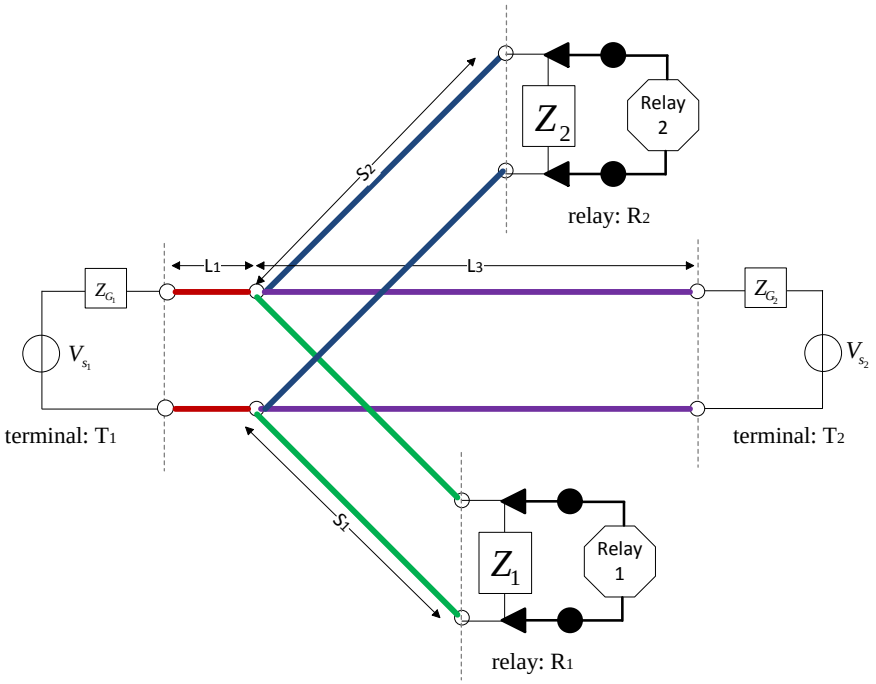

Figure 7.4: Four-segment testing network layout.

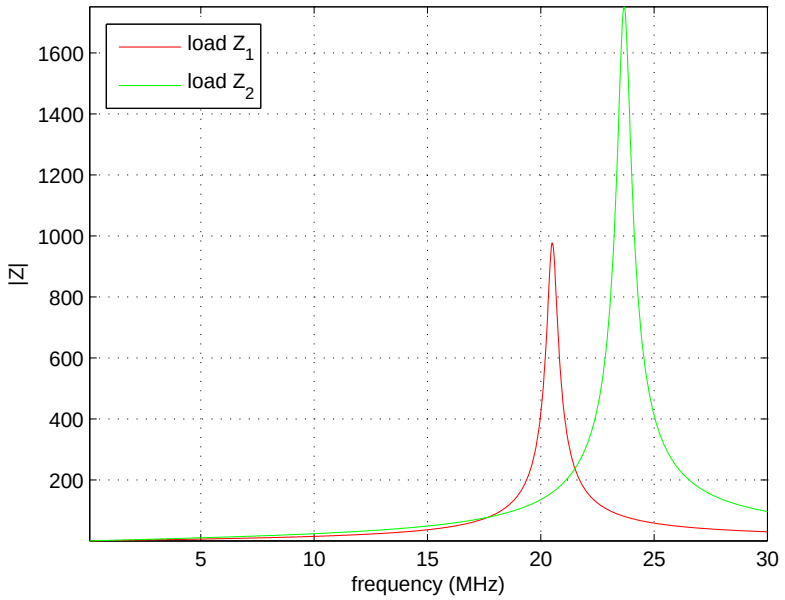

Figure 7.5: Frequency response of loads Z_1 and Z_2.

Table 7.2: Parameters for generating path gain $h_{T_1R_1}^{[k],(1)}$

line section name	length	cable type	terminated load
backbone 1	L_1=*10.6m*	n_{L1}=*5*	*N/A*
branch-tap 1	S_2=10.2m	n_{S1}=2	$Z_2 \,/\!/\, Z_{lR_2}$=$Z_2 \,/\!/\, 150\Omega$
backbone 2	L_2=*0m*	*N/A*	*N/A*
branch-tap 2	L_3=30.7m	n_{L3}=5	Z_{G_2}=5Ω
backbone 3	S_1=*21.4m*	n_{S2}=2	*N/A*
branch-tap 3	S_3=0	N/A	Z_3=∞
backbone 4	L_4=*0*	*N/A*	*N/A*
	Transmitting inner impedance:		Z_{G_1}=5Ω
	Receiving load impedance:		$Z_1 \,/\!/\, Z_{lR_1}$=$Z_1 \,/\!/\, 150\Omega$

Table 7.3: Parameters for generating path gain $h_{T_1R_2}^{[k],(1)}$

line section name	length	cable type	terminated load
backbone 1	L_1=*10.6m*	n_{L1}=*5*	*N/A*
branch-tap 1	S_1=21.4m	n_{S1}=2	$Z_1 /\!/ Z_{lR_1}$=$Z_1 /\!/ 150\Omega$
backbone 2	L_2=*0m*	*N/A*	*N/A*
branch-tap 2	L_3=30.7m	n_{L3}=5	Z_{G_2}=5Ω
backbone 3	S_2=*10.2m*	n_{S2}=2	*N/A*
branch-tap 3	S_3=0	N/A	Z_3=∞
backbone 4	L_4=*0*	*N/A*	*N/A*
	Transmitting inner impedance:		Z_{G_1}=5Ω
	Receiving load impedance:		$Z_2 /\!/ Z_{lR_2}$=$Z_2 /\!/ 150\Omega$

Table 7.4: Parameters for generating path gain $h_{T_2R_1}^{[k],(1)}$

line section name	length	cable type	terminated load
backbone 1	L_3=*30.7m*	n_{L3}=*5*	*N/A*
branch-tap 1	S_2=10.2m	n_{S2}=2	$Z_2 /\!/ Z_{lR_2}$=$Z_2 /\!/ 150\Omega$
backbone 2	L_2=*0m*	*N/A*	*N/A*
branch-tap 2	L_1=10.6m	n_{L1}=5	Z_{G_1}=5Ω
backbone 3	S_1=*21.4m*	n_{S1}=2	*N/A*
branch-tap 3	S_3=0	N/A	Z_3=∞
backbone 4	L_4=*0*	*N/A*	*N/A*
	Transmitting inner impedance:		Z_{G_2}=5Ω
	Receiving load impedance:		$Z_1 /\!/ Z_{lR_1}$=$Z_1 /\!/ 150\Omega$

Table 7.5: Parameters for generating path gain $h_{T_2R_2}^{[k],(1)}$

line section name	length	cable type	terminated load
backbone 1	L_3=*30.7m*	n_{L3}=*5*	*N/A*
branch-tap 1	S_1=21.4m	n_{S1}=2	$Z_1 /\!/ Z_{lR_1}$=$Z_1 /\!/ 150\Omega$
backbone 2	L_2=*0m*	*N/A*	*N/A*
branch-tap 2	L_1=10.6m	n_{L1}=5	Z_{G_1}=5Ω
backbone 3	S_2=*10.2m*	n_{S2}=2	*N/A*
branch-tap 3	S_3=0	N/A	Z_3=∞
backbone 4	L_4=*0*	*N/A*	*N/A*
Transmitting inner impedance:			Z_{G_2}=5Ω
Receiving load impedance:			$Z_2 /\!/ Z_{lR_2}$=$Z_2 /\!/ 150\Omega$

Table 7.6: Parameters for generating path gain $h_{R_1T_1}^{[k],(2)}$

line section name	length	cable type	terminated load
backbone 1	*0m*	*N/A*	*N/A*
branch-tap 1	0m	N/A	Z_1
backbone 2	S_1=*21.4m*	n_{S1}=2	*N/A*
branch-tap 2	L_3=30.7m	n_{L3}=5	Z_{T_2}=150Ω
backbone 3	*0m*	N/A	*N/A*
branch-tap 3	S_2=10.2m	n_{S2}=2	$Z_2 /\!/ Z_{GR_2}$=$Z_2 /\!/ 5\Omega$
backbone 4	L_1=*10.6m*	n_{L1}=5	*N/A*
Transmitting inner impedance:			Z_{GR_1}=5Ω
Receiving load impedance:			Z_{T_1}=150Ω

Table 7.7: Parameters for generating path gain $h_{R_1T_2}^{[k],(2)}$

line section name	length	cable type	terminated load
backbone 1	*0m*	*N/A*	*N/A*
branch-tap 1	0m	N/A	Z_1
backbone 2	S_1=*21.4m*	n_{S1}=2	*N/A*
branch-tap 2	L_1=10.6m	n_{L1}=5	Z_{T_1}=150Ω
backbone 3	*0m*	N/A	*N/A*
branch-tap 3	S_2=10.2m	n_{S2}=2	$Z_2 /\!\!/ Z_{GR_2}$=$Z_2 /\!\!/ 5\Omega$
backbone 4	L_3=*30.7m*	n_{L3}=5	*N/A*
	Transmitting inner impedance:		Z_{GR_1}=5Ω
	Receiving load impedance:		Z_{T_2}=150Ω

Table 7.8: Parameters for generating path gain $h_{R_2T_1}^{[k],(2)}$

line section name	length	cable type	terminated load
backbone 1	*0m*	*N/A*	*N/A*
branch-tap 1	0m	N/A	Z_2
backbone 2	S_2=*10.2m*	n_{S2}=2	*N/A*
branch-tap 2	L_3=30.7m	n_{L3}=5	Z_{T_2}=150Ω
backbone 3	*0m*	N/A	*N/A*
branch-tap 3	S_1=21.4m	n_{S1}=2	$Z_1 /\!\!/ Z_{GR_1}$=$Z_1 /\!\!/ 5\Omega$
backbone 4	L_1=*10.6m*	n_{L1}=5	*N/A*
	Transmitting inner impedance:		Z_{GR_2}=5Ω
	Receiving load impedance:		Z_{T_1}=150Ω

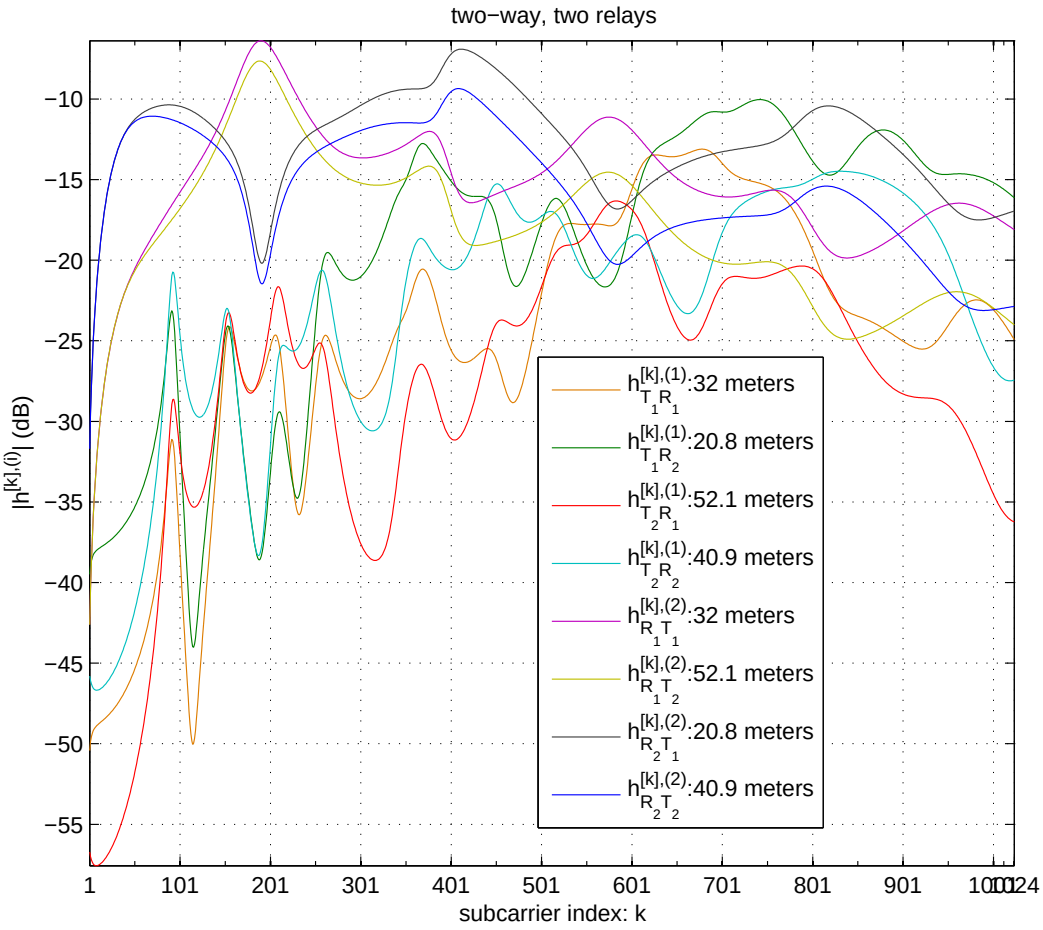

Figure 7.6: Generated testing path gains.

Table 7.9: Parameters for generating path gain $h_{R_2T_2}^{[k],(2)}$

line section name	length	cable type	terminated load
backbone 1	*0m*	*N/A*	*N/A*
branch-tap 1	0m	N/A	Z_2
backbone 2	*S_2=10.2m*	n_{S2}=2	*N/A*
branch-tap 2	L_1=10.6m	n_{L1}=5	Z_{T_1}=150Ω
backbone 3	*0m*	N/A	*N/A*
branch-tap 3	S_1=21.4m	n_{S1}=2	$Z_1 /\!/ Z_{GR_1}$=$Z_1 /\!/ 5\Omega$
backbone 4	*L_3=30.7m*	n_{L3}=5	*N/A*
	Transmitting inner impedance:		Z_{GR_2}=5Ω
	Receiving load impedance:		Z_{T_2}=150Ω

7.4 Numerical examples

Rather than using the optimal power allocation scheme, we simply set the relay gain factors $g_{R_1}^{[k]}$ and $g_{R_2}^{[k]}$ $(k = 1,2,...K)$ as 1, and terminals powers $p_{T_1}^{[k]}$ and $p_{T_2}^{[k]}$ as common constant values. Thus the relay powers $p_{R_1}^{[k]}$ and $p_{R_2}^{[k]}$ can be calculated by using (7.51) and (7.52), and the network total power can be found by using (7.53).

As an example, the SNR values of the STC (7.44), MAF (7.45) and ASTC (7.47) schemes at terminal T_1 on each subcarrier have been compared in Fig. 7.7. It is clearly shown that, unlike the ASTC scheme, neither the STC scheme nor the MAF scheme can guarantee the maximum SNR on each subcarrier to be obtained. This point is emphasized by the SNR difference value (7.46) shown in the figure.

Next, the one-direction capacity of the ASTC scheme (7.54) has been compared with the STC and MFA schemes, as shown in Fig. 7.8, with respect to the increasing of the total network power (7.53). We can see from Fig. 7.8 that, under a random power allocation configuration, the ASTC scheme outperform the two fixed schemes. Note if the optimization power allocation is applied to the ASTC scheme, a better performance can be expected.

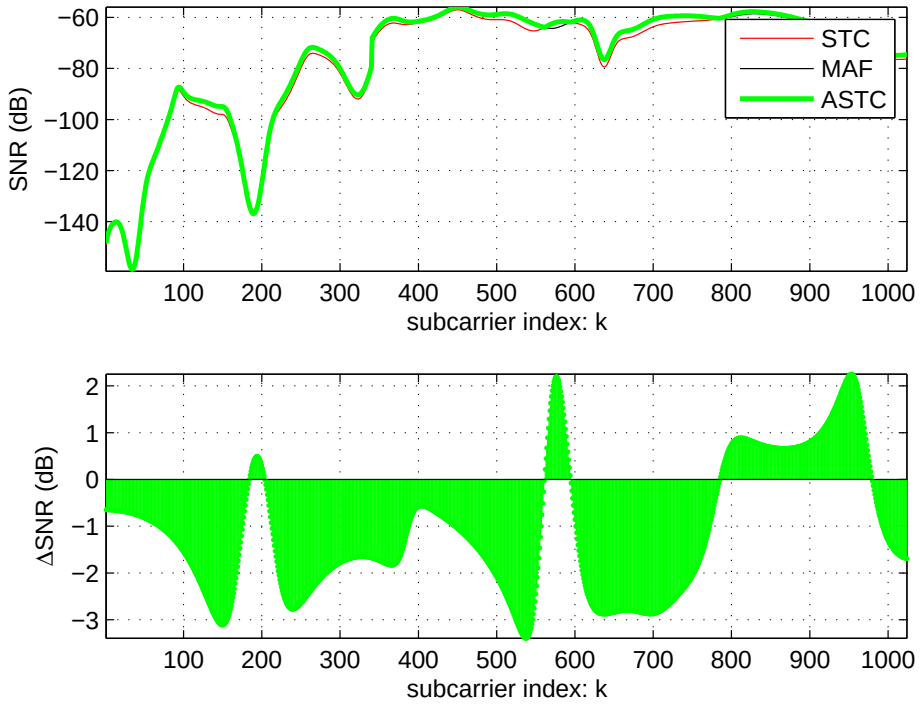

Figure 7.7: SNR values of the STC, MAF, and ASTC schemes on the first 256 subcarriers.

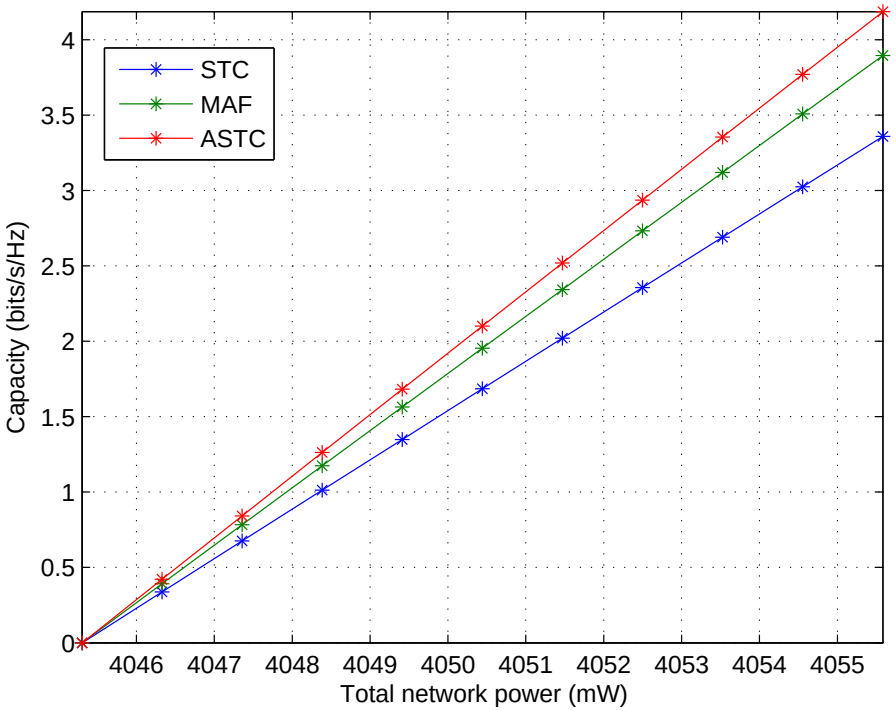

Figure 7.8: Capacity of ASTC, STC and MAF schemes.

7.5 Chapter summary

We have proposed an adaptive space-time coding scheme for the relay nodes, which works in the two-way multicarrier PLC system, where the two terminals exchange information with each other in two time-phases. In particular, we examined SNR and capacity performance of proposed system under the practical indoor PLC environment. Simulation results show that with respect to the fixed schemes, the proposed adaptive scheme can make the two-way relay system attain higher data-transmission capacity with the same total transmission power.

Chapter 8

Conclusion

Compared with other communication systems, PLC technology has its unique advantage that power cables are preexisting almost in every town of the world. With the emerging concept of smart grid, where communication infrastructures need to be used in the whole power grid, we believe this advantage will make PLC more and more important to the communication technology society.

In this thesis, we have focused on the indoor relay-assisted PLC networks. In particular, we have proposed a method to analyze a relay-involved PLC channel and its channel model generation approach. With this realistic channel condition, we examined several relay schemes which have been introduced in the indoor PLC network to improve the performance. The main points are summarized as follows.

8.1 Concluding remarks

The background knowledge has been reviewed in Chapter 2, where indoor power line topology, point-to-point (P2P) channel modeling method, some published channel models and different types of noise have been analyzed. In particular, we give a detailed description of Canete's hybrid P2P indoor PLC channel model[32] as it is a useful tool for our simulations.

On the other hand, we introduced Benyoucef's general background PLC noise model[38]. With this noise model, random noise samples have been obtained to examine the proposed relay schemes.

In Chapter 3, we pointed out that the relay-involved PLC channel cannot be treated as a simple extension of the P2P case, and the method of modeling it has been presented. In addition to giving the general procedures of building a relay-involved channel model from scratch, we also proposed a simple approach, which transforms the original problem into modeling a group of special P2P channels.

A practical problem has been studied in Chapter 4. When multiple outlets are available between the transceivers, to obtain the most benefits from the relay device, which outlet should be selected to deploy the relay device? As a result from our analysis, a location selection criteria has been given to guide the best-effort selection for one or more relay devices.

In Chapter 5, we considered the one-way relay-assisted data transmission system, where the source node transits an identical message twice, in the first and second signaling phase respectively. On one hand, this configuration makes the system benefit from the spacial diversity (which is based on the different location of the network nodes). On the other hand, time diversity can also be realized since the relay-involved PLC channel is naturally time-varying.

To avoid the system capacity loss due to the half-duplex constraint of relay devices, in Chapter 6, we applied a simple form of network coding into the two-way information exchange PLC system. Without missing QoS requirements on each traffic direction, an alternative optimization algorithm has been proposed to save the total network power.

As a further step, we introduced the space-time coding (STC) technology into this two-way PLC network in Chapter 7. Simulation results show that by switching the relay nodes between the STC mode and the normal multi-relay AF (MAF) mode in an adaptive manner, extra performance improvement can be obtained as a combined effect from both network coding and STC.

8.2 Future perspectives

As a final comment we would like to show some future perspectives which could represent further research topics.

Our research results show that if a relay device has been introduced into the PLC network, its time-varying impedance will affect the signaling path significantly. Although as has

been shown in Chapter 5, this affect can be positive; however the other side is also true. The reason behind this is the impedance of the relay device can either enhance or reduce the impedance matching status of the network. This problem can be solved if the impedance of the relay device is designed to be adaptive to the matching requirement of the grid circuit.

In addition, besides the optimal power allocation for different relay schemes that has been considered in this thesis, the related problems, such as optimal bit-loading and adaptive modulation, also need to be addressed. Because characteristics of the relay-involved channel condition are essentially different from the P2P case, previous solutions to these problems need to be re-examined.

Appendix A

Proof of Propositions in Chapter 5

LEMMA A.1: Compound function $-\log_2 f(x)$ is convex on $\{x \mid f(x) > 0\}$, if $f(x)$ is concave.[50]

LEMMA A.2: A non-negative weighted sum of convex (concave) functions is convex (concave) function.[50]

A.1 Proof of proposition 5.1

Considering there is at least one solution to problem (5.18)-(5.20), so that the Lagrange multiplier λ in (5.26)-(5.27) cannot take 0 value. Let us rewrite (5.19) as $\sum_{k=1}^{K} \log_2 f(x_k) \geq 2q$, where

$$f(x_k) = A_k + \frac{D_k}{B_k + C_k x_k} + \frac{E_k \sqrt{x_k}}{B_k + C_k x_k} \tag{A.1}$$

and

$$\frac{df(x_k)}{dx_k} = \frac{E_k}{2\sqrt{x_k}(B_k + C_k x_k)} - \frac{C_k D_k + C_k E_k \sqrt{x_k}}{(B_k + C_k x_k)^2}. \tag{A.2}$$

Note that $\frac{df(x_k)}{dx_k} = 0$ has the only solution on $\{x_k \mid x_k \geq 0, k = 1, 2, \ldots K\}$ as

$$s = \frac{\sqrt{C_k^2 D_k^2 + C_k B_k E_k^2} - C_k D_k}{C_k E_k} \tag{A.3}$$

and

$$f(s) \geq \lim_{x_k \to 0+} f(x_k) = A_k + \frac{D_k}{B_k} \tag{A.4}$$

$$f(s) \geq \lim_{x_k \to +\infty} f(x_k) = A_k. \tag{A.5}$$

It can be seen from (A.3)-(A.5) that the peak value of $f(x_k)$ always occurs at s. This leads to the conclusion that the optimal x_k satisfying (5.19) occurs at s.

In addition, we note that when $0 \leq x_k \leq \frac{3B_k+2\sqrt{3}B_k}{3C_k}$,

$$\frac{d^2 X_k}{dx_k^2} \leq 0. \tag{A.6}$$

Let us denote a subset of $\{x_k \mid x_k \geq 0, k = 1,2,\ldots K\}$ as

$$\mathscr{X} = \left\{ x_k \mid 0 \leq x_k \leq x_{0,k}, x_{0,k} = \frac{(1+\frac{2}{3}\sqrt{3})B_k}{C_k}, k = 1,2,\ldots K \right\}. \tag{A.7}$$

As $x_0 \geq s$, subset $\mathscr{X}$ includes the neighborhood of s.

Thus $f(x_k)$ is positive and concave on $\mathscr{X}$. By using Lemma A.1 and A.2, the LHS of (5.19) is convex on $\mathscr{X}$. Finally, as (5.18) and (5.20) are obviously convex on $\mathscr{X}$, so that the problem (5.18)-(5.20) is convex on $\mathscr{X}$.

Furthermore, from (A.3)-(A.5), we can see the LHS of (5.27) is a piecewise monotone function of x_k. And (A.6) shows that the LHS of (5.26) is monotonically decreasing on $\mathscr{X}$. □

A.2 Proof of proposition 5.2

It is easy to observe that μ cannot take 0 value. We rewrite the LHS of (5.31) as $2q - \sum_{k=1}^{K} \log_2 \left(F + G_k y_k + \frac{H_k}{L_k y_k + M_k} + Y_k \right)$, where

$$Y_k = \frac{R_k \sqrt{L_k y_k^2 + y_k}}{L_k y_k + M_k}. \tag{A.8}$$

We can find that

$$\lim_{x_k \to 0+} Y_k = 0 \tag{A.9}$$

$$\lim_{x_k \to \infty} Y_k = \frac{R_k}{\sqrt{L_k}}. \tag{A.10}$$

In addition, when $y_k \geq 0$,

$$\frac{dY_k}{dy_k} \geq 0 \tag{A.11}$$

$$\frac{d^2 Y_k}{dy_k^2} \leq 0. \tag{A.12}$$

So that Y_k is increasing and concave on $\{y_k \mid y_k \geq 0, k = 1,2,\ldots K\}$. In addition, as $H_k < 0$, $F_k, M_k > 1$ and $G_k, L_k, R_k > 0$, so that $\frac{H_k}{L_k y_k + M_k}$ is concave on $\{y_k \mid y_k \geq 0, k = 1,2,\ldots K\}$. From Lemma A.1 and A.2, the LHS of (5.31) is convex on $\{y_k \mid y_k \geq 0, k = 1,2,\ldots K\}$.

Furthermore, from (A.11) we can see the LHS of (5.40) is a monotone function of y_k. And (A.12) shows that the LHS of (5.39) is monotone to y_k. □

A.3 Proof of proposition 5.3

It is easy to observe that δ cannot take 0 value. From their definitions, we know that $S_k, T_k, U_k > 0$. In addition, it is obvious that z_k and $\sqrt{z_k}$ is concave and non-negative on $\{z_k \mid z_k \geq 0, k = 1,2,\ldots K\}$. Using Lemma A.1 and A.2 leads us to the result that the LHS of (5.44) is convex on $\{z_k \mid z_k \geq 0, k = 1,2,\ldots K\}$.

Furthermore, it is easy to see that the LHS of (5.49) is monotonically increasing with z_k and the LHS of (5.50) is a monotonously decreasing function of z_k, respectively. □

Appendix B

Proof of Propositions in Chapter 6

LEMMA B.1: Log-barrier $-\sum_{i=1}^{m} \log_2 (f_i(x))$ is convex on $\{x \,|\, f_i(x) > 0\}$ if $f_i(x)$ is concave, where $m \in Z^+$.[50]

LEMMA B.2: A non-negative weighted sum of convex (concave) functions is convex (concave) function.[50]

LEMMA B.3: $-\log_2 f(x)$ is quasi-convex, if $f(x)$ is quasi-concave on $\{x \,|\, f(x) > 0\}$.[50]

LEMMA B.4: $\sum_{i=1}^{m} f_i(x)$ is quasi-convex (quasi-concave), if $f_i(x)$ is non-increasing (non-decreasing), where $m \in Z^+$.[50]

B.1 Proof of proposition 6.1

As $B_k, C_k, F_k, G_k > 0$ and $D_k > 1$, the expressions $\left(-\frac{B_k}{C_k x_k + D_k}\right)$ and $\left(-\frac{F_k}{G_k x_k + D_k}\right)$ in (6.25) and (6.26), respectively, are concave on $\{x_k \mid x_k \geq 0, k = 1, 2, \ldots K\}$. From Lemma B.1 and B.2, it is easy to approve that the LHS of (6.25) and (6.26) are convex on $\{x_k \mid x_k \geq 0, k = 1, 2, \ldots K\}$. (6.24) and (6.27) are obviously convex, thus problem (6.24)-(6.27) is convex on

$$\{x_k \mid x_k \geq 0, k = 1, 2, \ldots K\}.$$

Furthermore, it can be easily observed that the LHS of (6.35) is increasing with x_k, while the LHS of (6.36)-(6.37) are decreasing functions of x_k. □

B.2 Proof of proposition 6.2

As $H_k, J_k, O_k > 0$ and $L_k, M_k, P_k > 1$, the expression $\left(M_k - \frac{O_k}{J_k y_k + P_k}\right)$ in (6.42) is increasing and concave on$\{x_k \mid x_k \geq 0, k = 1, 2, \ldots K\}$. From Lemma B.1, it is easy to approve that the LHS of (6.42) is convex on $\{x_k \mid x_k \geq 0, k = 1, 2, \ldots K\}$.

The expression $\left(1 + \frac{H_k}{J_k y_k + L_k}\right)$ in (6.41) is monotonically decreasing, so it is quasi-concave. From Lemma B.3 and B.4 , the LHS of (6.41) is quasi-convex, so that the problem (6.40)-(6.43) is quasi-convex on $\{x_k \mid x_k \geq 0, k = 1, 2, \ldots K\}$.

Furthermore, we can see that the LHS of (6.52) is decreasing with y_k, while the LHS of (6.50)-(6.51) are increasing functions of y_k. □

Appendix C

List of Acronyms

AF	amplify-and-forward
AGC	automatic gain control
AMM	automatic meter management
AMR	automatic meter reading
AP	access point
AWGN	additive white Gaussian noise
BB	broad band
BER	bit error rate
BF	broadcast-and-forward
BFSK	binary FSK
BMA	broadcast-and-multiaccess
BPSK	binary PSK
CB	circuit breaker
CCDF	complementary CDF

CDF	cumulative distribution function
CENELEC	European Committee for Electrotechnical Standardization
CP	cyclic prefix
CRC	cyclic redundancy check
CSI	channel state information
CSMA	carrier sense multiple access
CSMA/CA	CSMA with collision avoidance
CSMA/CD	CSMA with collision detection
DBPSK	differential BPSK
DF	decode-and-forward
DFT	discrete Fourier transform
DLL	data link layer
DPSK	differential PSK
DQPSK	differential QPSK
DSSS	direct-sequence spread spectrum
ESP	energy service provider
FCC	Federal Communications Commission
FEC	forward error correction

FFT	fast Fourier transform
FHSS	frequency-hopping spread spectrum
FSK	frequency shift keying
HAN	home area network
HD	high definition
HPAV	HomePlug AV
HPCC	HomePlug Command & Control
HPGP	HomePlug GreenPHY
HV	high voltage
HVAC	heating, ventilation and air conditioning
ITU	International Telecommunication Union
ITU-T	ITU- Telecommunication Standardization
KKT	Karush Kuhn Tucker
LAN	local area network
LLC	logical link control
LV	low voltage
MAC	medium access control
MIMO	multiple input multiple output

MP	main panel
MV	medium voltage
NB	narrow band
NL	network layer
OFDM	orthogonal frequency division multiplexing
pdf	probability density function
PLC	power line communication
PSD	power spectral density
PSK	phase shift keying
PS-OFDM	pulse shaped OFDM
QoS	quality of service
QPSK	quadrature PSK
SNR	signal to noise ratio
SOHO	small office home office
UTP	unshielded twisted pair
WLAN	wireless LAN

References

[1] A. M. Tonello and F. Versolatto, "Bottom-up statistical PLC channel modeling–Part I: Random topology model and efficient transfer function computation," *Power Delivery, IEEE Transactions on*, vol. 26, no. 2, pp. 891–898, 2011.

[2] A. M. Tonello, F. Versolatto, and S. D'Alessandro, "Opportunistic relaying in in-home PLC networks," in *Global Telecommunications Conference (GLOBECOM 2010), 2010 IEEE*, pp. 1–5, IEEE, 2010.

[3] H. C. Ferreira, L. Lampe, J. Newbury, and T. G. Swart, *Power Line Communications: Theory and Applications for Narrowband and Broadband Communications over Power Lines*. Wiley, 2010.

[4] H. C. Ferreira, H. Grove, O. Hooijen, and A. Han Vinck, "Power line communications: an overview," in *AFRICON, 1996., IEEE AFRICON 4th*, vol. 2, pp. 558–563, IEEE, 1996.

[5] M. S. Yousuf and M. El-Shafei, "Power line communications: An overview–Part I," in *the 4th International Conference on Information Technology*, pp. 218–222, IEEE, 2007.

[6] E. Bassi, F. Benzi, L. Almeida, and T. Nolte, "Powerline communication in electric vehicles," in *Electric Machines and Drives Conference, 2009. IEMDC'09. IEEE International*, pp. 1749–1753, IEEE, 2009.

[7] K. Kilani, V. Degardin, P. Laly, and M. Lienard, "Transmission on aircraft power line between an inverter and a motor: Impulsive noise characterization," in *Power Line Communications and Its Applications (ISPLC), 2011 IEEE International Symposium on*, pp. 301–304, IEEE, 2011.

[8] Z. Fan, P. Kulkarni, S. Gormus, C. Efthymiou, G. Kalogridis, M. Sooriyabandara, Z. Zhu, S. Lambotharan, and W. H. Chin, "Smart grid communications: Overview of research challenges, solutions, and standardization activities," *Communications Surveys & Tutorials, IEEE*, vol. 15, no. 1, pp. 21–38, 2013.

[9] S. Galli, A. Scaglione, and Z. Wang, "For the grid and through the grid: The role of power line communications in the smart grid," *Proceedings of the IEEE*, vol. 99, no. 6, pp. 998–1027, 2011.

[10] I. H. Cavdar, "A solution to remote detection of illegal electricity usage via power line communications," *Power Delivery, IEEE Transactions on*, vol. 19, no. 4, pp. 1663–1667, 2004.

[11] D. Hong, J. Lee, and J. Choi, "Power quality monitoring system using power line communication," in *Information, Communications and Signal Processing, 2005 Fifth International Conference on*, pp. 931–935, IEEE, 2005.

[12] M. Zimmermann and K. Dostert, "A multipath model for the powerline channel," *Communications, IEEE Transactions on*, vol. 50, no. 4, pp. 553–559, 2002.

[13] F. C. Corripio, J. A. C. Arrabal, L. D. del Rio, and J. E. Munoz, "Analysis of the cyclic short-term variation of indoor power line channels," *Selected Areas in Communications, IEEE Journal on*, vol. 24, no. 7, pp. 1327–1338, 2006.

[14] "Homeplug AV white paper." http://www.homeplug.org/products/whitepapers, 2007.

[15] L. Lampe and A. H. Vinck, "On cooperative coding for narrow band PLC networks," *AEU-International Journal of Electronics and Communications*, vol. 65, no. 8, pp. 681–687, 2011.

[16] B. Praho, M. Tlich, P. Pagani, A. Zeddam, and F. Nouvel, "Cognitive detection method of radio frequencies on power line networks," in *Power Line Communications and Its Applications (ISPLC), 2010 IEEE International Symposium on*, pp. 225–230, IEEE, 2010.

[17] T. Sartenaer and P. Delogne, "Powerline cables modelling for broadband communications," in *Proc. IEEE Int. Conf. Power Line Communications and Its Applications*, pp. 331–337, 2001.

[18] H. Furukawa, H. OKada, T. Yamazato, and M. Katayama, "Signaling methods for broadcast transmission in power-line communication systems," in *7th International Symposium on Power-Line Communications and its applications*, 2003.

[19] L. Lampe and A. H. Vinck, "A study on relay network techniques in PLC," in *The Workshop on Power Line Communications, 2011 (WSPLC)*, 2011.

[20] G. Bumiller, "Single frequency network technology for medium access and network management," in *6th International Symposium on Power-Line Communications and its applications*, 2002.

[21] S. D'Alessandro, A. M. Tonello, and F. Versolatto, "Power savings with opportunistic decode and forward over in-home PLC networks," in *Power Line Communications and Its Applications (ISPLC), 2011 IEEE International Symposium on*, pp. 176–181, IEEE, 2011.

[22] S. D'Alessandro and A. M. Tonello, "On rate improvements and power saving with opportunistic relaying in home power line networks," *EURASIP Journal on Advances in Signal Processing*, vol. 2012, no. 1, pp. 1–17, 2012.

[23] L. Lampe, R. Schober, and S. Yiu, "Distributed space-time coding for multihop transmission in power line communication networks," *Selected Areas in Communications, IEEE Journal on*, vol. 24, no. 7, pp. 1389–1400, 2006.

[24] L. Lampe and A. H. Vinck, "Cooperative multihop power line communications," in *Power Line Communications and Its Applications (ISPLC), 2012 16th IEEE International Symposium on*, pp. 1–6, IEEE, 2012.

[25] T. Esmailian, F. Kschischang, and P. Gulak, "An in-building power line channel simulator," in *International Symposium on Power Line Communications and Its Applications (ISPLC)*, pp. 27–29, 2002.

[26] T. Esmailian, F. R. Kschischang, and P. Glenn Gulak, "In-building power lines as high-speed communication channels: channel characterization and a test channel ensemble," *International Journal of Communication Systems*, vol. 16, no. 5, pp. 381–400, 2003.

[27] A. M. Tonello and T. Zheng, "Bottom-up transfer function generator for broadband PLC statistical channel modeling," in *Power Line Communications and Its Applications, 2009. ISPLC 2009. IEEE International Symposium on*, pp. 7–12, IEEE, 2009.

[28] S. Galli and T. C. Banwell, "Modeling the indoor power line channel: new results and modem design considerations," in *Consumer Communications and Networking Conference, 2004. CCNC 2004. First IEEE*, pp. 25–30, IEEE, 2004.

[29] S. Galli, "A novel approach to the statistical modeling of wireline channels," *Communications, IEEE Transactions on*, vol. 59, no. 5, pp. 1332–1345, 2011.

[30] H. Philipps, "Modelling of powerline communication channels," in *Conf. IEEE Int. Symp. on Power Line Communications and Its Applications*, pp. 14–21, 1999.

[31] F. Versolatto and A. M. Tonello, "Analysis of the PLC channel statistics using a bottom-up random simulator," in *Power Line Communications and Its Applications (ISPLC), 2010 IEEE International Symposium on*, pp. 236–241, IEEE, 2010.

[32] F. Canete, J. Cortes, L. Diez, and J. Entrambasaguas, "A channel model proposal for indoor power line communications," *Communications Magazine, IEEE*, vol. 49, pp. 166–174, December 2011.

[33] "PLC channel generator v2." http://www.plc.uma.es. Accessed: 2015-05-03.

[34] "User guide v2." http://www.plc.uma.es. Accessed: 2015-05-03.

[35] M. Zimmermann and K. Dostert, "Analysis and modeling of impulsive noise in broadband powerline communications," *Electromagnetic Compatibility, IEEE Transactions on*, vol. 44, pp. 249–258, Feb 2002.

[36] J. Cortes, L. Diez, F. Canete, and J. Sanchez-Martinez, "Analysis of the indoor broadband power-line noise scenario," *Electromagnetic Compatibility, IEEE Transactions on*, vol. 52, pp. 849–858, Nov 2010.

[37] D. Middleton, "Statistical-physical models of electromagnetic interference," *Electromagnetic Compatibility, IEEE Transactions on*, no. 3, pp. 106–127, 1977.

[38] D. Benyoucef, "A new statistical model of the noise power density spectrum for powerline communication," in *Proceedings of the 7th International Symposium on Power-Line Communications and its Applications, Kyoto, Japan*, pp. 136–141, 2003.

[39] D. M. Pozar, *Microwave Engineering*. John Wiley & Sons, 2009.

[40] C. Caloz and T. Itoh, *Electromagnetic Eetamaterials: Transmission Line Theory and Microwave Applications*. John Wiley & Sons, 2005.

[41] X. Cheng, R. Cao, and L. Yang, "On the system capacity of relay-aided powerline communications," in *Power Line Communications and Its Applications (ISPLC), 2011 IEEE International Symposium on*, pp. 170–175, April 2011.

[42] "NP508 user guide." http://www.netcommwireless.com/product/powerline/np505. Accessed: 2015-05-03.

[43] H. A. Latchman, S. Katar, L. Yonge, and S. Gavette, *Homeplug AV and IEEE 1901: A Handbook for PLC Designers and Users*. John Wiley & Sons, 2013.

[44] W. Zhang, U. Mitra, and M. Chiang, "Optimization of amplify-and-forward multicarrier two-hop transmission," *Communications, IEEE Transactions on*, vol. 59, no. 5, pp. 1434–1445, 2011.

[45] Y. Li, W. Wang, J. Kong, W. Hong, X. Zhang, and M. Peng, "Power allocation and subcarrier pairing in OFDM-based relaying networks," in *Communications, 2008. ICC'08. IEEE International Conference on*, pp. 2602–2606, IEEE, 2008.

[46] I. Hammerstrom and A. Wittneben, "On the optimal power allocation for nonregenerative OFDM relay links," in *Communications, 2006. ICC'06. IEEE International Conference on*, vol. 10, pp. 4463–4468, IEEE, 2006.

[47] Y. Ma, A. Liu, and Y. Hua, "A dual-phase power allocation scheme for multicarrier relay system with direct link," *Signal Processing, IEEE Transactions on*, vol. 62, no. 1, pp. 5–16, 2014.

[48] N. Papandreou and T. Antonakopoulos, "Bit and power allocation in constrained multicarrier systems: the single-user case," *EURASIP Journal on Advances in Signal Processing*, vol. 2008, p. 11, 2008.

[49] Y. Rong, X. Tang, and Y. Hua, "A unified framework for optimizing linear nonregenerative multicarrier mimo relay communication systems," *Signal Processing, IEEE Transactions on*, vol. 57, no. 12, pp. 4837–4851, 2009.

[50] S. Boyd and L. Vandenberghe, *Convex Optimization*. Cambridge University Press, 2004.

[51] R. Ahlswede, N. Cai, S.-Y. Li, and R. W. Yeung, "Network information flow," *Information Theory, IEEE Transactions on*, vol. 46, no. 4, pp. 1204–1216, 2000.

[52] C. Fragouli and E. Soljanin, "Network coding fundamentals," *Foundations and Trends in Networking*, vol. 2, no. 1, 2007.

[53] R. Koetter and M. Médard, "An algebraic approach to network coding," *Networking, IEEE/ACM Transactions on*, vol. 11, no. 5, pp. 782–795, 2003.

[54] S. Bhadra, S. Shakkottai, and P. Gupta, "Min-cost selfish multicast with network coding," *Information Theory, IEEE Transactions on*, vol. 52, no. 11, pp. 5077–5087, 2006.

[55] X.-B. Liang, "Matrix games in the multicast networks: maximum information flows with network switching," *IEEE/ACM Transactions on Networking (TON)*, vol. 14, no. SI, pp. 2433–2466, 2006.

[56] J. N. Laneman and G. W. Wornell, "Distributed space-time-coded protocols for exploiting cooperative diversity in wireless networks," *Information Theory, IEEE Transactions on*, vol. 49, no. 10, pp. 2415–2425, 2003.

[57] J. N. Laneman, D. N. Tse, and G. W. Wornell, "Cooperative diversity in wireless networks: Efficient protocols and outage behavior," *Information Theory, IEEE Transactions on*, vol. 50, no. 12, pp. 3062–3080, 2004.

[58] Y. Wu, P. A. Chou, S.-Y. Kung, *et al.*, "Information exchange in wireless networks with network coding and physical-layer broadcast," tech. rep., MSR-TR-2004, 2005.

[59] C. K. Ho, R. Zhang, and Y.-C. Liang, "Two-way relaying over OFDM: optimized tone permutation and power allocation," in *Communications, 2008. ICC'08. IEEE International Conference on*, pp. 3908–3912, IEEE, 2008.

[60] B. Tan and J. Thompson, "Relay transmission protocols for in-door powerline communications networks," in *Communications Workshops (ICC), 2011 IEEE International Conference on*, pp. 1–5, IEEE, 2011.

[61] M. Noori and L. Lampe, "Improving data rate in relay-aided power line communications using network coding," in *Global Communications Conference (GLOBECOM), 2013 IEEE*, pp. 2975–2980, IEEE, 2013.

[62] S. Fu, K. Lu, Y. Qian, and M. Varanasi, "Cooperative network coding for wireless ad-hoc networks," in *Global Telecommunications Conference, 2007. GLOBECOM'07. IEEE*, pp. 812–816, IEEE, 2007.

[63] T. Cover and A. E. Gamal, "Capacity theorems for the relay channel," *Information Theory, IEEE Transactions on*, vol. 25, no. 5, pp. 572–584, 1979.

[64] A. Sendonaris, E. Erkip, and B. Aazhang, "User cooperation diversity–Part I: System description," *Communications, IEEE Transactions on*, vol. 51, no. 11, pp. 1927–1938, 2003.

[65] V. B. Balakirsky and A. H. Vinck, "Potential performance of PLC systems composed of several communication links," in *Power Line Communications and Its Applications, 2005 International Symposium on*, pp. 12–16, IEEE, 2005.

[66] A. H. Vinck and B. Dai, "Multi-user power-line communication," in *Power Line Communications and Its Applications (ISPLC), 2013 17th IEEE International Symposium on*, pp. 13–17, IEEE, 2013.

[67] S. Alamouti, "A simple transmit diversity technique for wireless communications," *Selected Areas in Communications, IEEE Journal on*, vol. 16, no. 8, pp. 1451–1458, 1998.

[68] V. Tarokh, H. Jafarkhani, and A. R. Calderbank, "Space-time block codes from orthogonal designs," *Information Theory, IEEE Transactions on*, vol. 45, no. 5, pp. 1456–1467, 1999.

[69] R. U. Nabar, H. Bolcskei, and F. W. Kneubuhler, "Fading relay channels: performance limits and space-time signal design," *Selected Areas in Communications, IEEE Journal on*, vol. 22, no. 6, pp. 1099–1109, 2004.

[70] K. Dostert, *Powerline Communications*. Prentice Hall PTR, 2001.

[71] H. C. Ferreira, H. M. Grové, O. Hooijen, and A. Han Vinck, *Power Line Communication*. Wiley Online Library, 1999.

[72] L. T. Berger, A. Schwager, P. Pagani, and D. Schneider, *MIMO Power Line Communications: Narrow and Broadband Standards, EMC, and Advanced Processing*. CRC Press, 2014.

[73] M. S. Yousuf, S. Z. Rizvi, and M. El-Shafei, "Power line communications: An overview–Part II," in *Information and Communication Technologies: From Theory to Applications, 2008. ICTTA 2008. 3rd International Conference on*, pp. 1–6, IEEE, 2008.

[74] N. Pavlidou, A. H. Vinck, J. Yazdani, and B. Honary, "Power line communications: state of the art and future trends," *IEEE Communications Magazine*, vol. 41, no. 4, pp. 34–40, 2003.

[75] M. M. Rahman, C. S. Hong, S. Lee, J. Lee, M. A. Razzaque, and J. H. Kim, "Medium access control for power line communications: An overview of the IEEE 1901 and

ITU-T G.hn standards," *Communications Magazine, IEEE*, vol. 49, no. 6, pp. 183–191, 2011.

[76] H. Dai and H. V. Poor, "Advanced signal processing for power line communications," *Communications Magazine, IEEE*, vol. 41, no. 5, pp. 100–107, 2003.

[77] H. Meng, Y. L. Guan, and S. Chen, "Modeling and analysis of noise effects on broadband power-line communications," *Power Delivery, IEEE Transactions on*, vol. 20, no. 2, pp. 630–637, 2005.

[78] M. Katayama, T. Yamazato, and H. Okada, "A mathematical model of noise in narrowband power line communication systems," *Selected Areas in Communications, IEEE Journal on*, vol. 24, no. 7, pp. 1267–1276, 2006.

[79] L. Di Bert, P. Caldera, D. Schwingshackl, and A. M. Tonello, "On noise modeling for power line communications," in *Power Line Communications and Its Applications (ISPLC), 2011 IEEE International Symposium on*, pp. 283–288, IEEE, 2011.

[80] M. Gotz, M. Rapp, and K. Dostert, "Power line channel characteristics and their effect on communication system design," *Communications Magazine, IEEE*, vol. 42, no. 4, pp. 78–86, 2004.

[81] H. Hrasnica, A. Haidine, and R. Lehnert, *Broadband Powerline Communications: Network Design*. John Wiley & Sons, 2005.

[82] R. Olsen, "Technical considerations for wideband powerline communication-a summary," in *Power Engineering Society Summer Meeting, 2002 IEEE*, vol. 3, pp. 1186–1191 vol.3, July 2002.

[83] P. Popovski and H. Yomo, "Wireless network coding by amplify-and-forward for bi-directional traffic flows," *Communications Letters, IEEE*, vol. 11, no. 1, pp. 16–18, 2007.

[84] P. Larsson, N. Johansson, and K.-E. Sunell, "Coded bi-directional relaying," in *Vehicular Technology Conference, 2006. VTC 2006-Spring. IEEE 63rd*, vol. 2, pp. 851–855, IEEE, 2006.

[85] M. Sheikh-Hosseini, G. A. Hodtani, and M. Molavi-Kakhki, "Capacity analysis of power line communication point-to-point and relay channels," *Transactions on Emerging Telecommunications Technologies*, 2014.

[86] X. Cheng, R. Cao, and L. Yang, "Relay-aided amplify-and-forward powerline communications," *Smart Grid, IEEE Transactions on*, vol. 4, pp. 265–272, March 2013.

[87] K. Dostert, "Telecommunications over the power distribution grid–possibilities and limitations," *IIR-Powerline*, vol. 6, p. 97, 1997.

[88] A. Stefanov and E. Erkip, "Cooperative coding for wireless networks," *Communications, IEEE Transactions on*, vol. 52, no. 9, pp. 1470–1476, 2004.

[89] T. Esmailian, P. G. Gulak, and F. R. Kschischang, "A discrete multitone power line communications system," in *Acoustics, Speech, and Signal Processing, 2000. ICASSP'00. Proceedings. 2000 IEEE International Conference on*, vol. 5, pp. 2953–2956, IEEE, 2000.

[90] M. Yu and J. Li, "Is amplify-and-forward practically better than decode-and-forward or vice versa?," in *Acoustics, Speech, and Signal Processing, 2005. Proceedings.(ICASSP'05). IEEE International Conference on*, vol. 3, pp. iii–365, IEEE, 2005.

[91] D. S. 11/03, "Broadband power-line communications systems: a background brief," tech. rep., Australian Communications Authority, Radiofrequency Planning Group, Spectrum Planning Team, 2003.